Spatial and Temporal Dynamics of Microorganisms Living Along Steep Energy Gradients and Implications for Ecology and Geologic Preservation in the Deep Biosphere

Thesis by

Sean William Alexander Mullin

In Partial Fulfillment of the Requirements for

the degree of

Doctor of Philosophy

CALIFORNIA INSTITUTE OF TECHNOLOGY

Pasadena, California

2020

(Defended 8 June 2020)

Sean W. A. Mullin
ORCID: 0000-0002-6225-3279

What is any man's discourse to me, if I am not sensible of something in it as steady and cheery as the creak of crickets? In it the woods must be relieved against the sky. Men tire me when I am not constantly greeted and refreshed as by the flux of sparkling streams. Surely joy is the condition of life. Think of the young fry that leap in ponds, the myriads of insects ushered into being on a summer evening, the incessant note of the hyla with which the woods ring in the spring, the nonchalance of the butterfly carrying accident and change painted in a thousand hues upon its wings…

—Henry David Thoreau, "Natural History of Massachusetts"

ACKNOWLEDGEMENTS

Seven years is a long time. Beyond four years, the collective memory of a university is misty and gray, and if it were a medieval map, would be marked simply, “Here be dragons.” The number of times I have been mistaken this past year for an aged staff scientist or long-suffering post-doc would be amusing if not for my deepening wrinkles serving to confirm my status as a relative dinosaur. Wrinkles aside, I can happily say that my time spent in the Orphan Lab has been one of tremendous growth and exploration. I am extremely fortunate to have enjoyed the company of brilliant people who have inspired, challenged, amused, supported, and comforted me through it all. I have grown in grad school as both a scientist and a person, in no small part due to their impact on my life.

First, I want to thank Victoria. I already appreciate the amount of work you do behind the scenes to keep the lab running, obtain opportunities for students, and maintain connections with the outside world, but I suspect that as time passes, I will appreciate those things even more. I have learned a tremendous amount from you, not least of which are the ways to communicate my science to the outside world to spark their interest. In a world of increasingly chaotic noise, I suspect these skills will be invaluable for the rest of my life. Getting to know you better on cruises has been a real joy and your passion for science has been infective — a real boon whenever my pessimism threatens.

I also need to thank my fellow geobiology students and post-docs, both former and current, for being a tremendous support network. I still vividly recall starting out at Caltech. Coming from a large school, I expected to feel alone, particularly once I found out that I was the only geobiology student of the year. The warmth with which the older students so thoroughly accepted me took me aback but has since become aspirational as I have aged into the role of elder grad student. In particular, I want to thank Jena Johnson, Sarah Slotznick, Elizabeth Trembath-Reichert, and Lewis Ward for their welcome and friendship. Y’all are amazing. Of course, those students have since graduated, but the new geobiology crew has never ceased to impress, especially my officemates in 102. Special thanks to John Magyar, Usha Lingappa, Gray Chadwick, Kyle Metcalfe, Cecilia Sanders, Aditi Narayanan, and Alon Philosof for their friendship and willingness to celebrate each other’s successes and commiserate with the setbacks.

A few scientific thanks are also deeply required here, in particular to a handful of postdocs who helped teach me the ways. Thank you to Greg Wanger, who was a driving force behind getting the

BLM-1 project off the ground, and to Brittany Kruger, who helped see it to completion. Thank you also to Kat Dawson, who I had met in lab but really got to know in Costa Rica. Seventy cores was a tall order for a two-person team, but we managed. I am glad to call you a friend and collaborator (plus somehow you are able to hear me perfectly even when I mumble and it honestly surprises me every time). Haley Sapers has also been a constant scientific sounding board for the past several years, someone with a seemingly boundless capacity to give and think, as well as a great travel companion. Your desire to do everything to the maximum degree and my tendency to efficiency (perhaps born of laziness) has been a potent combination. I absolutely must thank Stephanie Connon, the Orphan Lab Manger, as well. I honestly do not understand how you keep everything straight in the lab will all the projects running. Somehow, though, you handle it all with both diligence and grace.

I have been lucky to have made many friends outside of the Orphan Lab, too, and I cannot imagine what my life would have been like without their personal support. Giuliana Viglione, Kelvin Bates, Elle Chimiak, Al Chan, and Ollie Stephenson — thank you. You mean the world to me. Nancy Sulahian of the Glee Club and Taso Dimitriadis of the Center for Diversity have also been critical parts of my life here, giving me the opportunity to use some different parts of my brain and good friends besides. I want to thank my friends outside of Caltech too, for when I just need a break: Andrew Chen, Matt Franscioni, David Binsacca, Katie Papoe and Erik Wong, and Martín Hernandez. Thank you for reminding of the world abroad.

To my parents and my family in general, thank you. I am fortunate to have you so close and your support has never stopped. My cousins Ken and Nick showed me around LA when I first visited to convince me to come here, and it worked! Aunt Donna and Bennet — I have so appreciated your interest in my life and my science. And of course to my parents, I cannot express enough thanks. I wrote in my application for Caltech that my scientific curiosity came from you, and that remains true. You have been patient, interested, supportive, and kind. Problems never feel unsurmountable when I talk to you.

Lastly, I want to thank James. The past four years with you have been a delight, truly, and I cannot imagine them any differently. You are the rarified air keeping me afloat, and I keep thoughts of you close at hand at all times as a little source of joy and light my life. I look forward to our future.

ABSTRACT

The deep biosphere represents a massive repository of life with unknown effects on global biogeochemical cycles. Even the fundamental life strategies of the endemic microorganisms that inhabit this biome remain enigmatic; some studies have indicated that subsurface organisms subsist in energetic regimes below the theoretical lower limit for life. A boom-bust life cycle, mediated by tectonic disturbances and subsurface fractures, may help explain these phenomena. This work addresses and expands on this question, first by exploring the response of continental deep biosphere microorganisms to an *in situ* organic matter amendment, then by analyzing the microbial community dynamics of the sediments and carbonate along a naturally-occurring energy gradient at a methane seep. Our experiments in the continental deep biosphere confirmed that mineralogical heterogeneity can drive differential colonization of the native microorganisms, implying that selection and adaptation to *in situ* conditions occurs, differentiating individual microbial niches. We also observed the formation of secondary framboidal iron sulfide minerals, a well-known phenomenon in marine sediments but not extensively observed in the deep subsurface, that were correlated to the presence of abundant sulfur-metabolizing microorganisms. Chapters 2 and 3 are instead focused on the microbial ecology of a methane seep on the Pacific margin of Costa Rica. Cold methane seeps themselves represent sharp boundaries between the generally low-energy background seafloor and abundant chemical energy in the form of methane. Chapter 2 describes that the microorganisms living at these seeps occupy a significantly narrower spatial scale than the endemic megafauna. In addition, by correlating community dissimilarity and geographic distance, the functional center of the seep was identified, allowing for insight into the ecological differentiation between clades of anaerobic methanotrophic archaea (ANME). Chapter 3 examines in greater detail the endolithic microbial community, principally composed of ANME-1. By conducting transplantation experiments of carbonates on the seafloor, we tested the response of the *in situ* endolithic communities and found that carbonates moved distinctly outside the active zone changed less than communities moved to regions of less activity.

PUBLISHED CONTENT AND CONTRIBUTIONS

Mullin, S.W. et al. (2020). "Patterns of In Situ Mineral Colonization by Microorganisms in a ~60°C Deep Continental Subsurface Aquifer". *Frontiers in Microbiology* (accepted).

S.W.M. participated in the conception of the project, gathered field data, extracted and analyzed the DNA, performed the microscopy, and wrote the manuscript.

Mullin, S.W., et al. (2020). "Correlating the Microbial and Animal Communities with Biogeochemistry at a Cold Methane Seep in the Costa Rica Pacific Margin". In prep

S.W.M. participated in the conception of the project, participated in the cruise, participated in extracting DNA, analyzed all DNA data, geochemistry, and spatial mapping, and wrote the manuscript.

Mullin, S.W., et al. (2020). "Microbial community dynamics and succession in methane seep carbonates". In prep

S.W.M. participated in the conception of the project, participated in the cruise, participated in extracting DNA, analyzed all DNA data, and wrote the manuscript.

TABLE OF CONTENTS

LIST OF ILLUSTRATIONS AND/OR TABLES

Introduction

One of the most common questions that I have been asked during my Ph.D. studies is a simple one: "What is geobiology?" This is a fair question, certainly, since geobiology itself is a relatively young field with fluid boundaries touching on microbiology, ecology, evolutionary biology, geochemistry, and paleontology. Laurens Baas Becking coined the term "geobiology" in the 1930's, drawing inspiration from the work of Beyerinck, Vernadsky, and Vinogradsky, pioneers in the field of microbial ecology (Baas Becking and Canfield, 2015). I have always appreciated both the breadth and humility of his original definition: "an attempt to describe the relationship between organisms and the Earth." In considering relationships between the biosphere and geosphere, geobiologists often construct frameworks called biogeochemical cycles that describe how a nutrient moves through the biotic and abiotic spheres on Earth (*e.g.* the carbon cycle, nitrogen cycle, marine nutrient cycle, etc.). Great progress has been made over the past century in uncovering various fluxes within these cycles and their magnitudes, but almost without exception, each cycle considers the deep subsurface (everything below about 5 m into the sediment) to be a black box (Battin et al., 2009; Canfield et al., 2010). Once a nutrient is buried, it is considered to have effectively exited the cycle, typically balanced with inputs from volcanism and tectonic uplift. The deep subsurface, however, contains a massive reservoir of life—about 14% of the total biomass on earth—which possesses the capacity to metabolize many of the various chemical species that get buried (Bar-On et al., 2018). The kilometers of rock and sediment beneath the surface of the Earth hold staggering numbers of microorganisms; they outnumber surface microorganisms—of which there are already a million times more than the number of stars in the universe—by more than 4:1. There is little information to suggest one way or another if the biogeochemical cycles of the deep subsurface and the surface are connected.

Part of the reason for the lack of integration of subsurface microorganisms into global models is simply that these environments are difficult to access. Even beyond securing site access, collecting samples often requires elaborate drilling and sampling equipment. Laboratory-based experiments also suffer from the challenges in reproducing subsurface conditions *in vitro*, such as the pressure and temperature or the extreme lack of labile organic matter and strong

oxidants. Perhaps more importantly, the redox geochemistry of the subsurface also means that many deep subsurface microorganisms grow on timescales longer than humans can realistically detect. *In situ* doubling times for virtually all subsurface organisms are unknown. Many studies that examine questions of growth in the deep biosphere instead rely on single-cell activity measurements using isotopic labels and nanometer-scale secondary ion mass spectrometry (nanoSIMS) (Morono et al., 2011; Trembath-Reichert et al., 2017), rRNA gene transcripts (Blazewicz et al., 2013; Orsi et al., 2013), or amino acid racemization (Onstott et al., 2014; Braun et al., 2017). These studies indicate that subsurface organisms complete biomass turnover (but not reproduction) on timescales ranging from several months to thousands of years.

The extremely slow turnover times of the deep biosphere also present an ecological and evolutionary puzzle — if an organism does not reproduce for thousands of years, how do principles like selection, competition, succession, or genetic drift work in the subsurface? In some of the most oligotrophic subsurface environments, models have suggested that the resident microorganisms are either operating at power limits below the theoretical minimum for life or are simply on a "slow march to death," competing against each other only in the sense of which will survive the longest (LaRowe and Amend, 2015; Starnawski et al., 2017; Bradley et al., 2018). The subsurface does hold endemic organisms, however, implying that adaptation and selection must occur (Inagaki et al., 2006; Chivian et al., 2008; Biddle et al., 2011; Osburn et al., 2014; Momper et al., 2017). Notably, subsurface studies have demonstrated that higher cell densities do occur in some locations, mostly in places with higher organic matter content, such as coal seams or sapropels, or in locations with exposed rock faces, perhaps as a result of high tectonic activity or glacial erosion (Coolen and Overmann, 2000; Coolen et al., 2002; Inagaki et al., 2003; Jørgensen and Boetius, 2007; Sahl et al., 2008; Inagaki et al., 2015; Riedinger et al., 2015; Telling et al., 2015; Trembath-Reichert et al., 2017; Morono et al., 2019). Human activity can even speed up the exposure of these areas to microbial activity, as in the case of hydraulic fracturing ("fracking"), where hydrocarbons and freshly fractured rock surfaces are exposed by means of water pressure (Mouser et al., 2016). Although it is not unexpected to find more biomass in locations with higher energy inputs, these findings also hint at a possible life strategy for deep subsurface organisms: persisting in low-energy environments with extremely reduced metabolic function until a rare event delivers a richer energy source (Sleep and Zoback, 2007; Hirose et al., 2011).

Of course, it is virtually impossible to monitor a subsurface site and wait for one of these rare events to alter the local geochemistry so as to observe the microbial response. Whalefalls, for example, can happen virtually anywhere on the ocean floor and deliver a massive amount of organic carbon to an energy-poor environment (Goffredi and Orphan, 2010), but the ocean floor is far too vast to monitor at once (although it is still smaller than the deep subsurface as a whole). A better strategy is to either intentionally perturb the community, perhaps by intentionally sinking a dead whale in a known location (Braby et al., 2007), or to examine environments that already exist along steep energy gradients, such as a methane seep on the ocean floor, even if they are not in the deep subsurface (Levin et al., 2016; Ashford et al., 2020). Both of these approaches require careful examination of the relationships between the local microorganisms and their environment in order to interpret how and why the microbial community responds to changes in the energetic landscape.

As Baas Becking said of geobiology, the research presented here is an attempt to describe some of these organismal-environmental relationships. Chapter 1 describes several years of observation at Inyo-BLM1, a ~755 m borehole outside of Death Valley, California. For the first nine months, we tracked the resident organisms in various niches — in particular, preferential attachment to different lithologies. Subsequently, the borehole was perturbed by the addition of an organic carbon source. The community responded within just a few months; the relative proportions of various species changed drastically, despite the fact that we added just one gram of carbon to the system. Our experiments not only allowed us to observe various niches in the terrestrial deep biosphere (planktonic versus surface-attached, carbonate versus silicic rock-preferring, etc.), they also demonstrated that the deep biosphere community was capable of comparatively rapid response to organic carbon loading significantly above what had been observed in other studies that only examined biomass turnover.

Chapters 2 and 3 focus on a mud volcano and methane seep west of Costa Rica, where hydrothermal fluids bearing methane gently suffuse the seafloor and give rise to unique oases of life within the typically stark seafloor. Chapter 2 describes the general ecology of the seep, especially with regard to its boundaries. We found that the functional "edge" for the chemosynthetic communities was sharper and closer to the seep's center for sediment microorganisms than for benthic seep fauna. We also sought to identify useful indicators for

seep activity, which can be nebulous to define. One particular crab, *Kiwa puravida*, was generally found close to the seep center, as was a particular group of archaea, ANME-1.

In Chapter 3, we specifically focused on carbonate rocks present at the seep and their endolithic microorganisms. Again, these rocks served as a steep energy gradient to the microorganisms — abundant energy-rich methane outside and presumably little inside — but the carbonates came with the added complication that the endolithic microorganisms themselves were responsible for creating the rock matrix. We conducted *in situ* transplants of seep carbonates on the seafloor between various zones of seepage activity and monitored the change in endolithic microbial communities over a 12-month period. Rocks moved within areas of active methane oxidation changed significantly, demonstrating that the communities were alive and responding dynamically to environmental conditions. Intriguingly, the communities of rocks moved completely beyond the active zone of the seep changed very little; perhaps the lack of metabolic substrate caused them to enter their persisting, low-metabolic activity lifestyle.

Steep energy gradients, such as those we examined, can provide significant insight into an environment that historically has been nearly impossible to study effectively. Furthermore, when those gradients change dynamically, they have the potential to mimic long timescales, where the microbial community may go many years without significant energy input. By studying the ecology and microbiology along these gradients, we can better understand the lasting impacts of human intervention (fracking, deep seabed mining, etc.) in the subsurface. More importantly, we can finally incorporate this massive repository of life into global biogeochemical models and come to a deeper understanding of our planet.

Chapter 1

PATTERNS OF *IN SITU* MINERAL COLONIZATION BY MICROORGANISMS IN A ~60°C DEEP CONTINENTAL SUBSURFACE AQUIFER

Abstract

The microbial ecology of the deep biosphere is difficult to characterize, owing in part to sampling challenges and poorly understood response mechanisms to environmental change. Pre-drilled wells, including oil wells or boreholes, offer convenient access, but sampling is frequently limited to the water alone, which may provide only a partial view of the native diversity. Mineral heterogeneity demonstrably affects colonization by deep biosphere microorganisms, but the connections between the mineral-associated and planktonic communities remain unclear. To understand the substrate effects on microbial colonization and the community response to changes in organic carbon, we conducted an 18-month series of in situ experiments in a warm (57°C), anoxic, dolomitic aquifer at 752 m depth using replicate flow-through cartridges containing different solid substrates, with a proteinaceous organic matter perturbation halfway through this series. Samples from these cartridges were analyzed microscopically and by Illumina (iTag) 16S rRNA gene libraries to characterize changes in mineralogy and the diversity of the colonizing microbial community. The substrate-attached and planktonic communities were significantly different in our data, with some taxa (e.g. Candidate Division KB-1) rare or undetectable in one fraction and abundant in the other. The substrate-attached community composition also varied significantly with mineralogy, such as with two Rhodocyclaceae OTUs, one of which was abundant on carbonate minerals and the other on silicic substrates. Secondary sulfide mineral formation, including iron sulfide framboids, was observed on two sets of incubated carbonates. Notably, microorganisms were attached to the framboids, which were correlated with abundant Sulfurovum and Desulfotomaculum sp sequences in our analysis. Upon organic matter perturbation, mineral-associated microbial diversity differences were temporarily masked by the dominance of putative heterotrophic taxa in all samples, including OTUs identified as Caulobacter, Methyloversatilis, and Pseudomonas. Subsequent experimental deployments included a methanogen-dominated stage (Methanobacteriales and Methanomicrobiales) six months after the perturbation, and a return to an assemblage similar to the pre-perturbation community after nine months. Substrate-associated community differences were again significant within these subsequent phases, however, demonstrating the value of in situ time course experiments to capture a fraction of the microbial assemblage that is frequently difficult to observe in pre-drilled wells.

Introduction

The continental deep biosphere represents approximately 5-15% of the biomass on Earth, or about 27-64 Gt of carbon, yet the ecological conditions that govern community structure and activity remain poorly constrained (McMahon and Parnell, 2014; Bar-On et al., 2018; Magnabosco et al., 2018). One factor that complicates our understanding of this vast habitat is that microbial community composition is often predicated on highly heterogeneous local mineralogy and geochemistry (Orcutt et al., 2011; Sylvan et al., 2013; Toner et al., 2013; Jones and Bennett, 2014). Most cells in the deep subsurface are attached to surfaces, not planktonic, with attached cells estimated to outnumber free-living cells by a factor of 10 to 10^3 (Wanger et al., 2007; McMahon and Parnell, 2014). Evidence suggests that not only does the mineralogical composition and crystallographic axes affect which microbes attach via electrostatic interactions (Yee et al., 2000; Edwards and Rutenberg, 2001), but also that microbes actively weather minerals to access scarce nutrients or by way of their central metabolism (Lovley et al., 1989; Rogers et al., 1998; Caccavo and Das, 2002; Roberts, 2004). These effects can often be challenging to detect *in situ* due to the difficulty of accessing underground fracture networks, and because mineralogy typically varies concurrently with changes in geochemistry, temperature, porosity, and pressure along a depth axis. *In situ* experiments in terrestrial boreholes drilled from the surface are an attractive option because they provide direct access to rock surfaces in the native subsurface biogeochemical context. Subseafloor biosphere studies, such as (Orcutt et al., 2010), which deployed flow-through columns containing mineral colonization substrates of interest, can provide a good model for terrestrial experiments. *In situ* incubation of a variety of mineral substrates enables the study of microorganisms adhering to differing mineral surfaces, and further reveals the differences in composition between mineral-adhered and free-living microbial populations. Although drilling in terrestrial environments is comparatively more accessible than in marine systems as described in other studies (Orcutt et al., 2010), such experiments are not without their own challenges (Wilkins et al., 2014). Drilling always carries a risk of contamination, but drilling contamination can be mitigated in pumped or free-flowing boreholes by flushing with local groundwater to remove contaminants and re-establish the indigenous community (Moser et al., 2003; Davidson et al., 2011).

Describing the ecology of the subsurface can also prove difficult because of the extremely slow growth and metabolism of many resident microorganisms. *In situ* doubling times

for virtually all deep biosphere organisms are unknown and most studies rely on biomass turnover rates instead, calculated from cell-specific activity measurements and amino acid racemization studies (Kieft and Phelps, 1997; Morono et al., 2011; Onstott et al., 2014; Braun et al., 2017; Trembath-Reichert et al., 2017). These studies suggest biomass turnover rates in the deep biosphere range from several months to thousands of years. In fact, in the most oligotrophic environments such as the ocean gyre subseafloor, reactive transport models indicate that resident cells, if they are growing, either have energy requirements below the reported power usage minimum required for cellular maintenance (LaRowe and Amend, 2015) or are not growing at all, but slowly dying (Bradley et al., 2018). In less austere environments, such as the coastal marine subsurface or the terrestrial deep biosphere, microbial community analyses do not indicate that these environments only host poorly-adapted surface organisms. Instead, these environments are home to their own endemic, uncultivated, and previously unknown organisms such as the aptly named Deep Sea Archaeal Group, novel branches of Chloroflexi, or Candidate Phyla (Takai et al., 2001; Inagaki et al., 2006; Jørgensen and Boetius, 2007; Osburn et al., 2014). The terrestrial deep biosphere, accessed via boreholes or mines, has proven especially fruitful for the discovery of novel microbial diversity, including from the site in this study (**Fig. 1.1**) (Chivian et al., 2008; Sahl et al., 2008; Teske and Sørensen, 2008; Breuker et al., 2011; Osburn et al., 2014; Momper et al., 2017; Momper et al., 2018; Sackett, 2018; Sackett et al., 2019). Little is known, however, about the changes in deep subsurface systems of yearly or longer timescales. It may be possible that deep biosphere organisms persist with little to no growth until a rare nutrient or energy delivery, perhaps mediated by tectonic disturbance (Riedinger et al., 2015). Controlled substrate addition experiments performed *in situ* offer a novel experimental approach to understand the influence of transient energy influx on deep biosphere community structure and help constrain the energy requirements and maximum metabolic rates of these organisms.

Here we describe an 18-month series of five *in situ* microbial colonization experiments to characterize and constrain the microbial community and activity of a warm, continental biosphere from a ~775 m-deep borehole (Inyo-BLM 1) hosted in a fractured, Paleozoic carbonate beneath the Mojave Desert, CA, USA (**Fig. 1.1**). We demonstrate that not only is the mineral-hosted microbial community significantly different from the planktonic community, but that mineral-hosted communities vary based on the mineralogy. We also demonstrate that a controlled organic substrate addition strongly affected the *in situ* microbial community

composition and revealed subsurface taxa that were poised to take advantage of introduced complex organic matter.

Materials and Methods

Field site

The Inyo-BLM 1 well was completed in 2007 to a total depth of 884 m below land surface (mbls) by The Hydrodynamics Group, LLC (Edmonds, WA) on behalf of Inyo County, California (Belcher et al., 2009; Bredehoeft and King, 2010). The well pad is on the eastern flank of the Funeral Mountains in the Amargosa Valley, proximal to the California-Nevada border near Death Valley National Park (36º 24'04.19 N / 116º 28'06.58 W). Inyo-BLM 1 was drilled to test hypotheses concerning deep groundwater flow across the Funeral Mountains and intersects a variety of lithologies (e.g. sandstone, tuff), ultimately encountering Hidden Valley Dolomite (Silurian-Devonian, 423-393 Ma, in age) at 744 mbls (Fridrich et al., 2012), which is associated with the Lower Carbonate Aquifer (LCA), a warm, fractured rock aquifer in the discharge zone of the Death Valley Regional Flow System (Belcher et al., 2001; Bredehoeft et al., 2008). (**Fig. 1.1**). Inyo-BLM 1 was pumped for development and hydrologic testing in both 2007 and 2011 by pumping out approximately 1.6 million liters of water (~100 times total volume of groundwater in Inyo-BLM 1) and then allowed to re-equilibrate with the surrounding anoxic aquifer. Other than these two pumping events in 2007 and 2011, the hole sat undisturbed apart continuous monitoring of the static water level by the National Park Service to measure water table elevation until our sampling began in 2014. Although originally drilled to a total depth of 884 m, at the time of sampling, Inyo-BLM 1 was only accessible to 755 mbls, presumably due to collapse of unstable rock below the casing. Inyo-BLM 1 is continuously cased in unscreened low-carbon steel and cemented in a step-down manner (Bredehoeft et al., 2008); caliper measurements were completed in 2015 showing that the inner diameter decreases from 14.5 - 15 cm diameter (0 to 610 mbls) to 8.4 to 8.6 cm diameter (610-750 mbls), with the final 5 m open to the host rock and the warm (57°C) reducing fluids of the LCA. The borehole passes through several lithologies, including sandstone, siltstone, and mixed siliciclastic and tuff lake sediments, however the open hole section is entirely hosted within the Hidden Valley Dolomite within the Lost Burro Formation, roughly Silurian-Devonian (423 – 393 Ma) in age (Fridrich et al., 2012). Although the Inyo-BLM 1 drill pad is located hundreds of meters above the valley

floor (694 m above sea level), hydrostatic pressure maintains the groundwater at approximately 28 m below the surface (USGS, 2018). A study by Thomas, et al. (Thomas et al., 2013) indicated that although this hole likely shares the same hydrological recharge area as other wells in the area, including Ash Meadows springs, it is likely primarily sourced from a deeper and older portion of aquifer. A thermal flowmeter was deployed on August 21st, 2015 to test for flow within the open portion of the well, but none was detected (ie. < 0.08 L per min) (data not shown).

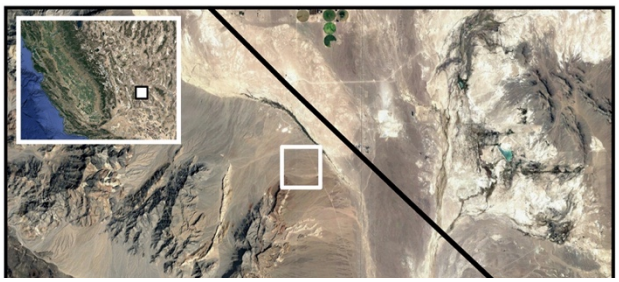

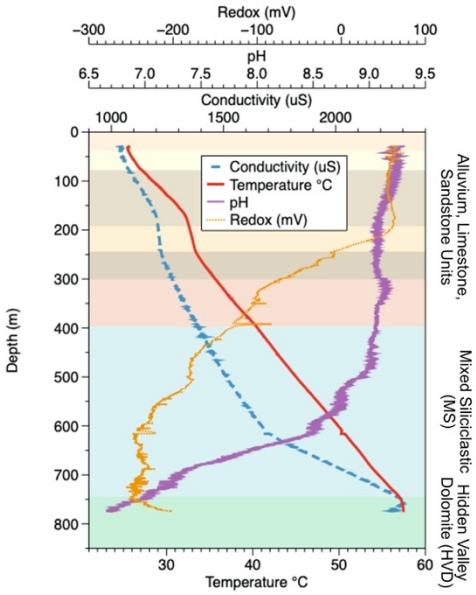

Fig. 1.1: Site location and borehole profile. (Left) BLM-1 is located northeast of Bat Mtn. in the Funeral Mountain Range. Image retrieved from Google Earth. (Right) Geochemical profile of the borehole overlaid with lithological units as described in Friedrich CJ, et al (2012). The borehole itself is cased in steel down to 750 m depth, at which point it is open to the Hidden Valley Dolomite unit. Geochemical data from the groundwater within the borehole, which begins at around 33 m depth from surface, is displayed. Although the borehole was originally drilled to 884 m depth, infilling of soft sediments now limits access to approximately 755 m.

In situ incubations

To characterize the rock-associated microbial community, several sterilized solid substrates of defined or native materials were incubated *in situ* within polytetrafluoroethylene (PTFE) open-ended cartridges (2 cm inner diameter, approximately 18 cm long) screened with 1 mm nylon mesh. Cartridges were filled with pre-characterized substrates, which consisted of either mineral standards or cuttings of the appropriate lithologic units obtained during the drilling process and archived at the USGS Core Library and Data Center (Mercury, NV). Incubated standard substrates included glass wool (Sigma Aldrich #18421), dolomite (Ward's Science #470025-558), pyrite (Ward's Science #470205-736), optically clear calcite (Ward's Science 470025-522), pyrrhotite (Ward's 470025-750), and 3 mm diameter low-carbon steel ball bearings (McMaster-Carr 96455K49) as a proxy for the well casing. Natural lithologies tested

included Hidden Valley Dolomite (HVD), a fine-grained dark-gray dolomite with nodular chert, and mixed siliciclastic lake sediments and tuff (MS). Crushed minerals ranged in size from 2 - 5 mm. *In situ* incubations containing dolomite, HVD, calcite, or MS were always conducted in duplicate (n = 2 cartridges) for each time point. Cartridges were assembled into bundles of three, secured with 200-test Dyneema™ high-strength line (**Fig. 1.8**). Duplicate cartridges were always assembled into separate bundles. Three 5 mm PTFE rods acted as a cage for the bundles. The entire assembly was autoclaved and maintained in a sterile bag until deployment. During the deployment of the cartridges, an A-frame was constructed over the well cap, and the cartridge string was lowered into the well affixed to both 200-test and 500-test Dyneema™ fishing line as a failsafe. At regular intervals (~75-100 m) a series of polyurethane foam blocks (PUR) (Identi-plug™, Fisher Scientific Inc.) were attached to the fishing line with nylon cable ties (McMaster-Carr 70215K96) following (Imachi et al., 2011). The incubation package was suspended in the open hole portion of the borehole at ~752 m depth, within the HVD unit, for periods of 3-6 months before retrieval with 5 total incubations over 18 months (**Table 1.2**). Upon retrieval, cartridges were stored at ambient temperature in oxygen impermeable mylar bags with sterile oxygen scrubbing packets (Oxy-Sorb; Harrisburg, NC) until they could be disassembled and subsampled under sterile conditions in a laboratory anaerobic chamber the following day. Subsamples were frozen at -80°C for DNA analysis or fixed individually in electron microscopy-grade 2% paraformaldehyde or 2.5% glutaraldehyde (Electron Microscopy Sciences; Hatfield, PA) for microscopy. The dates and mineral substrates included for each deployment are provided in **Table 1**.2.

Incubation Number	Date Deployed	Date Recovered	Total Days in situ	Mineral Cartridges	Notes
1	11/3/14	2/5/15	94	Glass Wool, Ward's Calcite, Ward's Dolomite, Hidden Valley Dolomite (HVD), Tuff & Mixed Siliciclastic Lake Sediments (MS), Low-Carbon Steel	
2	2/5/15	8/21/15	197	Glass Wool, Ward's Calcite, Ward's Dolomite, HVD, MS, Low-Carbon Steel	Well-logging and geochemical analysis performed after recovery.
3	8/23/15	11/5/15	74	Glass Wool, Ward's Dolomite, HVD, MS, Low-Carbon Steel, Ward's Pyrite, Ward's Pyrrhotite,	5 Natural Sea Sponges attached to line above minerals.
4	11/5/15	2/4/16	91	Glass Wool, Ward's Calcite, Ward's Dolomite, HVD, MS, Low-Carbon Steel	Only one natural sponge from Inc. 3 recovered. Others were degraded and fell off the line.
5	2/4/16	5/11/16	97	Glass Wool, Ward's Calcite, Ward's Dolomite, HVD, MS, Low-Carbon Steel	

Table 1.2: Contents and timetable of all *in situ* Incubations

Groundwater geochemistry and microbiology

In the period following retrieval of Incubation 2 and prior to deployment of Incubation 3, the borehole was chemically and physically characterized using a QL40-OCEAN Idronaut wellbore logging probe (Mount Sopris Instruments; Denver, CO), operated by the Desert Research Institute. This device consists of calipers which continuously measure and record borehole diameter and a multiprobe (Idronaut, S.R.L; Brugherio, Italy) that concurrently measures temperature, pH, relative oxygen reduction potential (ORP), and conductivity over the entire depth profile. Several liters of water from 579 and 752 m were also collected at this time by successive collection at ambient pressure with gas-tight discrete samplers ("bailers," Comprobe, Inc; Fort Worth, TX) for extensive aqueous geochemical and dissolved gas characterization, with the shallower depth sampled first to prevent mixing the water column. Dissolved metals and ions were quantified by ACZ Laboratories (Steamboat, CO), and organic carbon (DOC), particulate organic carbon (POC), and total organic carbon (TOC) were quantified by Anatek Labs (Spokane, WA), both of which are accredited environmental testing

facilities. The methodologies and standard error values for these analyses are included in **Table 1.8**, with the error values from ACZ Laboratories generated from duplicate analyses of a standard and the error values from Anatek Labs from duplicate sample analyses. Samples from two depths were analyzed (579 mbls and 752 mbls). Sulfide was measured using the methylene blue method with a field detection kit (detection limit ~0.02 mM) (ChemMet, LLC.; Buffalo, New York), following the manufacturer's protocol. We also conducted a qualitative *in situ* test for dissolved sulfide using silver nitrate-coated film, following (Fike et al., 2017). The environmental detection limit of this method has not been well-quantified, but data suggests that 20 minutes of exposure to a 0.9 mM sulfide solution is more than sufficient for visualization. The film was attached to the discrete water sampler, lowered to 752 m depth in the uncased portion of the borehole, left stationary for two minutes, and then recovered to the surface, for a total time of ~45 minutes.

To measure dissolved gases in the well waters (**Table 1.8**), sterilized 160 mL serum bottles were prepared with 50 μL saturated (0.07 g/mL) HgCl solution and capped with butyl rubber stoppers. The HgCl solution was then evaporated away to dryness under constant vacuum, leaving only the 3.5 mg of HgCl behind. Water samples were collected by draining the first ~50 mL fluid fractions from three separate 750 m depth water samples through platinum-cured silicone tubing (Masterflex LS-24) and a 25 G needle into the pre-evacuated serum bottles. The filled vials were stored upside down until their analysis within 8 weeks. Headspace concentrations of H_2, O_2, N_2, CO_2, CO, ethane, and propane were measured using a Shimadzu GC-2014ATF headspace GC equipped with a Haysep 80/100 (5 m) and MS-5A 60/80 (2.5 m) molecular sieve columns and TCD and FID detectors. Samples were measured twice (relative percent differences listed in **Table 1.8**) and were compared against a 1% standard mixture (Restek; Bellefonte, PA). See (Rowe et al., 2017) for details.

Microbial cell counts of the groundwater were performed in two ways (live and fixed) on fluids from 579 mbls and 752 mbls collected August 20th - 21st, 2015. Samples collected from three separate casts for each depth were counted in each way. Live samples were stored at 4°C until they were processed (August 21st, 2015). Samples were also fixed in the field with 1% paraformaldehyde and stored at 4°C until they were processed on August 23rd, 2015. Live samples were counted with a Petroff-Hausser counting chamber, and fixed samples were stained

with 4',6-diamidino-2-phenylindole (DAPI) and counted on fluorescence microscope (Olympus BX51, Olympus Scientific Solutions; Waltham, MA) at 1000× magnification (**Table 1.13**).

Amendment of complex organic matter *in situ*

As part of a separate experiment, five natural sea sponges (Constantia; Hawthorne, CA) were attached to the line directly above the mineral cartridges (~752 mbls) during Incubation 3 as well as higher up on the suspension line at 579 mbls. All sponges from the 752 mbls set, closest to the experimental cartridges, were consumed by microbial activity by the time of recovery; one sponge set at 579 mbls remained at the end of the experiment, however, this sponge was noticeably degraded with a gelatinous consistency. This degraded material was salvaged from the line and frozen for microbial community analysis.

To approximate the amount of organic carbon and nitrogen introduced into the deep aquifer and potentially consumed by in situ microorganisms, the composition of the sponges was estimated. The purchased sea sponges deployed in Incubation 3 belong to the family Dictyoceratida, which have minimal or no calcareous spicules in their skeleton and are primarily composed of spongin, a collagenous halogenated glycoprotein with high thermal stability up to ~360 □ C (Ehrlich et al., 2003; Green et al., 2003; Ehrlich et al., 2010; Norman et al., 2016). Prior to deployment, the sponges were washed, bleached with hydrogen peroxide and rinsed, and sterilized by autoclaving for 30 minutes. Spongin's chemical formula is unknown, but the carbon and nitrogen content has been quantified (carbon = 47.44%, nitrogen = 16.15%) (Gamgee, 1880). Each sponge was on average 0.37 g, and based on the observation that all sponges from the region proximal to the Incubations appeared to be entirely degraded by the time Incubation 3 was recovered, we estimate the total carbon and nitrogen added to the system in the proximity of the mineral cartridges was ~0.88 g and ~0.30 g, respectively.

We developed a rough diffusion-based model to approximate the time for degradation and dispersal of the sponge-derived organic matter. As no vertical flow was detected within the well, we assumed dispersal of the solubilized, degraded sponge substrate occurred through molecular diffusion. This model was simplified to a one-dimensional diffusion in two directions, described by the thin-film (Gaussian) solution to Fick's Second Law:

$$C(x,t) = \frac{N}{2\sqrt{\pi D t}} * e^{\frac{-x^2}{4Dt}}$$

where $C(x,t)$ is the concentration of the molecule of interest at position x and time t, N is the moles of the molecule per unit area at x_0 and t_0 (12.58 mol C/m^2, given well diameter of ~8.6 cm), and D is the diffusion coefficient (Mehrer, 2007). We bounded the time range for the diffusion of the sponge nutrients by setting t_0 as either the moment the sponges are in place or halfway through Incubation 3, which assumes that the sponge organics do not diffuse for the first 37 days and then become completely diffusible after that time ($37 \leq t_0 \leq 74$). Diffusion coefficients, D, are normally only determined empirically, which was not possible here. As an approximation, we used the D for lactose at 55°C: $1.06 * 10^{-9}$ m^2/s (Ribeiro et al., 2006). Based on the cartridge bundle dimensions, which extended from approximately 0.25 to 2.0 m from the sponges, and accounting for the well casing with an average diameter of 0.086 m, we estimate 10.6 L of water surrounded the cartridge bundle. Using all of these parameters, we determined a rough estimate of the total moles of organic carbon released into the water surrounding the cartridges by integrating $C(x)$ over the distance at either t = 37 days or t = 74 days (depending on which t_0 is used) and multiplying by the volume, which translates to values in the range of 160 μmol carbon to 3.01 mmol carbon, respectively. We thus assume that retrieval of the experiment would mix any remaining dissolved carbon species upward into the remaining 733 m of the water column; diffusion downward from these distances over the remaining time scale of our experiments is trivial.

Abiotic H_2 production from steel

Hydrogen production from the steel alloy used in the well casing was verified (**See Fig. 1.15**) by adding one of several Fe-bearing substrates to a defined medium (**Table 1.7**) designed to approximate well fluids at 579 mbls as determined by the geochemistry suite from 8/21/15 described above (**Table 1.8**). The substrates tested for hydrogen production were low-carbon steel analogous to the well casing material (McMaster-Carr 96455K49), 304 stainless steel (McMaster-Carr 9291K43), 316 stainless steel (McMaster-Carr 96415K71), and hematite (Ward's Science 470025). Three replicate vials were measured for each substrate. For steel incubations, three steel ball bearings were added to the sterilized defined medium, and for hematite, 2-5 mm crushed rock was weighed to be volumetrically equivalent to the steel. The headspace of each tube was measured with the same headspace gas chromatograph program as was used to measure the natural samples, as described above.

DNA sequencing:

DNA was extracted from environmental samples with the Qiagen PowerSoil DNA Extraction Kit (Qiagen; Hilden, Germany; 12888) according to the kit protocol except for the following changes during the lysis step. Following the addition of 0.25 - 0.5 g of sample to the lysis tubes, the tubes were flash frozen in liquid nitrogen. The samples were thawed at room temperature, and then the lysis buffer (30 μL C1 buffer) was added and the samples were incubated in a 65°C water bath for 30 minutes, with each sample vortexed for 1 minute every 10 minutes. The samples were then placed in a bead beater (FastPrep FP120, Thermo Fisher Scientific; Waltham, MA) at 5.5 m/s speed for 45 seconds. The samples were then centrifuged at 10,000 × *g* for 30 s and processed according to the rest of the manufacturer's instructions. To keep extraction conditions consistent, raw water samples were extracted with the same kit by adding 250 μL of Inyo-BLM-1 water to the PowerSoil lysis tubes. Filtered water samples consist of 250 mL of raw water passed through a 0.22 μm PES filter (UX-06730-43, Thermo Scientific; Waltham, MA). ~0.25 g of this filter was then processed as above.

Microbial diversity was assessed by Illumina iTAG sequencing of the V4 region of the 16S rRNA gene, using a protocol recommended by the Earth Microbiome project (Caporaso et al., 2012) and sequenced with Illumina TAG sequencing by Laragen, Inc (Los Angeles, CA) as previously described (Caporaso et al., 2012; Case et al., 2015). The V4 region of the 16S rRNA gene was amplified using degenerate 515F and 806R primer pairs (5'-GTGCCAGCMGCCGCGGTAA-3' and 5'-GGACTACHVGGGTWTCTAAT-3'). Each sample was amplified in duplicate. Each reaction was 15 μL total: 7.5 μL Q5 Hot Start High-Fidelity 2x Master Mix (New England BioLabs, Inc.), 5 μL DNAse-free water, 0.75 μL of each primer at 10 μM, and 1 μL of gDNA extract (~0.5 ng/μL) from the sample. Reations were held at 98°C for 2 minutes to denature the DNA, with amplification proceeding for 30 cycles at 98 °C for 10 s, 54°C for 20 s, 72°C for 20 s; a final extension of 72°C for 2 minutes was added for complete amplification. These PCR products are checked for purity via gel electrophoresis and the DNA concentration quantified by Qubit HS (Bio-Rad, Inc.) before they are barcoded for sequencing. Barcoding primers include the original primer sequence as well as linkers, adapters, and on the reverse primer, a unique barcode denoted with X: 515f-bc: 5'-AATGATACGGCGACCACCGAGATCTACACTATGGTAATTGTGTGCCAGCMGCC

GCGGTAA-3'; 806r-bc:5'-CAAGCAGAAGACGGCATACGAGAT-XXXXXXXXXXXX-AGTCAGTCAGCCGGACTACHVGGGTWTCTAAT. The reaction used 5 μL of the 16s rRNA DNA product, 12.5 μL of Q5 Host Start Master Mix, 1.25 μL of 10 μM forward primer, 5 μL of 2.5 μM reverse primer, and 1.25 μL DNAse-free water. Reaction temperatures were the same as above.

Extraction controls and no-template controls were included in every sequencing run; controls were amplified with 45 reaction cycles in the initial PCR reaction to produce a quantifiable PCR product. Autoclaved control minerals that were not incubated *in situ* were also extracted and sequenced after 45 cycles of amplification (control minerals amplified 30 times did not produce a detectable gel electrophoresis band) to control for DNA that may have survived sterilization. **Fig. 1.9** is a comparison of mineral controls versus incubated minerals. Sequencing sample metadata is listed in **Table 1.17,** and the resulting OTU table with the associated sequence and taxonomic identification is available at the NCBI SRA database with accession number PRJNA605006.

Illumina amplicon sequence analysis

In-house amplicon processing was completed with QIIME 1.8.0 and included joining paired-ends, quality trimming, 99% OTU clustering, singleton removal, 0.01% relative abundance threshold removal (Caporaso et al., 2010). Remaining OTUs were then manually checked against sequenced extraction and no-template controls and non-incubated mineral controls to remove contaminating sequences. OTUs with relative abundance ≥ 0.05% in the controls were removed from the dataset. A total of 118 OTUs were removed during this step, leaving 520 OTUs remaining after all filtering steps. The average number of reads per sample remaining after quality-score filtering and removal of singletons, threshold filtering, and manual contaminant filtering was 23,742, with a range of 5,287 – 47,225. The Shannon diversity index and Chao1 richness estimate were computed for each sample and are listed in **Table 1.17**. Although some studies examining high-throughput sequencing data rarefy each sample to the lowest sequence sample, we chose not to rarefy due to several recent studies which indicate this transformation is not appropriate and can impede detection of differential abundance (McMurdie and Holmes, 2014; Weiss et al., 2017). These studies indicate that transforming sequence counts into relative abundance is more effective at detecting true differential

abundance and does not require discarding valid data. Taxonomic assignments for each OTU were generated by comparing against the Silva 138 database (90% cutoff). Further statistical analyses, including non-metric multidimensional scaling (NMDS), analysis of similarity (ANOSIM), similarity percentage (SIMPER), and one-way analysis of variance (ANOVA) were conducted in R (R Core Team, 2014) with the *vegan* ecological statistics package . NMDS analyses were conducted after performing a fourth root transformation to the relative abundance data, following studies indicating that this is a simple but effective way to evaluate differential abundance in microbial communities (McMurdie and Holmes, 2014; Weiss et al., 2017). These analyses construct *de novo* ordinations based on ranked dissimilarities, and the fit of the ordination is measured by the "stress." In general, stress values below 0.2 are acceptable, and all NMDS ordinations presented here have stress < 0.2. In our ANOSIM tests, p-values < 0.05 were considered significant. ANOSIM R values indicate the strength of dissimilarity between groups from 0 to a maximum of 1. SIMPER tests were applied in R to identify specific OTUs with different relative abundances between sample groups, such as between mineral types or between individual incubations. OTUs identified by SIMPER that contributed most to sample differentiation were included for presentation, with the significance of the differential abundance of individual OTUs assessed by ANOVA (**Fig. 1.6**); these OTUs showed up most frequently in the top 10 contributors to the variance between sampling groups and the significance of the differential abundance of these OTUs was assessed by ANOVA. Venn diagrams of community overlap (**Fig. 1.16**) were made with Venny (Oliveros, 2007-2015).

Imaging of *in situ* incubated minerals

All mineral samples were imaged both pre- and post-incubation to record any incubation-associated mineralogical changes. 2.5% glutaraldehyde-fixed mineral samples for Scanning Electron Microscopy (SEM) were dehydrated with an ethanol dehydration series (25%, 50%, 75% 90% 100%; each step 30 minutes), then critical-point dried with liquid CO_2 to preserve cell morphology. Briefly, this involves washing out the ethanol with liquid CO_2 in a pressure chamber kept cold with an ice water bath, then raising the temperature to 31°C and adjusting the internal pressure to 74 bar (the critical point of CO_2), and then slowly bleeding away the remaining CO_2. The samples were mounted on aluminum stubs with carbon tape and sputter-coated with 10 nm of 80:20 Platinum:Palladium to minimize charging effects. Scanning electron microscopy was carried out on a Hitachi SU3500 microscope (Hitachi High-

Technologies; Tokyo, Japan) equipped with an Oxford X-Max 150 Energy Dispersive X-ray Spectroscopy (EDX) unit (Oxford Instruments; Abingdon, United Kingdom).

Mineral composition

The calcite and dolomite standards, along with the HVD and MS natural samples, were first powdered manually with an aluminum oxide mortar and pestle. The resulting powder was then analyzed by X-Ray Fluorescence (XRF) with an INAM Expert 3L tabletop XRF under helium purge with a Ti target using INAM's built-in fundamental parameters software. Data was acquired over 60 seconds with 15 kV excitation energy for light elements, followed by an additional 60 seconds with 45 kV excitation voltage for heavier elements. The resulting comparative elemental analyses (as the corresponding elemental oxides) are listed in **Table 1.14.**

Results

Well logging and geochemistry

Well logging and geochemical analyses of Inyo-BLM 1 in August, 2015 were consistent with well logging data collected in 2011. Over the 18-month period of our experiments, the water level in the borehole was 28.7 m ± 0.03 mbls (USGS, 2018). The temperature increased by 4.8°C per 100 m from 25.7°C at the surface to 57°C at the bottom of the well (**Fig. 1.1**). The pH of the fluids down to 500 mbls was slightly alkaline (9.0-9.2), transitioning to more acidic conditions (6.9) in the uncased portion of the well (depth > 750 mbls). Water samples were collected at 752 mbls (in the uncased portion) and at 579 mbls (**Table 1.8**). Both samples showed brackish conditions (9.7 and 9.4 mM Na^+ and 1.5 and 1.4 mM Cl^-, respectively [222, 215, 52.4, 49.2 ppm]) (**Table 1.8**). Ferrous iron concentrations increased by 60% (0.90 to 1.4 μM; 0.05 to 0.08 ppm) and sulfate levels were three times higher (reaching 1.6 μM) in the uncased portion of the hole at 752 mbls relative to 579 mbls (**Table 1.8**). Calcium, magnesium, and silica concentrations also increased below the casing. Sulfide was not detected by an onsite Cline assay, and a qualitative *in situ* test for dissolved sulfide using the silver nitrate-coated film method also indicated sulfide concentrations were below detection (Fike et al., 2017). Continuous ORP data obtained with the Idronaut well-logging tool showed a dramatic drop in potential at about 200 mbls (or 167 m below water level), indicative of anoxia (**Fig. 1.1**). Within the open hole portion at the bottom, the ORP drifts towards positive values, but these types of probes are sensitive to

flocculent material in the water. We cannot determine whether the drift is due to an actual increase in the ORP or the presence of suspended particles at depth. Upon recovery of Incubation 2 on 8/21/15, average planktonic cell counts at 752 mbls were 4.1×10^6 cells per mL $\pm$ 2.8×10^6, the large standard deviation owing to the tendency of cells to form small clumps. (**Table 1.13**).

H_2 production by anaerobic corrosion of steel.

Analyses of dissolved gases in water samples obtained from 579 mbls and 752 mbls in Inyo-BLM 1 immediately preceding the carbon amendment (start of Incubation 3) revealed up to 30-fold more dissolved hydrogen in the cased section of the well relative to the open section (200 vs 7 μM). The increase in hydrogen co-occurred with a 10-fold increase in dissolved methane (100 vs 10 μM) (**Table 1.8**). By contrast, the fluids at 752 mbls contained elevated dissolved CO_2, consistent with a carbonate-hosted aquifer.

To test whether the steel casing could have produced hydrogen (via the Schikorr reaction), we incubated three alloys of steel as well as hematite (Fe_2O_3) in sterile media mimicking the water chemistry in the borehole (Schikorr, 1929; Linnenbom, 1958; Ma et al., 2013). These experiments verified that low-carbon steel similar to that used in the well casing (and used in our experimental cartridges) produced significantly more H_2 than stainless steel alloys or hematite (**Fig. 1.15**). Within 13 days, the low-carbon steel produced 14.3 μmol H_2, approximately 70-fold more hydrogen than the 304 stainless steel, and 700-fold more hydrogen than the 316 stainless steel alloy or hematite, which produced barely detectable hydrogen peaks during chromatography analysis.

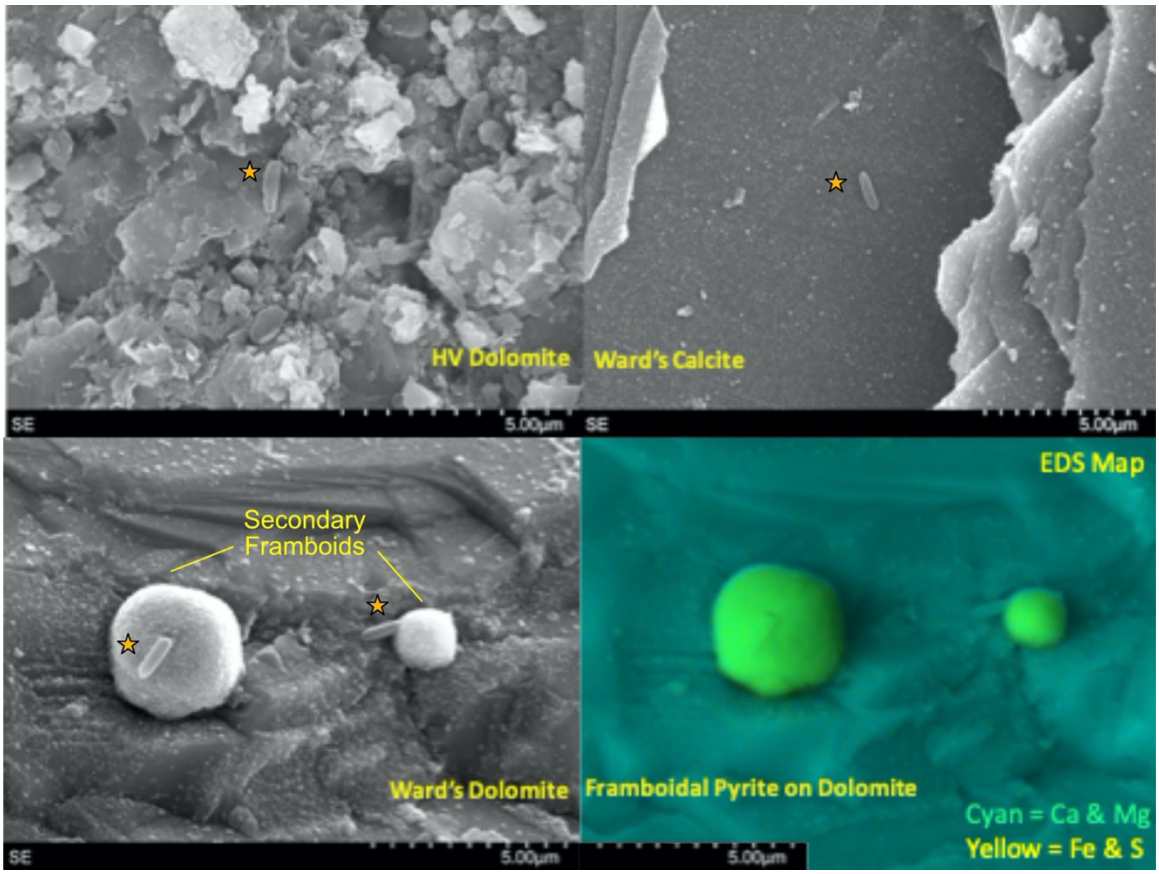

Fig. 1.3: Scanning Electron Micrograph and Energy Dispersive X-Ray Spectroscopy (EDX) overlays of carbonates from Inc. 1, with microorganisms marked with orange stars. (Top Left) Natural dolomite sample (HVD) with putative cell in center. The texture of the rock presented difficulties in distinguishing cells from surroundings. (Top Right) Although calcite standard was easiest to image, few cells and no iron sulfide framboids were visible. (Bottom Left) Cells attached to secondary framboidal structures. (Bottom right) EDX map of bottom left panel which confirms that secondary framboids are iron sulfide.

Mineralogic analysis and *in situ* secondary iron sulfide mineral formation

Unincubated calcite, dolomite, Hidden Valley dolomite (HVD), and mixed siliciclastic (MS) substrates were analyzed by XRF spectroscopy to compare their compositions (**Table 1.14**).The elemental composition of the substrates was consistent with their mineralogical identification and in the case of the natural HVD and MS samples, with previous geological descriptions (Fridrich et al., 2012). The HVD and dolomite standard differed in their trace element composition, with the dolomite standard higher in iron and manganese and the HVD higher in silicon. The MS sample was consistent with mixture of potassium and calcium

aluminosilicates, with a wide array of trace elements detected, including significant amounts of iron, manganese, and titanium.

All mineral substrates were imaged by scanning electron microscopy (SEM) pre- and post-incubation in Inyo-BLM 1. Apart from microbial attachment, the majority of incubated minerals displayed no obvious mineralogical alteration over the course of their incubation. Notable exceptions included the two dolomitic rocks (dolomite standard and native Hidden Valley Dolomite [HVD]) recovered from the three-month long Incubation 1 (2/5/15), which showed widespread precipitation of 1-5 μm diameter secondary minerals with framboidal structure (~10 per 100 μm square viewing area); energy dispersive X-ray spectroscopy (EDX) characterized these secondary minerals as iron sulfides (**Fig. 1.3**). While large anhedral pyrite crystals were observed in both the standard dolomite and HVD samples prior to deployment, nothing resembling the framboidal precipitates were observed on any samples prior to deployment, indicating they formed *in situ*. These secondary minerals were typically associated with 1-3 microbial cells. Sulfide framboid generation was only detected in the first set of incubations, prior to the organic matter amendment experiment. Sulfide mineral formation was also observed on minerals from the six-month long Incubation 2 (recovered 8/21/15), in this case producing scattered zinc sulfide spheroids, rather than iron sulfide framboids, but spheroid-attached cells were not observed. In both cases, secondary mineral formation was only detected on the dolomitic minerals (HVD and Ward's dolomite, $n = 8$) across two separate incubations, and not on any glass wool, mixed siliciclastic (MS), low-carbon steel, or calcite minerals incubated in parallel ($n = 14$). Incubations 1 and 2 occurred prior to the organic matter addition in Incubation 3 on 8/23/15, and no further secondary mineral formation was observed via SEM following the organic matter addition.

Microbial community analyses

After removing potential contaminants found in the sequencing controls, analysis of the Illumina 16S rRNA gene amplicons (iTag) of all samples taken from the site, including incubated mineral substrates from cartridges suspended at 752 mbls, polyurethane foam blocks (PUR) from the suspension line, and water from 579 mbls and 752 mbls, revealed a system dominated by Firmicutes, Nitrospira, Alpha- and Betaproteobacteria, and Candidate Division KB-1 (also known as Candidate Division Acetothermia), with a moderate relative abundance of Chloroflexi,

Epsilonproteobacteria, and Euryarchaeota, including two putative methanogens of the Methanobacteriales and an OTU related to the South African Gold Mine Group of Thermoplasmata. The samples demonstrated low diversity overall; the maximum observed Shannon Index was 4.03, and the maximum Chao1 richness was 360. Reflecting the low diversity, the dominant OTU in 60 of the 71 samples represented >15% of the total community for that sample. Across all samples and incubations, two broad groups appeared when visualizing the microbial community by NMDS: one group consisting of water (including unfiltered and filtered water) and the other consisting of solid substrates, including minerals and glass (**Fig. 1.12**). PUR samples occupied ordination space between water samples and mineral samples but contained no unique OTUs. Instead, the PUR-colonized community represented a mixture of planktonic and surface-attached microorganisms (**Fig. 1.16**).

ANOSIM analyses of the samples were conducted to assess which parameters correlated most strongly with community variance; ANOSIM R values range from 0-1 with increasing correlation. When examined across the entire dataset, the most important parameter in the variation between samples was the Incubation number ($R = 0.4535$, p-value = 0.001), with type of substrate showing secondary importance for community differences ($R = 0.2667$, p-value = 0.001). Interestingly, carbonate samples, which included calcite, dolomite, and HVD, grouped together in all but one incubation (Incubation 1). Across all incubations, the communities colonizing carbonate minerals were not significantly different from each other (p-value = 0.558). We also assessed the difference between filtered and unfiltered water samples and found no significant difference (p-value = 0.2). Although we had originally hypothesized that the community colonizing the PUR samples would group with the water samples, these samples were significantly different from the water samples (p-value = 0.001). Based on the ANOSIM analyses and the similarity between the sample types, we therefore grouped the calcite, HVD, and dolomite samples into one "carbonate" bin, and the water samples (filtered and unfiltered) into one "background" bin, which increased the contribution of substrate to the variance ($R = 0.3235$, p-value = 0.001). The apparent dominance of the incubation reference number in describing the community structure was largely due to the organic matter amendment during Incubation 3. On an individual Incubation basis, colonizing substrate (e.g. carbonate, MS, silica glass wool) was generally a strong determinant of variability (**Fig. 1.5**). The ANOSIM R statistic and significance values for mineralogical variation when comparing within individual

Incubations were as follows: Incubation 1 (R = 0.9733, p = 0.005), Incubation 2 (R = 0.5774, p = 0.006), Incubation 3 (not significant, p = 0.053), Incubation 4 (R = 0.6406, p = 0.026), Incubation 5 (R = 0.3900, p = 0.026). ANOSIM analysis comparing Incubations 1 and 2 (which occurred prior to organic amendment) revealed strong effect of substrate type (using the carbonate bin) over Incubation (R = 0.7669, p-value = 0.001 vs. R = 0.2167, p-value = 0.006). When carbonate minerals in these two incubations were treated as independent, the effect is still significant but less impactful (R = 0.6764, p-value = 0.001).

To understand which OTUs were most affected by mineralogical variation, we focused on a subset of data least affected by the organic matter amendment (Incubations 1, 2, 5). After confirming that the substrate bins were still a significant contributor to the variance in these three incubations (R= 0.3871, p-value = 0.001), we used pairwise SIMPER to identify OTUs contributing most toward the variance between substrate bins (**Fig. 1.6**). The patterns in colonization of these OTUs indicate whether they are more commonly found in water samples or on one of the different lithological substrates. For example, the Candidate Division KB-1 OTU was the most abundant OTU recovered from water and PUR samples (17.3% relative abundance on average) and was moderately abundant in glass wool cartridges (8.9%), but consistently represented <5% of the community on mineral samples. Other OTUs that were enriched in planktonic samples included an *Nitrospiraceae* OTU (14.1%) and an OTU matching *Desulforudis* sp., a putative hydrogenotrophic, sulfate-reducing Firmicute discovered in deep strata accessed by a South African mine (7.7% abundance, 100% sequence ID) (Chivian et al., 2008). Several OTUs which were abundant in water samples were also found on the low-carbon steel, including the OTU matching *Desulforudis* (5% average, 15.5% max abundance). Other OTUs appear to show a preference for solid or mineral substrates. For example, an OTU identified as a *Geobacillus* sp. consistently represented 1-5% of the community on glass, steel and mineral samples (up to 19% on a glass sample), but was only detected in 1 of 17 water or PUR samples at 0.08% relative abundance.

In general, analysis of relative abundance values can be difficult; values can change significantly depending on total community composition. It is important, therefore, to apply a transformation to these values to minimize the effect of small number variance (e.g. fourth-root transform, as we have done) and to contextualize relative abundance shifts by examining OTU overlap between different sample bins. Overall, across all incubations and samples, 75% of the

OTUs identified on lithological substrates (carbonate, mixed siliciclastic [MS], silica glass wool, steel) were detected at least once on each substrate (**Fig. 1.16**). Carbonate and MS shared the most OTUs unique to two categories (3.2%) and carbonate, MS, and silica glass wool shared the most unique to three categories (8.4%). Most of the variance, therefore, between substrate types was caused by differential abundance rather than strict OTU presence or absence.

We also used these techniques to attempt to identify which, if any, OTUs were correlated with the presence of the framboidal iron sulfides found on dolomite and HVD samples in Incubation 1. By subsetting our data to Incubations 1 and 2, which contained the same substrates and differed only in length of incubation, we attempted to identify microbial community shifts concurrent with iron sulfur framboid precipitation. Variance analysis (ANOSIM) confirmed that the community colonizing dolomite samples (HVD and dolomite standard) significantly differed between Incubations 1 and 2 ($R = 0.8125$, $p = 0.04$) and a SIMPER analysis identified the top two taxa responsible for driving the difference between dolomite samples in Incubation 1 and 2 as *Sulfurovum* sp., an *Epsilonproteobacteria*, and *Desulfotomaculum* sp., a Firmicute, which were detected in Incubation 1 at high abundances but in Incubation 2 were either completely absent (*Sulfurovum*) or at much lower relative abundance (*Desulfotomaculum*). Cultured representatives of the two genera are sulfide-oxidizers and sulfate-reducers, respectively.

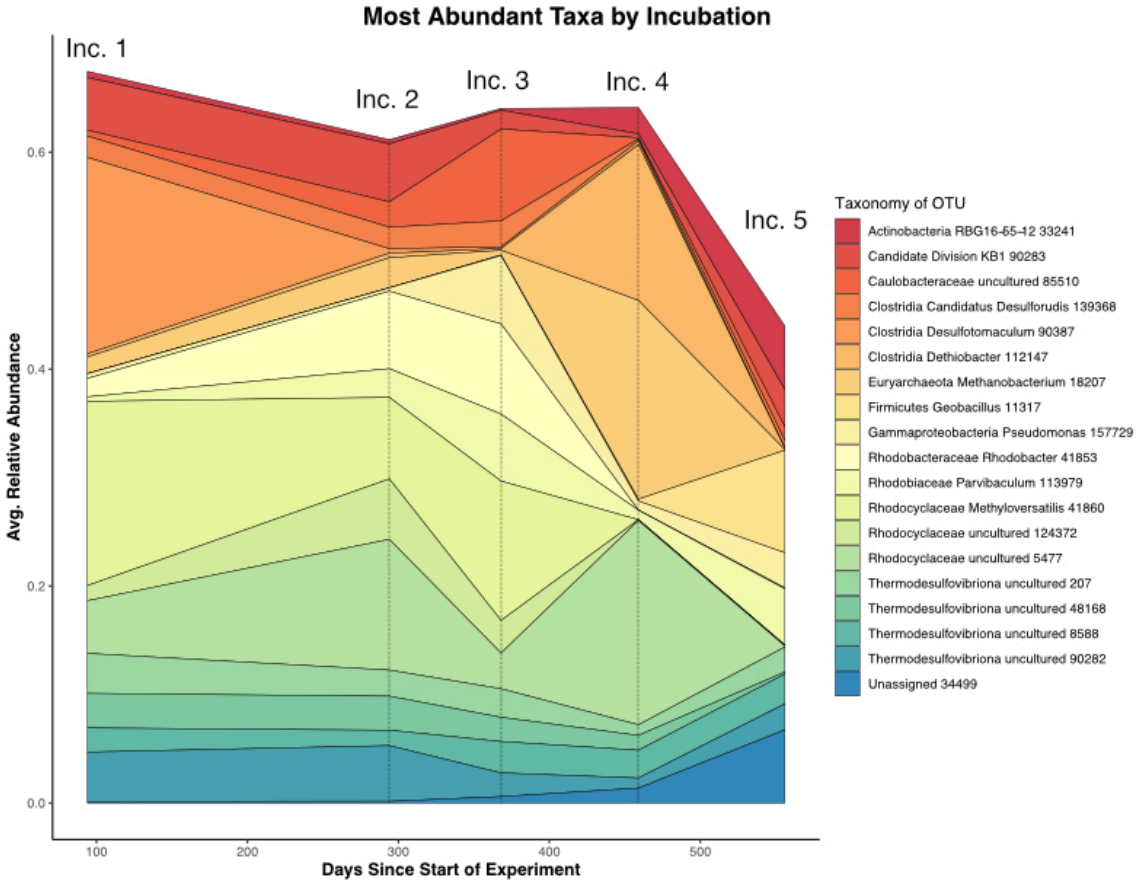

Fig. 1.4: Average relative abundance of most abundant taxa by days since the start of the experiment, with individual incubation collection points noted above.. The relative abundance as measured by 16S rRNA iTag data from mineral substrates common to all incubations was averaged at each time point. The data demonstrate the large relative abundance decrease in the *Desulfotomaculum* OTU co-occurent with the loss of framboidal iron sulfides in Incubation 2 as well as the large bloom in a *Methanobacter* OTU in Incubation 4 (6 months after organic substrate amendment). Incubation 5 displays a general increase in the proportion of rare taxa relative to the whole.

Community response to organic substrate amendment

Upon retrieval of the Incubation 3 deployment, organic sponges from the 752 mbls region were missing, although the zip ties used to attach them were still on the line. We assume the 752 mbls sponges were degraded during the incubation as a significantly degraded, gelatinous sponge was still attached to the line from the 579 mbls set. The close relationship between Incubations 1 and 2 and the dramatic community shift in Incubation 3 demonstrated the profound impact that the organic matter amendment had on the microbial community. Biological replicates of substrates in 4 of the 5 incubations (1, 2, 4, and 5) were closely clustered

in the NMDS, but replicates from Incubation 3, which were incubated concurrent with the organic matter amendment, displayed the greatest separation from each other as well as from samples from the other incubations (**Fig. 1.5**). Changes in relative abundance of the most abundant OTUs across all incubations are summarized in **Fig. 1.4**.

The microbial assemblage colonizing the degraded sea sponges from the organic matter amendment experiment was distinct from that recovered on the mineral substrates during the same incubation. The top three OTUs recovered from the organic sponges are most closely related to *Fervidobacterium,* a Thermotogae (20.3% of recovered sequences), *Anaerolinea,* a Chloroflexi (19.0%), and *Thermodesulfovibrio,* a Nitrospiraceae (18.6%). These organisms dominated the sponge assemblage, but were only rare OTUs in samples from previous mineral incubations and water samples. We did observe these OTUs in the microbial assemblage on minerals adjacent to the organic sponge in Incubation 3, but at much lower relative abundance. For example, the next highest relative abundance of any of these sponge-dominating OTUs on any mineral substrate from this *in situ* deployment was an OTU related to *Anaerolinea* in the pyrrhotite cartridge (5.3% relative abundance). These findings indicate that a small subset of the microbial community was stimulated by spongin protein amendment but that shifts in the mineral-hosted community cannot be solely attributed to cells directly transferred from the organic matter-associated community. Mineral substrate assemblages from Incubation 3 displayed a relative increase in a few key taxa, including a putative carbon-degrading Rhodocyclales matching *Methyloversatilis* sp. (8.1% to 13.6%, 100% nucleotide identity) and an OTU identified as an uncultured *Caulobacteraceae* (2.3% to 8.5%), while the relative abundance of taxa commonly detected on minerals in previous incubations showed a marked decrease. These *Methyloversatilis* and *Caulobacteraceae* OTUs were undetected and 0.00013% of the community on the organic sponge, respectively, further suggesting their presence on the neighboring mineral substrates in Incubation 3 was not simply due to cross-contamination from the organic sponge associated microbial assemblage.

The subsequent set of mineral cartridges in Incubation 4, recovered six months after the organic carbon amendment, had very few sequences of *Methyloversatilis* sp., with all but three cartridges (one dolomite, one HVD, one MS) containing any detectable sequences from the *Methyloversatilis* OTU. Instead, a shift in community composition featuring methanogens was observed, with an OTU annotated as a *Methanobacter* sp. representing nearly 15% of the

recovered diversity across all samples. The *Methanobacter* OTU, along with other archaea (*Methanothermobacter*, South African Gold Mine group Thermoplasmata), was detected in previous incubations but at much lower relative abundance (less than 2%) (**Fig. 1.4**).

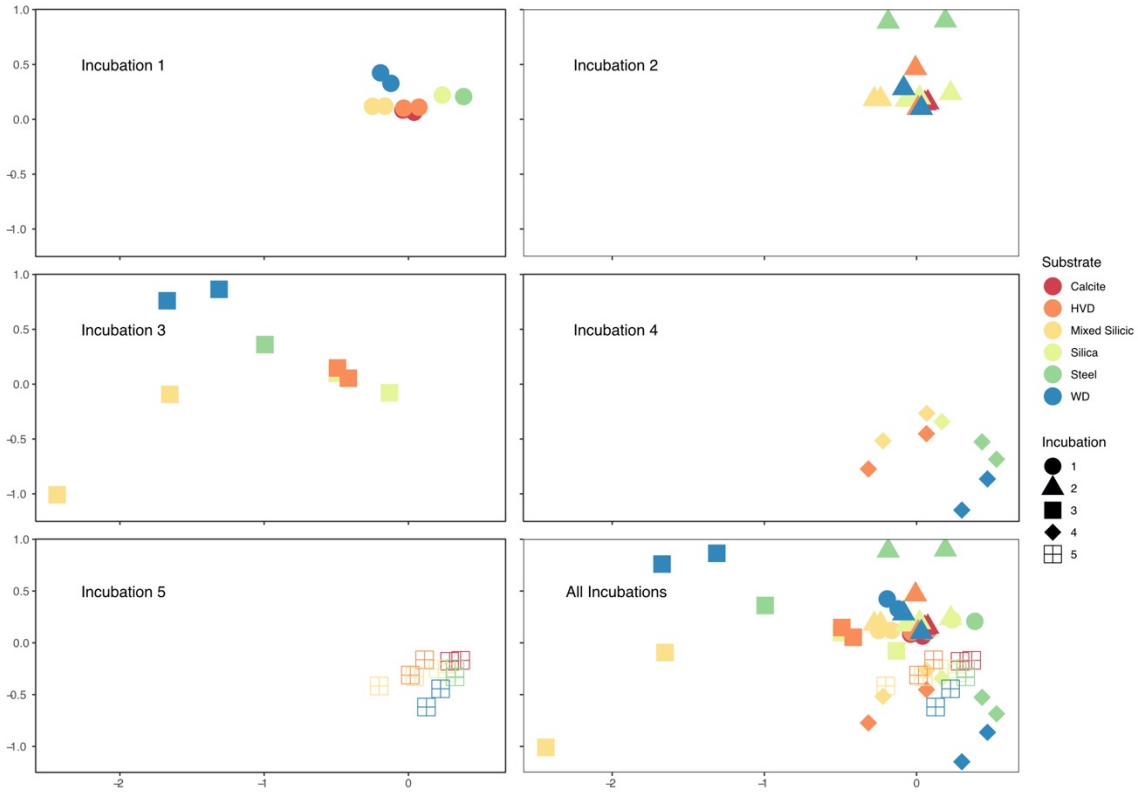

Fig. 1.5: Faceted NMDS of microbial relative abundance of solid substrates used in each Incubation with combined NMDS bottom right. Each point on the plot represents an individual cartridge from an incubation; two points of the same color and shape are biological replicates of substrates from the same incubation but incubated in separated cartridges *in* situ. Incubations 1 & 2 are the most closely related and both occurred before the addition of the organic carbon substrate. Incubation 3 represents the first samples obtained after the carbon amendment and displays the widest variation amongst biological replicates and among mineral substrates. Incubation 4 is dominated by methanogenic Archaea which pulls the samples into a cluster towards the left, and by Incubation 5, the samples are again tightly clustered and close to their starting position on the NMDS axes.

The microbial assemblage recovered from Incubation 5, nine months after the organic matter experiment, appeared to more closely resemble the original community composition in Incubations 1 and 2. Groups such as the Candidate Division KB-1, *Nitrospira* sp., and *Sulfurovum*, which decreased in their relative abundance during Incubations 3 and 4 likely due to a

proportional increase in fast-growing microorganisms responding to organic matter amendment, returned to their original relative abundance in Incubation 5. Other OTUs became more prominent, and Incubation 5 samples had a comparatively higher diversity with higher Shannon indices (**Table 1.17**). One OTU recovered from this incubation (4% average rel. abundance) matched sequences with no known phylum according to our cutoff (90% ID). This OTU had 99% similarity to a bacterial sequence recovered from hot springs (NCBI BLAST accession number KM740594.1), and was distantly related to Aminicenantia (87% ID) in the Silva database but was below our identity cutoff (National Library of Medicine (US), 1988). Other microbial lineages remained at low levels in Incubation 5, including members of the *Desulfotomaculum,* which was closely associated with the presence of iron-sulfide framboids in Incubation 1. The *Sulfurovum* OTU, which was also implicated in framboid formation, did recover to roughly the same relative abundance as Incubation 1. Notably, the difference in *Desulfotomaculum* was identified in SIMPER analyses as the primary factor distinguishing communities in Incubation 1 and 5. Apart from these differences, however, the net result of these analyses indicated that much of the community composition within this borehole environment was reestablished less than a year after organic matter perturbation.

Discussion

Comparison of Inyo-BLM-1 to other deep biosphere environments

Although the timescale for mineral substrate colonization in the deep biosphere is not well constrained, we infer that the substrate-attached microbial assemblages we detected in our experiments were representative of natural assemblages and likely not introduced contaminants. Prior to our experiments, the anoxic and 57°C Inyo-BLM 1 borehole sat undisturbed for three years, creating conditions that are generally unfavorable to the persistence of contaminating microbial organisms (Pedersen et al., 1997). A previous study in a deep South African mine borehole demonstrated that natural microbial assemblages and the *in situ* condition of anoxia returned within two months of perturbation (Moser et al., 2003). Additionally, the microorganisms observed in Inyo-BLM 1 were remarkably similar to 16S rRNA gene clone library observations originally reported in this South African gold mine (Moser et al., 2005). Conditions at this site were similar to Inyo-BLM 1, characterized by warm (54°C), anoxic, paleometeoric waters upwelling from 4-5 km depth into a metabasaltic unit underlying dolomite

in South Africa. Clone libraries in that study detected four main taxa in the community: *Desulfotomaculum, Comamonadaceae* (Betaproteobacteria), *Candidatus* Desulforudis audaxviator, and *Methanobacterium*. Inyo-BLM 1 contains OTUs identified as all of these groups at high relative abundance, including *Methanobacterium* as the dominant archaeon. Since their identification in 2008, the putative sulfate-reducing hydrogenotrophs *Desulforudis* have been reported from an array of deep biosphere environments (Chivian et al., 2008; Tiago and Verissimo, 2013; Jungbluth et al., 2017). Interestingly, many of these studies, including the original description, were performed in boreholes with steel casings, as is the case for Inyo-BLM 1. It is likely that steel casings, especially low-carbon steel, may be contributing to local H_2 production that enriched these organisms. Beyond the taxa it shares with other deep biosphere studies, Inyo-BLM 1 contains a number of unusual bacterial lineages, including representatives from Candidate Divisions KB-1 and Aminicenantes (formerly OP8). Candidate Division Aminicenantes was initially described from the Obsidian Pool thermal spring in Yellowstone National Park and have since been detected in a diverse marine and terrestrial subsurface environments (Hugenholtz et al., 1998). Although no cultured representatives are available, recent metagenomic analysis of Aminicenantes recovered from a Siberian deep thermal aquifer indicated a potential for complex carbohydrate and proteinaceous substrate fermentation as well as heterotrophic nitrite respiration (Kadnikov et al., 2019). Originally discovered in the Kebrit deep brine basin in the Red Sea (Eder et al., 1999), Candidate Division KB-1 bacteria have since been identified in a number of other hypersaline environments, including other deep hypersaline brine lenses, salterns, and hypersaline lakes and sediments (Nigro et al., 2016). Today, the Inyo-BLM 1, and the Lower Carbonate Aquifer that feeds it, are low salinity, but the Amargosa Desert region was home to evaporitic, fluvial lakes in the Paleozoic (Khoury et al., 1982) and it is interesting to consider whether these as yet uncultured bacteria may have adapted over time to the freshening groundwater environment.

Substrate specificity of microorganisms

The physical and chemical environment in the terrestrial deep biosphere are often extremely heterogeneous both in terms of the mineralogy as well as the nature of the permeating fluids. While fluid sampling is common in deep rock-hosted biosphere studies through legacy boreholes and mines, the ability to study mineral-associated microbial assemblages in the deep subsurface is more challenging (Moser et al., 2003; MacLean et al., 2007; Davidson et al., 2011;

Ino et al., 2016). Previous work in the shallow subsurface has demonstrated that planktonic and mineral-attached communities are distinct, with some species significantly more abundant in one fraction or the other (Flynn et al., 2013). Here, we attempted to understand the distinction between the planktonic and mineral-attached communities as well as the role that mineral heterogeneity plays on microbial colonization by incubating a set of minerals representing the *in situ* lithologies at Inyo-BLM 1 alongside mineral standards and comparing the attached microbial assemblages to the planktonic community recovered from the aqueous phase. Similar types of mineral colonization experiments in both terrestrial and marine environments have pointed to local mineralogy as a primary factor linked to *in situ* microbial diversity (Roberts, 2004; Edwards et al., 2005; Orcutt et al., 2010; Toner et al., 2013). In some cases, microbial attachment is associated with direct mineral respiration, as occurs with iron-reducing bacteria (Lovley et al., 1989; Caccavo and Das, 2002), and in other circumstances, attachment may be controlled by the surface chemistry or electrostatic interactions between cell membranes and the mineral surface (Hermansson, 1999; Yee et al., 2000; Tuson and Weibel, 2013).

Nearly all of the OTUs we recovered from Inyo-BLM 1 were recovered from the solid substrates; 27.2% of the OTUs were exclusively detected on solid substrates, whereas only 0.4% were unique to the water samples (**Fig. 1.16**). Of the OTUs that were the most common contributors to substrate differentiation, a Candidate Division KB-1 OTU (bin90283) was abundant both in the water samples and on the PUR samples, and a *Geobacillus* OTU (bin11317) was only abundant on solid substrates (**Fig. 1.6**). Notably, the abundance of *Geobacillus* was not significantly different as assessed by ANOVA, because many samples, even the solid substrates, had no detectable sequences from this lineage. The variance on solid substrates, however, was much higher, with abundance on carbonate samples ranging from 0 – 21.9%. An F-test for significantly different variance confirmed that all of the solid substrates (carbonates, MS, silica, and steel) all had significantly higher variance than water samples for the relative abundance of this OTU, implying that the *Geobacillus* species only rarely colonized the minerals in the cartridges, but that when this occurred, these organisms frequently occurred at relatively high abundance.

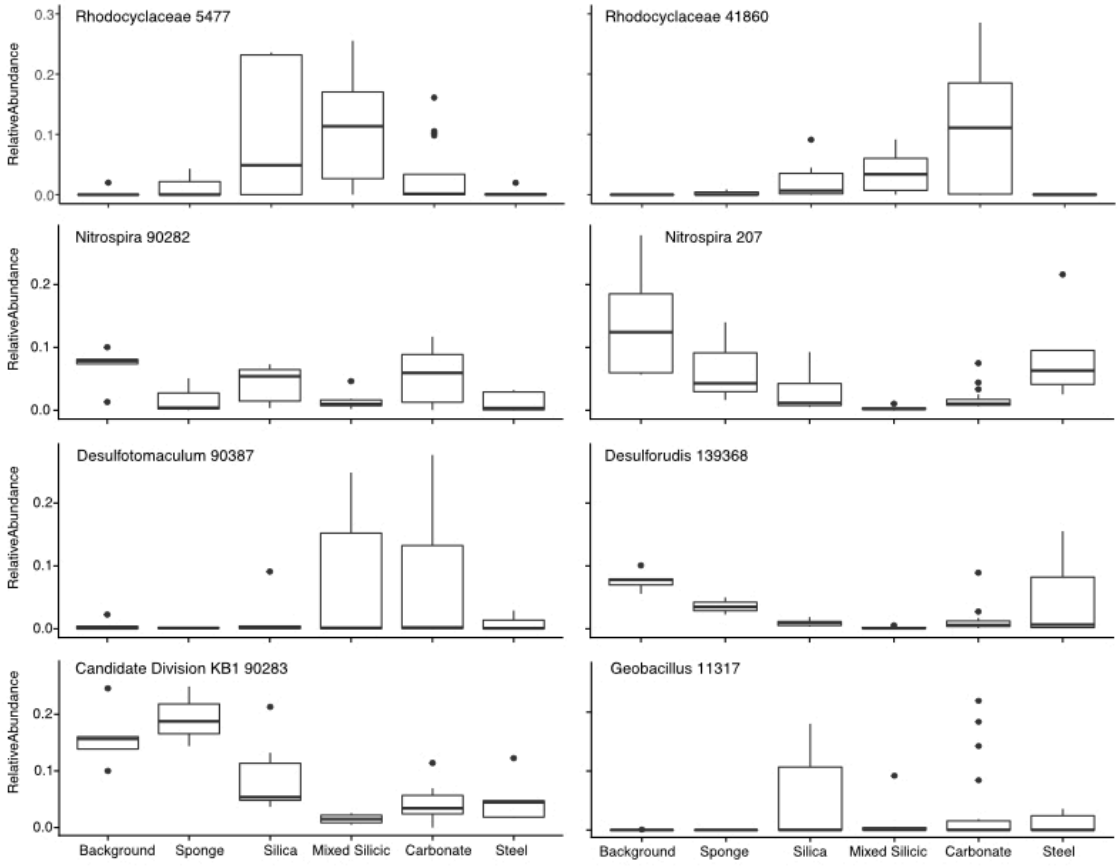

Fig. 1.6: Tukey-style box and whiskers plot showing the average relative abundance of SIMPER-identified important taxa by substrate group. For each grouping of samples, the box represents the upper and lower quartiles surrounding the median (line in the box). Whiskers represent the remaining spread of the data, apart from outlying data points (defined as points further from the median than 1.5 × Interquartile Range). We isolated 16S data from Incubations 1, 2, and 5 (since they are least impacted by the organic substrate addition) and identified the eight most common OTUs to appear in SIMPER pairwise analysis of substrates (ANOSIM by substrate: R value = 0.3863, p-value = 0.001). The relative abundances for these OTUs were averaged across the three Incubations in order to analyze mineral preference across the microbial community. "Background" samples include bailed filtered and unfiltered water (n = 5); "PUR" indicates polyurethane foam block samples (n = 3); "Carbonates" include calcite, dolomite, and HVD samples (n = 18); "Silica" indicates glass wool samples (n = 6); "Mixed" indicates MS lithology (tuff and lake sediments) (n = 6); "Steel" indicates low carbon steel ball bearings (n = 5). Plots are additionally labeled with the one-way ANOVA p-value if significant (p-value < 0.05). The lack of significance for the *Desulfotomaculum* and *Geobacillus* OTUs was indicative of the fact that the *Desulfotomaculum* population crashed after Incubation 1 and that the *Geobacillus* was infrequently found on minerals, but that, when present, it was often in high abundance, supporting the idea that this organism is infrequently detected but typically detected at high abundance.

Of the 518 OTUs found on the solid substrates, 72% of the OTUs were detected on least one sample from each lithological substrate, while only 5% of the OTUs were unique to a single lithological substrate type (**Fig. 1.16**). The mineralogy seems to play a significant role in governing the relative abundance of many OTUs and recruiting specific microbial lineages, both at the class and genus level, and differentiating amongst predicted microbial guilds (**Fig. 1.6**). Twenty-nine OTUs of *Rhodocyclaceae,* a family of Betaproteobacteria, were identified in our survey, with very different colonization patterns. For example, a *Methyloversatilis*-affiliated OTU was more than twice as abundant on average on the carbonate minerals (calcite, dolomite, HVD) than on glass wool or the MS sediments, while another *Rhodocyclaceae* OTU was most abundant on the glass wool and silica-rich MS. The underlying ecological or physiological factors influencing mineral colonization preference for these uncultured groups is not known, but the persistent partitioning by mineral substrate across the different incubations is notable. In another example, two OTUs affiliated with *Desulforudis* sp. (bin139368) and *Desulfotomaculum* sp. (bin90387), both putative sulfate-reducing Firmicutes, demonstrated different patterns of colonization – *Desulforudis* was most abundant on the low-carbon steel and *Desulfotomaculum* was

most abundant on carbonate minerals. Notably, the ANOVA analysis of the *Desulfotomaculum* species across Incubations 1, 2, and 5 did not indicate that the difference was statistically significant, because that particular OTU was detected only at very low abundance after Incubation 1. Within Incubation 1, however, that *Desulfotomaculum* OTU averaged 20.9% of the recovered community from the carbonates versus 1.4% of the community on the steel. Although inferring metabolic potential from 16S rRNA data represents a tentative assignment only, sequenced genomes *Desulforudis* indicate they are capable of autotrophic growth through hydrogen-coupled sulfate reduction, and we hypothesize *Desulforudis* in Inyo-BLM 1 may be locally consuming H_2 produced by the anaerobic corrosion of the steel (Chivian et al., 2008; Jungbluth et al., 2017) (**Fig. 1.15)**. Sequenced genomes and cultivated representatives of *Desulfotomaculum* are typically heterotrophic sulfate-reducers (Aüllo et al., 2013; Sousa et al., 2018), and although the exact reason for their preferential association with carbonates in our data is unclear, the natural tendency of those minerals to entrain organic matter as they form may be one possibility (Roberts et al., 2013). A distinct colonization pattern was observed with yet another *Desulfotomaculum*-identified OTU (bin86994), which was most abundant on low-carbon steel, pyrite, and pyrrhotite mineral substrates. The intra-genus colonization differences between putative sulfate-reducing Gram-positive bacteria across different mineral substrates highlights the value of examining colonization patterns at the OTU level rather than higher-order taxonomic clustering.

The three carbonate species we used in our flow-through cartridges (calcite, dolomite, HVD) demonstrated overall similar communities and were not significantly different in the iTag sequencing data when comparing across all samples. These findings differ from some studies examining authigenic calcite, aragonite, and dolomite at deep-sea methane seeps, which did observe community variations between calcite and dolomite substrates (Case et al., 2015). SEM scans did reveal, however, that both Incubation 1 dolomite mineral samples (HVD and dolomite standard) were substantially modified *in situ* by the precipitation of framboidal iron sulfides, whereas calcite samples from the same incubation had no observable secondary mineral precipitation (**Fig. 1.3**). It is possible that the difference in colonization patterns observed in marine studies was due to increased sensitivity of marine microorganisms to carbonate mineralogy because carbonate is a more dominant lithology in marine environments than terrestrial. The colonization differences between carbonate minerals may be more subtle than

the differences between carbonate phases and other mineral families. Increasing the sample size of calcite and dolomite incubations in future deployments may help resolve whether there are discernable differences between the colonization of different carbonate minerals.

The specific mechanisms underpinning mineral preferences are currently unknown, but the repeatable patterns observed at the Inyo-BLM 1 site highlight potential ecological partitioning between subsurface taxa associated with minerals. Mineralogical groupings were a significant determinant of microbial community variance in most of our samples. Aside from Incubation 3, when complex organic matter was introduced, cartridges with duplicate lithologies acted as robust biological replicates, closely associated in the NMDS analysis (**Fig. 1.5**) and ANOSIM R statistics for mineral type variation for were high (>0.35). In Incubation 1, nearly all of the variation between samples was attributable to mineral type (R = 0.9733). The Incubation number, partially representing the temporal distance from the organic carbon amendment, was a more important component when considering the entire data set, but perturbations on the scale of our experiment are likely infrequent. Since the vast majority of microorganisms in the deep biosphere are presumed to be mineral-attached (McMahon and Parnell, 2014), our experiments highlight the potential for targeting certain metabolisms and organisms based on the geology of their environment.

Framboidal iron sulfide precipitation

Framboidal iron sulfides, especially pyrite, have long been considered a potential biomarker, owing to the fact that they are often found in areas of high microbial activity, such as peat bogs and biofilms (Popa et al., 2004; Picard et al., 2016). It remains unknown, however, whether framboids are formed as a direct result of microbial activity or abiotically due to geochemical conditions (Sweeney and Kaplan, 1973; Graham and Ohmoto, 1994). As MacLean noted (Maclean et al., 2008), however, laboratory abiotic syntheses have only been accomplished at high-temperatures (above 60°C), well above the temperatures at nutrient- and biomass-rich systems where framboids are frequently found (Sawlowicz, 2000; Popa et al., 2004). It has been demonstrated that organic matter may play a role in aggregating the individual crystals into the framboid formation (MacLean et al., 2007), and (Maclean et al., 2008) observed individual crystals developing within an organic matrix. Particularly interesting in our study was the correlation between the presence of secondary iron sulfide framboids on two independent

dolomite incubations and two OTUs corresponding to *Desulfotomaculum,* a presumed sulfate-reducer, and *Sulfurovum,* a putative sulfide-oxidizing bacterium. Mineralogical heterogeneity of the substrate did not appear to explain the observed variation. Although both dolomites contained potential mineralogical sources for the framboids (higher iron content in the dolomite standard and micron-scale, anhedral iron- and sulfur-rich regions in the HVD), the secondary framboids formation was only observed during Incubation 1, although the same minerals were used for the incubations throughout the 18-moth experimental series. Precipitation of iron sulfides also could not be attributed to incubation time, as under optimal conditions, pyrite framboid have been shown to form within days (Rickard, 2019). Even if the organic matter amendment during Incubation 3 disrupted the ecological conditions, therefore, we would have expected to observe framboid formation in the Incubation 2 (197 days long). While sulfide concentrations were below detection in the water recovered from the borehole, it is possible that localized sulfur metabolism by *Desulfotomaculum* and/or *Sulfurovum* directly influenced framboid precipitation. The groundwater feeding Inyo-BLM 1 does contain trace iron and zinc (1.4 μM and 0.06 μM, respectively) (**Table 1.8**), which can react with sulfide and may contribute to undetectable aqueous sulfide concentrations in our water samples.

In addition to their ability to respire sulfate, it has been shown that some *Desulfotomaculum* are capable of growth as fermentative syntrophs coupled with hydrogenotrophic methanogens, rather than heterotrophic sulfate reducers (Imachi et al., 2000; Plugge et al., 2002; Moser et al., 2005; Imachi et al., 2006). Based on our 16S rRNA data alone, it is difficult to assess the physiology of these taxa in Inyo-BLM 1. On one hand, the detection of hydrogenotrophic methanogens affiliated with *Methanobacterium* in Inyo-BLM 1, the common partner of *Desulfotomaculum* when growing syntrophically (Imachi et al., 2000; Moser et al., 2005), suggests a similar syntrophic interaction could occur in our system, however, the co-occurrence of *Desulfotomaculum* (bin90387) with iron sulfides points also supports a possible role in sulfur metabolism. Our laboratory experiments with steel alloys confirmed that the steel we added in each of the *in situ* incubations could have resulted in elevated H_2 via anaerobic corrosion (the Schikorr reaction, e.g. $Fe^0 + 2H_2O \rightarrow Fe^{2+} + 2OH^- + H_2$) (Schikorr, 1929; Linnenbom, 1958; Ma et al., 2013). Therefore, we cannot dismiss the possibility that these organisms are syntrophs, that their disruption following Incubation 1 was due to inhibitory concentrations of

hydrogen, and that their correlation with pyrite formation was related to their role in producing small organic carbon molecules which aid in aggregating iron sulfide framboids rather than the production of sulfide.

Organic nutrient amendment

In most environments, oxidation of organic matter proceeds by the sequential reduction of O_2, NO_3^-, Fe^{3+}, SO_4^{2-}, and CO_2, in order of decreasing electron potential (Ponnamperuma, 1972). Because organic matter is thought to be move extremely slowly through the deep biosphere, most of these electron acceptors are long depleted at depth (Canfield, 1994; Hedges and Keil, 1995; Arndt et al., 2013; Osburn et al., 2014; Bradley et al., 2020). This results in a typically reduced system with low energy availability to the inhabiting organisms; Inyo-BLM 1 both has low dissolved organic carbon levels (0.431 ppm DOC) and few available electron acceptors (No detectable nitrate or nitrite and < 2 mM sulfate) (**Table 1.8**). Deep biosphere microorganisms are therefore thought to have low energy requirements (LaRowe and Amend, 2015), and grow extremely slowly, with estimated turnover rates varying orders of magnitude from months to thousands of years (Morono et al., 2011; Xie et al., 2013; Onstott et al., 2014; Trembath-Reichert et al., 2017). Because of the long growth times and slow metabolic rates, ecological principles such as succession, competition, or dispersal are likely reduced in impact and difficult to constrain (Biddle et al., 2011). By taking advantage of the addition of organic sponges to our system, we were able to observe the community response and some of these ecological forces at work in an unusual system. The microorganisms colonizing the sponges themselves were significantly different from the mineral-associated community, and in fact, the microbial diversity recovered from the incubated sponge mostly did not include OTUs that were abundant on the minerals, suggesting that the changes in the mineral-hosted community were driven by downstream degradation products of the sponges, analogous to the detrital matter that the deep biosphere likely subsists upon. The results imply that the planktonic BLM-1 assemblage is a reservoir for microorganisms that are capable of colonizing and rapidly metabolizing complex organic matter. The mineral-colonizing community, by contrast, may be taking advantage of the small organic molecules released during the breakdown of the proteinaceous sponge biomass.

This organic matter amendment experiment also provides with an opportunity to estimate community-wide carbon oxidation rates. The natural sponges introduced during

Incubation 3 provided ~0.9 g of proteinaceous organic carbon and 0.3 g of fixed nitrogen. While tracing the organic degradation process and associated end-product production in this open system was not possible, we used the shifts in the microbial community as a general indicator of the ecological conditions after the organic matter addition. In our rough model, we assume during Incubation 3, when the sponges are first added to the well, that the microbial community is exposed to the most labile organic carbon species. A dramatic enrichment in *Methyloversatilis* sp. on the mineral substrates (**Fig. 1.6**), but not on the sponge itself, indicates that this group perhaps is capable of rapid colonization and metabolism of organic molecules released by the sponge degradation. Cultured members of *Methyloversatilis* are methylotrophs that can oxidize a wide variety of C1 compounds coupled with oxygen or nitrate respiration (Lu et al., 2012; Doronina et al., 2014) and have been recovered in high abundances from oil reservoirs and hot springs (Lenchi et al., 2013; Doronina et al., 2014). The sudden dominance of these organisms in Incubation 3 and decrease in their relative abundance in subsequent incubations (**Fig. 1.4**) suggests they may represent a subset of the community poised to take advantage of carbon spikes to the system with a boom-bust lifestyle.

To our knowledge, this dolomitic aquifer is the first time organisms from Candidate Division KB-1 have been found in abundance in a terrestrial, low-salinity system. KB-1 is now classified as a subgroup of phylum Acetothermia (formerly OP1), which has been detected in anaerobic digesters as well as hot springs and other deep biosphere studies (Takami et al., 2012; Zaitseva et al., 2017; Hao et al., 2018), although the recovered diversity of related organisms in our system fall within the more narrowly defined KB-1 clade (sometimes referred to as class Acetothermiia) and we have therefore retained that name here. The only sequenced and published genome for Candidate Division KB-1, recovered from the Red Sea, points to a central metabolism based on glycine betaine degradation, a common N-containing organic osmolyte in hypersaline environments but less likely to be found in abundance in non-marine environments (Nigro et al., 2016). Although it is difficult to predict the metabolism of the as-yet uncultured KB-1 organisms in the groundwater due to the lack of extensive genomic characterization of this clade, the dynamics of community changes during the *in situ* organic matter addition, where the KB-1 OTUs dropped to very low abundance values over Incubations 3 and 4, suggest they were not stimulated (**Fig. 1.4**). There are a number of possibilities for the observed decrease in KB-1 relative abundance, including that the KB-1 strains in this environment do not metabolize

amino acids or that they perhaps were outcompeted by other microbes following the perturbation. Acetothermia and KB-1 organisms detected in other studies have revealed that the clade is capable of thriving in a range of organic matter concentrations, but if the KB-1 organisms in Inyo-BLM 1 are indeed heterotrophic (as are all the physiologically described representatives of this clade), our results imply that they are likely better adapted to *in situ* organic levels than to the excess provided during our amendment (Nigro et al., 2016; Zaitseva et al., 2017; Hao et al., 2018).

The recovery of Incubation 4 occurred six months after the introduction of the sponges to the well, and at this time, the microbial assemblage appeared to transition to a methanogenic phase. A small number of methanogen-affiliated sequences were detected in Incubation 1, including *Methanobacterium, Methanothermobacter,* and *Methanolobus,* however, samples from Incubation 4 were dominated by the OTU affiliated with *Methanobacterium.* All characterized isolates belonging to the *Methanobacterium* genus are hydrogenotrophic or formate-utilizing methanogens. Unexpectedly, although many OTUs associated with syntrophic clades (e.g. *Syntrophomonadaceae, Syntrophobacterales*) were observed during the organic enrichment in Incubation 3, few were recovered from Incubation 4, suggesting that much of the complex fermentable carbon was consumed. By the time Incubation 5 was recovered (nine months after organic matter addition), the diversity of organisms colonizing the experimental substrates was largely consistent to the community composition observed during Incubations 1 and 2 prior to organic matter amendment, suggesting that the community had reset to the state prior to the perturbation (**Fig. 1.5**).

The timing of the community shifts can provide bounds for order-of-magnitude activity estimates of the whole community in the borehole. Estimates for total carbon added to the system via diffusion were calculated above: 0.160 – 3.01 mmol. The lower activity estimate used the lower estimate for carbon diffusion (0.160 mmol C) and assumed that the methanogens detected were primarily using formate. Thus, the total estimated time for carbon oxidation to CO_2 is 177 days, extending from midway through Incubation 3 through midway through Incubation 5 (the midpoints of the incubations were used approximately to allow time for methanogen abundance to decrease). Based on a cell count of 4.1×10^6 cells/mL from Incubation 3, each cell is estimated to oxidize 0.02 fmol C per day on average. To calculate the upper bound

on activity, we used the higher diffused carbon value (3.01 mmol) and instead assumed that the detected methanogen, *Methanobacterium*, is hydrogenotrophic, thus assuming that the maximum value for methanogen relative abundance is a proxy for the maximum in hydrogen concentration the exhaustion of reduced carbon species. Based on these assumptions, we estimate that the complete oxidation of the carbon amendment occurred halfway between the recovery of Incubation 3 and 4, which translates to a total oxidation time of approximately 120 days and an average activity rate of 0.577 fmol C per cell per day. This exercise serves as a rough order-of-magnitude estimation and predicts oxidation rates that are high, but within the margin of error as compared to carbon oxidation rates measured from other deep biosphere systems using more direct methods (0.002 – 0.0067 fmol C per cell per day) (Morono et al., 2011; Trembath-Reichert et al., 2017; Moreno-Ulloa et al., 2019).

Conclusion

The terrestrial deep biosphere is characterized by its phylogenetic, physiological, and geological heterogeneity. Mineralogical changes occur both regionally, as in lithological units, and at the microscale, with secondary mineral formation such as iron sulfides potentially a product of the local micro-environment. This heterogeneity, along with the massive volume of the subsurface biome and difficulty in obtaining samples has meant that it is difficult to generate predictions as to the microbial population size, structure, or activity (Magnabosco et al., 2018). Although efforts are ongoing to address these questions, experiments performed in the laboratory are generally unable to capture all of the complexity of the subsurface. Our experiments serve as a wide-ranging *in situ* exploration of the factors controlling microbial populations and microbial colonization in one deep, warm dolomitic aquifer and enabled us to distinguish between populations of microorganisms living planktonically and those that preferentially adhere to a mineral surface. These observations provide some preliminary insight into the niche partitioning that occurs within the deep biosphere and emphasize the need for more comprehensive sampling of subsurface ecosystems. In addition to examining mineral-microbe associations, we utilized a complex N-rich organic matter amendment *in situ* to explore the response of the deep biosphere community to stimulation at this location. By observing this environment over a period of nine months after the carbon amendment, we observed this community oxidize the organic carbon in several phases, with putative heterotrophic organisms

closest to the carbon source, putative syntrophic organisms on neighboring mineral surfaces three months after the organic carbon was first deployed, and the dominance of methanogenic organisms six months after the original amendment. After nine months, the community returned to the assemblage that closely resembled its undisturbed state. Our experiments indicate that the microbial community is highly responsive to shifts in geochemistry and nutrient availability; tracking these community changes can even provide coarse estimates for the activity of these microorganisms. More precise activity measurements could be obtained, perhaps utilizing stable isotopic tracers, but avoidance of contamination of the slow-moving environmental system may require any such measurements be *ex situ*. In any case, careful consideration of the activity of deep biosphere organisms will aid in our understanding of the dynamics of this massive and understudied system.

Supplemental Figures

CaCl2*2H2O	9.9
MgCl2	25.1
KCl	30.5
NaCl	87.1
NaHCO3	582.5
KH2PO4	0.3
Na2SO4	65.6
SL-10 Trace Metal solution	1 mL
KOH added until pH9	

Table 1.7: Composition per liter of artificial BLM-1 media mimicking geochemistry at 579 m. (in mg / L unless otherwise noted).

	579 m	754 m	%Error	Analysis Method (EPA Reference)	Dilution	MDL (mg/L)
Al	0.03	0.008	1	M200.8.ICP-MS	1	0.001
Sb	0.0008	0.0004	4	M200.8.ICP-MS	1	0.0004
As	0.19	0.0778	1	M200.8.ICP-MS	100,1	0.0002
Ba	0.018	0.1096	2	M200.8.ICP-MS	1	0.0005
Be	U	U	2	M200.8.ICP-MS	100	0.005
B	1.82	1.74	0	M200.8.ICP-MS	100	0.05
Cd	U	0.0002	4	M200.8.ICP-MS	1	0.0001
Ca	2.7	31.7	2	M200.7.ICP	1	0.1
Cs	0.0003	0.0037	4	M200.8.ICP-MS	1	0.0002
Cr	U	U	3	M200.8.ICP-MS	1	0.0005
Co	U	0.00016	1	M200.8.ICP-MS	1	0.00005
Cu	U	0.0006	1	M200.8.ICP-MS	1	0.0005
Fe	0.05	0.08	3	M200.7.ICP	1	0.02
Pb	0.0002	0.0006	2	M200.8.ICP-MS	1	0.0001
Mg	3	12.1	2	M200.8.ICP-MS	1	0.2
Mn	0.002	0.0958	1	M200.8.ICP-MS	1	0.0005
Mo	0.1201	0.0533	4	M200.8.ICP-MS	1	0.0005
Ni	0.002	0.0092	2	M200.8.ICP-MS	1	0.0006
K	16.1	17	2	M200.7.ICP	1	0.2
Se	0.0005	U	4	M200.8.ICP-MS	1	0.0001
Si	10.6	43.8	3	M200.7.ICP	1	0.2
Ag	U	U	9	M200.8.ICP-MS	1	0.00005
Na	215	222	3	M200.7.ICP	1	0.2
Te	U	U	5	M200.8.ICP-MS	1	0.001
Tl	U	U	5	M200.8.ICP-MS	1	0.0001
Th	U	U	3	M200.8.ICP-MS	1	0.001
Sn	U	U	2	M200.8.ICP-MS	20	0.002
U	0.0002	0.0002	3	M200.8.ICP-MS	1	0.0001
V	U	U	2	M200.8.ICP-MS	1	0.0002
Zn	0.049	0.004	1	M200.8.ICP-MS	1	0.002
HCO_3^-	328	437	13	SMB2320B- Titration	1	2
CO_3^{2-}	88.1	U	13	SMB2320B- Titration	1	2
Hydroxide	U	U	13	SMB2320B- Titration	1	2
Total Alkalinity	416	437	13	SMB2320B- Titration	1	2
Hardness	19	129	13	SM2340B-calc	NA	0.8
TOC	1.64	4.21	16	SM5310B	1	0.1
DOC	0.813	0.431	2	SM5310B	1	0.1
POC	0.83	3.78	17	calculation from TOC-DOC	1	0.1
NO_3^-	0.02	U	1	calculation from total nitrate/nitrate and nitrite	1	0.02
NO_3^-/NO_2^-	0.02	U	1	M353.2 - Automated Cadmium Reduction	1	0.02
NO_2^-	U	U	0	M353.2 - Automated Cadmium Reduction	1	0.01
NH_3	U	0.22	0	M350.1	1	0.05
PO_4^{3-}	0.19	0.12	31	Calculation based on dissolved orthophosphate	1	0.03

Phosphorus, ortho, dissolved	0.06	0.04	31	M365.1 Automated Ascorbic Acid	1	0.01
SO_4^{2-}	44.4	158	1	D516-02/07 Turbidimetric	5	5
Cl^-	49.2	52.4	8	SM4500Cl-E	1	0.5
F^-	3.93	3.98	15	SM4500F-C	1	0.05
H_2	0.02	U	21			
N_2	U	U	NA			
CO_2	U	0.22	22	Described in main text		
CH_4	0.19	0.12	36			
CO	0.06	0.04	10			
O_2	44.4	158	62			

Table 1.8: Major ions and nutrients found in the groundwater within the borehole were measured at two depths, one inside the casing (579 m) and one below the casing (754 m). The ground water samples were obtained by successive sampling with 3 and 1 L discrete sampling devices (respectively) on 8/22/15-8/23/15, before the organic matter amendment was added to the system on 8/23/15. "U" indicates measured values below the minimum detection limit (MDL). The Environmental Protection Agency (EPA) or National Environmental Methods Index (NEMI) method reference number is listed, and the percent error of detection method was also quantified by technical duplicates. Because of the inherent error introduced by sampling from a dissolved gas bottle, percent error is significantly higher in our dissolved gas measurements. The microbial community contains no indication that the system is aerobic at any point, and is dominated primarily by putative fermentative organisms and methanogens. We therefore consider the dissolved oxygen data as a sampling artefact and indicative of amount of leak in the gas sampling process.

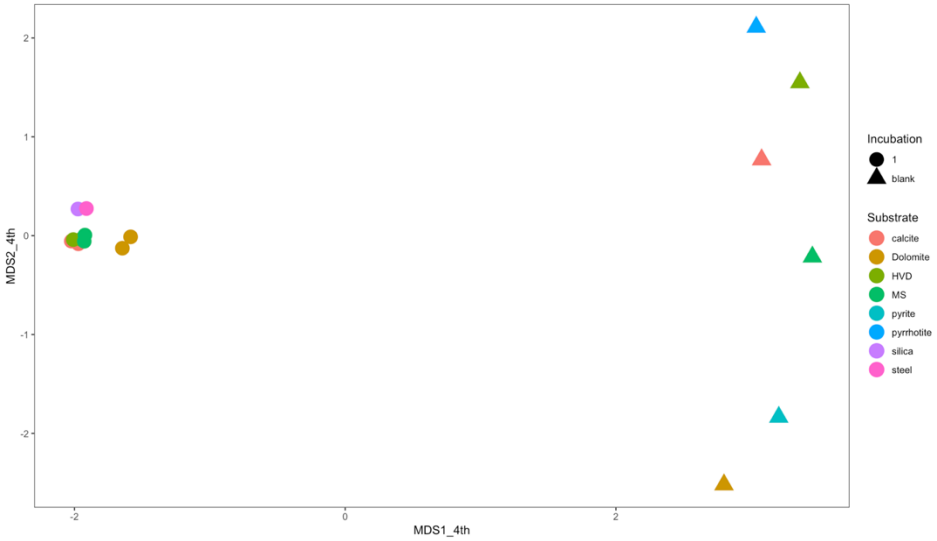

Fig. 1.9: NMDS of blank substrates versus Incubation 1. All Incubation substrates were autoclaved before incubation in the borehole. 16S rRNA genes did not amplify from these samples under standard conditions, but we were able to force a band to appear by increasing total PCR cycles to 45. Those amplified genes were also analyzed via Illumina iTag . The NMDS shown is for all amplicons, including contaminants identified by a no-template PCR control, which makes these points even closer than they would be after contaminant removal. ANOSIM analysis indicates that 95% of the variance is explained by whether the point was a blank sample or from Incubation 1 (R value = 0.9689, p-value = 0.001).

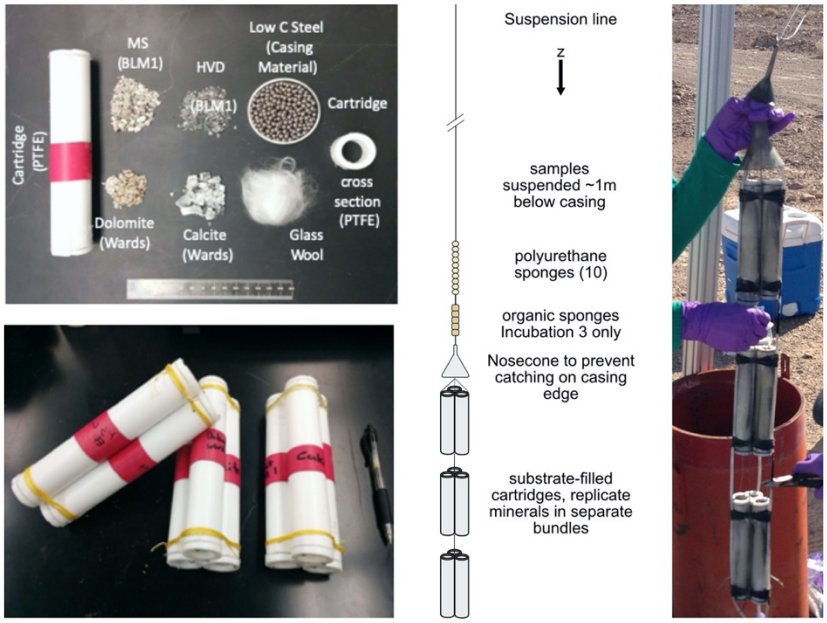

Fig. 1.10: (Left) Images of PTFE cartridges with mineral substrates. (Center) Schematic of bundles and sponge deployment in borehole. (Right) Image of post-incubation of cartridge bundle. The borehole cap and aluminum suspension frame are visible in the background.

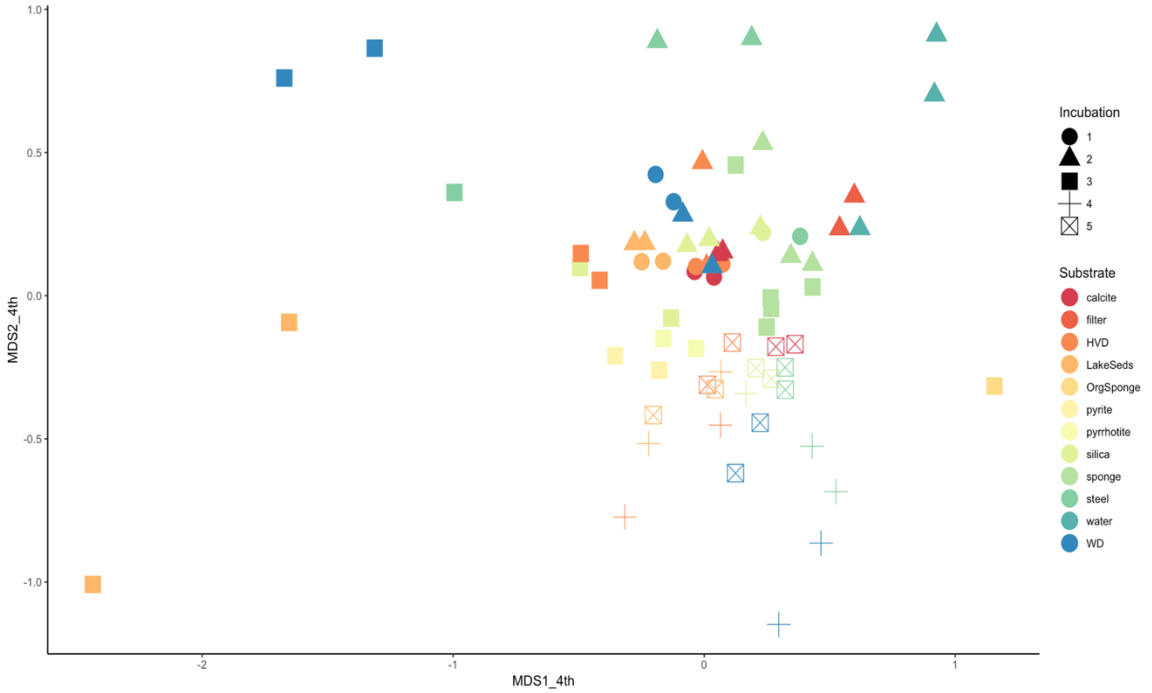

Fig. 1.11: NMDS of all samples taken from BLM-1, including raw and filtered water, minerals, polyurethane sponges, and the single recovered organic sponge. ANOSIM statistics for the complete dataset are as follows for the following variables: Incubation Number (0.4535, p-value = 0.001), substrate (0.2667, p-value = 0.001), substrate bin (0.3235, p = 0.001). There are three bins of substrates: carbonate (calcite, dolomite, HVD), sulfide mineral (pyrite, pyrrhotite), and planktonic (raw water, filtered water); other substrates are treated as their own bin.

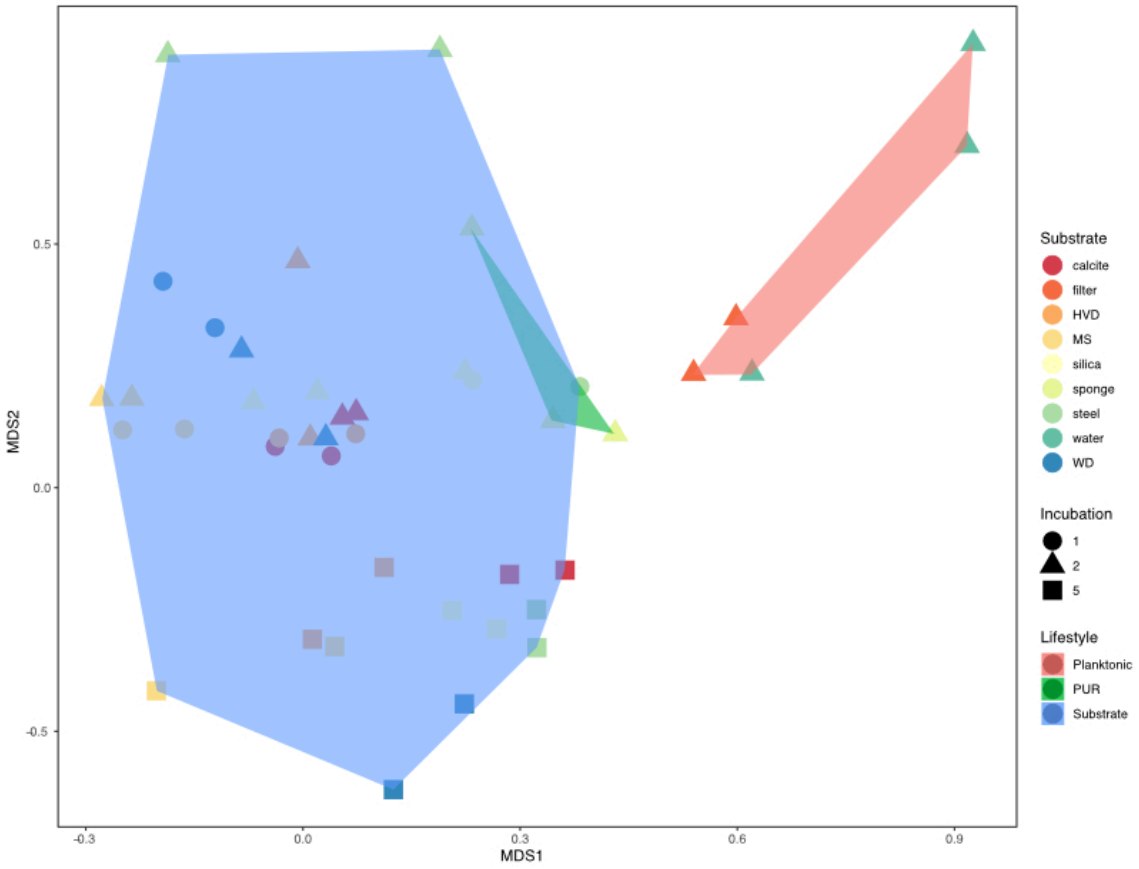

Fig. 1.12: NMDS of substrates for Incubations 1, 2, and 5, with hulls drawn around planktonic versus substrate groupings. The statistical significance of the lifestyle designations (planktonic, PUR, or substrate-attached) was assessed by ANOSIM (R = 0.4672, p-value = 0.001).

Cells counted using a Petroff-Hausser counting chamber, using 10 "samplings" of counted areas for each actual water samples from BLM-1				
Counted on 8-21-2015				
Sample 8-20-2015 1900' NO-glutaraldehyde				
Sample #	Average cell count per square	Cells/mL	Average (cells/mL)	Stdev
#1	0.15	3.0E+06	4.0E+06	1.0E+06
#2	0.25	5.0E+06		
#3	0.2	4.0E+06		
Sample 8-21-2015 2465' NO-glutaraldehyde				
Sample #	Average cell count per square	Cells/mL	Average (cells/mL)	Stdev
#1	0.09375	1.9E+06	4.1E+06	2.8E+06
#2	0.156	3.1E+06		
#3	0.36	7.2E+06		

Counted on 8-25-2015				
Sample 8-20-2015 1900' NO-glutaraldehyde				
Sample #	Average cell count per square	Cells/mL	Average (cells/mL)	Stdev
#1	0.175	3.5E+06	3.8E+06	5.5E+05
#2	0.219	4.4E+06		
#3	0.169	3.4E+06		
Sample 8-21-2015 2465' NO-glutaraldehyde				
Sample #	Average cell count per square	Cells/mL	Average (cells/mL)	Stdev
#1	0.281	5.6E+06	5.3E+06	7.6E+05
#2	0.219	4.4E+06		
#3	0.288	5.8E+06		

Table 1.13: Cell counts of water samples from two depths.

	Weight percentage			
Oxide	**Calcite**	**Dolomite**	**Hidden Valley Dolomite (HVD)**	**Mixed Siliclastic (MS)**
CaO	99.781	71.238	70.187	17.291
MgO	—	25.259	25.818	4.103
SiO_2	—	1.544	3.295	58.151
Al_2O_3	—	—	—	11.116
Fe_2O_3	0.000356	1.576	0.53	3.054
K_2O	—	—	—	5.631
Ni_2O_3	0.00012	—	—	0.000013
MnO_2	0.058	0.343	0.138	0.106
TiO_2	—	—	—	0.418
CuO	0.00018	—	—	0.00002
ZnO	—	0.000115	0.000067	0.000087
SrO	0.112	0.000263	0.00021	0.0005
PbO	—	—	0.00021	—
Y_2O_3	—	0.000029	—	0.000026
Total	**99.951656**	**99.960407**	**99.968487**	**99.870646**

Table 1.14: X-Ray Fluorescence (XRF) mineral composition data. The four primary minerals including the calcite and dolomite standards and HVD and MS natural samples were analyzed for their elemental composition. Although the data are reported as weight percentages of the mineral oxides, XRF cannot detect light elements (including carbon or oxygen) or the redox state of elements. These values are therefore useful as a comparative tool, but are not an absolute measurement of composition or mineralogy.

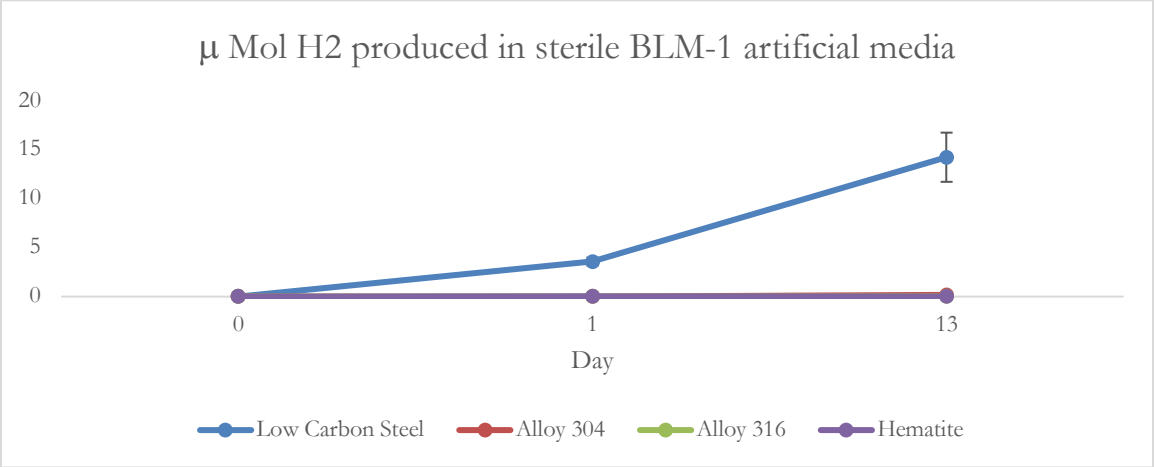

Fig. 1.15: H_2 production from different iron sources. *n*=2 for each iron source: low carbon steel, 304 stainless steel, 316 stainless steel, and crushed hematite. For each tube, three 3 mm ball bearings of steel alloy or 0.5 g crushed hematite were incubated anaerobically, in the dark, at room temperature in 10 mL defined sterile media, with pH and salt concentrations matching those of the 579 m water sample taken from the borehole. Each tube was sampled destructively—that is, we did not perform repeat measurements from individual tubes.

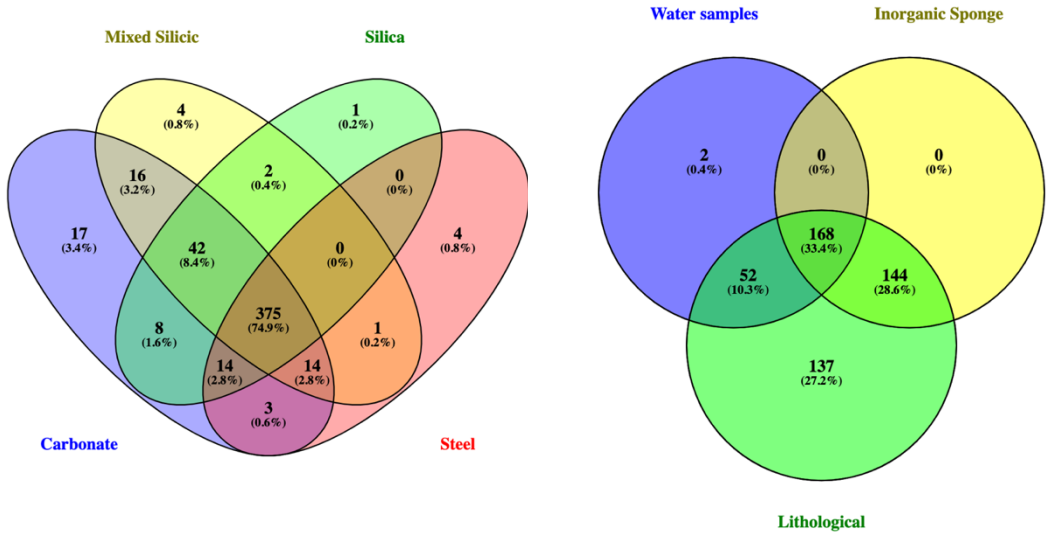

Fig. 1.16: Venn diagrams of OTU overlap between substrate types across all Incubations. (Left) Four categories of lithological substrates displayed. The carbonate bin contains the most unique OTUs but also has the highest number of samples. Overall, 375/520 (72%) of the OTUs were shared across all the lithological substrates. (Right) Venn diagram of carbonate bin versus water and sponge samples. Sponge samples contained no unique OTUs and water samples contained only 2, indicating that although some cells were more abundant in the planktonic fraction, most cells can be found attached to rocks. This is in agreement with evidence that rock-associated microorganisms outnumber planktonic cells by a factor of 10-10^3.

Sample Name	Incubation	Substrate	Substrate Group	Depth of Sample (mbls)	Shannon Index	Chao1 Richness Estimate
SM-Calcite-Mid	1	calcite	Carbonate	752	3.19989414	310.483871
SM-Calcite-Top	1	calcite	Carbonate	752	3.35433726	351.8125
SM-GlassWool	1	silica	Silica	752	3.16863452	277.2
SM-HidValDol-Mid	1	HVD	Carbonate	752	3.1462708	360.384615
SM-HidValDol-Top	1	HVD	Carbonate	752	3.36209629	317.55
SM-LakeSeds-1	1	MS	Mixed_Silicic	752	3.35520088	303.032258
SM-LakeSeds-2	1	MS	Mixed_Silicic	752	3.17815657	290.869565
SM-SteelBalls	1	steel	Steel	752	3.18296613	288.588235
SM-WardDol-Mid	1	WD	Carbonate	752	2.86291954	220.428571
SM-WardDol-Top	1	WD	Carbonate	752	2.88388839	218.375
SWM-BLM-BlCalc	blank	calcite	Control	NA	NA	NA
SWM-BLM-BlHVD	blank	HVD	Control	NA	NA	NA
SWM-BLM-BlLS	blank	MS	Control	NA	NA	NA
SWM-BLM-BlPrh	blank	pyrrhotite	Control	NA	NA	NA
SWM-BLM-BlPyr	blank	pyrite	Control	NA	NA	NA
SWM-BLM-BlWD	blank	WD	Control	NA	NA	NA
SWM-BLM-glass	3	silica	Silica	752	2.73443244	176.5
SWM-BLM-glasspyr	3	silica	Silica	752	3.41151595	291.15625
SWM-BLM-HVD12	3	HVD	Carbonate	752	3.18572767	187
SWM-BLM-HVD17	3	HVD	Carbonate	752	3.21036709	156
SWM-BLM-LS15	3	MS	Mixed_Silicic	752	2.02806733	50
SWM-BLM-LS4	3	MS	Mixed_Silicic	752	0.80877542	25.5
SWM-BLM-Osp7	3	OrgSponge	Osponge	752	2.22501753	106
SWM-BLM-prh11	3	pyrrhotite	pyrrhotite	752	3.21760052	326.2
SWM-BLM-prh6	3	pyrrhotite	pyrrhotite	752	3.26659205	297.146341
SWM-BLM-pyr1	3	pyrite	pyrite	752	3.23594744	214.647059
SWM-BLM-pyr7	3	pyrite	pyrite	752	3.07742261	245.666667
SWM-BLM-sp1	3	PUR	PUR	200	3.60594114	228.3125
SWM-BLM-sp10	3	PUR	PUR	752	3.82881942	343.5
SWM-BLM-sp7	3	PUR	PUR	579	3.23304088	250.136364
SWM-BLM-sp8	3	PUR	PUR	690	3.98379116	326.5
SWM-BLM-sp9	3	PUR	PUR	720	3.84795824	334.689655
SWM-BLM-steel	3	steel	Steel	752	2.19999003	81
SWM-BLM-WD13	3	WD	Carbonate	752	2.2976857	37.5
SWM-BLM-WD16	3	WD	Carbonate	752	2.27990826	77
SWM-BLM1-F4-glass-2	4	silica	Silica	752	2.85991087	283.774194

SWM-BLM1-F4-HVD6-2	4	HVD	Carbonate	752	2.48336084	176.12
SWM-BLM1-F4-HVD7-2	4	HVD	Carbonate	752	3.12718576	260.956522
SWM-BLM1-F4-LS10-2	4	MS	Mixed_Silicic	752	3.34106855	308.333333
SWM-BLM1-F4-LS12-2	4	MS	Mixed_Silicic	752	2.81113412	208.714286
SWM-BLM1-F4-steel2-2	4	steel	Steel	752	3.10856099	232.052632
SWM-BLM1-F4-steel3-2	4	steel	Steel	752	3.34276801	167
SWM-BLM1-F4-WD8-2	4	WD	Carbonate	752	2.53717628	109.153846
SWM-BLM1-F4-WD9-2	4	WD	Carbonate	752	2.70382705	127.461538
SWM-BLM1-F5-calc1	5	calcite	Carbonate	752	3.71801354	253.166667
SWM-BLM1-F5-calc2	5	calcite	Carbonate	752	3.91285026	279.105263
SWM-BLM1-F5-glass2	5	silica	Silica	752	3.48644325	235.25
SWM-BLM1-F5-glass4	5	silica	Silica	752	3.53811768	291.75
SWM-BLM1-F5-HVD1	5	HVD	Carbonate	752	3.55635476	276.848485
SWM-BLM1-F5-HVD2	5	HVD	Carbonate	752	3.54892251	314.344828
SWM-BLM1-F5-LCsteel	5	steel	Steel	752	4.03233343	277.30303
SWM-BLM1-F5-LS1	5	MS	Mixed_Silicic	752	3.48988961	251.090909
SWM-BLM1-F5-LS2	5	MS	Mixed_Silicic	752	3.40385856	196.666667
SWM-BLM1-F5-steel4	5	steel	Steel	752	3.55466346	273.875
SWM-BLM1-F5-WD1	5	WD	Carbonate	752	3.72015496	228.545455
SWM-BLM1-F5-WD2	5	WD	Carbonate	752	3.49377313	182
SWM-calc-2-5	2	calcite	Carbonate	752	3.74181087	282.6
SWM-calc-2-6	2	calcite	Carbonate	752	3.77444219	291.28125
SWM-deep-1	2	water	Background	752	2.83047299	53
SWM-deep-2	2	water	Background	752	2.65615232	48
SWM-filter-1	2	filter	Background	579	3.51828474	103.428571
SWM-filter-2	2	filter	Background	752	3.63184943	158.5
SWM-glass-2-9	2	silica	Silica	752	3.62974867	280.12
SWM-glass-2-mid	2	silica	Silica	752	3.01011486	277
SWM-glass-2-top	2	silica	Silica	752	3.8324139	316.391304
SWM-HVD-2-10	2	HVD	Carbonate	752	3.07718906	186.545455
SWM-HVD-2-12	2	HVD	Carbonate	752	3.85002118	310.529412
SWM-Lake-2-7	2	MS	Mixed_Silicic	752	3.31235757	244.045455
SWM-Lake-2-8	2	MS	Mixed_Silicic	752	3.29308608	214.545455
SWM-shallow	2	water	Background	579	2.79256109	161.5
SWM-sponge-2-1	2	PUR	PUR	200	3.57701852	186.368421
SWM-sponge-2-15	2	PUR	PUR	752	3.5749791	234.322581

SWM-sponge-2-9	2	PUR	PUR	579	3.2195543	243.444444
SWM-steel-2-mid	2	steel	Steel	752	2.46988761	100.545455
SWM-steel-2-top	2	steel	Steel	752	2.29920794	120.214286
SWM-WD-2-3	2	WD	Carbonate	752	3.62745517	247.833333
SWM-WD-2-4	2	WD	Carbonate	752	3.36669682	178.555556
C-Q5lot0141505-Neg	blank	PCR_no_template	Control	NA	NA	NA
SWM-NegCtrl-1	blank	DNA_extraction	Control	NA	NA	NA
SWM-NegCtrl-2	blank	DNA_extraction	Control	NA	NA	NA

Table 1.17: List of all sequenced samples with metadata and general diversity statistics, including Shannon Diversity and Chao1 richness estimate.

C h a p t e r 2

CORRELATING THE MICROBIAL AND ANIMAL COMMUNITIES WITH BIOGEOCHEMISTRY AT A COLD METHANE SEEP IN THE COSTA RICA PACIFIC MARGIN

Abstract

Marine methane seeps are globally distributed, highly dynamic features that serve as hotspots for chemosynthetic and communities and geochemical activity on the seafloor. Careful studies of the ecotone, or transition zone, between the localized seepage activity and surrounding deep sea environment are necessary to understand the impacts of seeps on the broader ocean biome, but these ecotones remain poorly understood. We describe the geochemical (major ions and carbon isotopes) and biological (megafauna and microbial 16S rRNA gene) diversity of 267 carbonate samples and sediment cores (up to 24 cm deep) retrieved from 13 Deep Submersible Vehicle (DSV) *Alvin* dives between 2017-2018 at Mound 12, a methane seep on the Costa Rica Pacific Margin. To provide a first-order spatial analysis of the seep, each sediment core was initially classified as "active," "transition," or "inactive" based on *in situ* megafaunal observations, the presence of bacterial mat, or methane seepage (shimmering water). Spatial correlation analysis of geochemical and microbial community data indicated that sites colonized by *Kiwa puravida,* the Costa Rica yeti crab, were among the most active, and consistently had high sulfide concentrations, ^{13}C-depleted dissolved inorganic carbon, and increased relative abundance of anaerobic methane-oxidizing consortia belonging to ANME-1a and 1b. Transition zones were characterized by less abundant chemosynthetic seep fauna, but were colonized by hydroids and other families of polychaetes. Inactive zones had few observable fauna outside of fish, brittle stars, or anemones. There was no significant difference, however, between the microbial assemblages recovered from push cores from the transition sites and inactive sites, indicating a narrower range for seep-associated microbial taxa than for megafauna reliant on active seep methane venting. Interestingly, authigenic seep carbonates colonized by transition zone animals harboured similar microbial communities, regardless of the activity classification, supporting previous work that suggests the endolithic microorganisms colonizing carbonates may be slower to change than those in the sediments. We also conducted photomosaic mapping of the site in both 2017 and 2018 using autonomous underwater vehicle (AUV) *Sentry*, which indicated that *K. puravida* populations had moved 5-15 m southwest. Evidence of new seep activity, along with abundant sediment ANME-1 organisms, was detected to the southwest of the main site.

Introduction

Methane seeps are highly dynamic regions on the seafloor characterized by widespread, diffuse, upward flow of methane-rich fluids permeating the sediment. Similar to hydrothermal vents, methane seeps are often found close to convergent boundaries of tectonic plates. As advected ocean water passes through fractured and weathered basaltic crust, heat and compression from the subducting plate aid in liberating volatile metals and gasses, and the enriched fluids infiltrate the sediments by way of deep fractures (Hovland, 2002; Tivey, 2007; Tryon et al., 2010). 50-80% of the methane sourced from these sites is oxidized in the sediment by microorganisms, principally anaerobic methane-oxidizing archaea (ANME) and their sulfate-reducing bacterial partners (SRB), with the remaining 200 Tg (0.2 Gt) of methane escaping to the hydrosphere (Reeburgh, 2007b; Boetius and Wenzhöfer, 2013; Levin et al., 2016). Less than 10 Tg of oceanic methane ultimately reaches the atmosphere, however, with the balance consumed by planktonic aerobic methanotrophs throughout the water column (Mau et al., 2006; Reeburgh, 2007b; Tavormina et al., 2008). Since methane is known to be more than 30 times more potent than carbon dioxide in terms of global warming potential, the role that benthic microbial communities play in controlling methane communities to the atmosphere also has a drastic impact on global climate (Shindell et al., 2009; Etminan et al., 2016).

The geologic underpinnings of methane seeps also give rise to unique habitats on the ocean floor colonized by endemic animals. Authigenic minerals also form in seep environments, chiefly as extensive carbonate pavements (Naehr et al., 2007; Marlow et al., 2014b; Case et al., 2015; Mason et al., 2015; Georgieva et al., 2019). Carbonate precipitation is driven by the *in situ* oxidation of methane with sulfate in the sediments by the syntrophic partnership between ANME and SRB (Boetius et al., 2000; Orphan et al., 2001a; Orphan et al., 2001b). The resulting increase in alkalinity drives authigenic carbonate precipitation with a $\delta^{13}C$ isotope signal reflective of the seep methane (Han et al., 2004; Crémière et al., 2016; Oppo et al., 2020). The increased flux of chemical energy at methane seeps and vents also frequently supports a complex food web (Levin et al., 2016). Sulfate reduction in the sediments with methane generates significant concentrations of sulfide that, in some areas, diffuses to the benthic water column. The sulfide, both in the sediments and the water column, is then used by the symbiotic bacterial partners of a variety of chemosynthetic animals, including bathymodiolin mussels, clams, and tubeworms

(Treude et al., 2003; Joseph, 2017). An intriguing example of this chemosynthetic symbiosis occurs between yeti crabs, genus *Kiwa,* and their sulfide-oxidizing bacterial epibionts that live on setae covering the crabs' bodies, especially the pereopods (Thurber et al., 2011; Goffredi et al., 2014). The yeti crabs feed their bacteria by waving their pereopods over the sulfide-rich fluids emanating from the sediment, presumably to stimulate sulfide oxidation by their epibionts, and then feed on the resulting bacterial biomass.

Thousands of methane seeps and vent sites have been located on the seafloor (Beaulieu et al., 2013; Beaulieu et al., 2015), but the extent to which these seeps interact with broader benthic ecology is still an area of active study (Levin et al., 2016; Ashford et al., 2020; Soares Pereira, 2020). While megafauna are generally easy to identify and enumerate, even when viewed from a remote operated vehicle (ROV) or autonomous underwater vehicle (AUV), the connections between seep fauna, geochemistry, and underlying sediment microbial community structure remain poorly studied. Although seep fauna are known to inhabit different zones surrounding the seep center, the specific environmental conditions shaping animal distribution are not well quantified, making the inference of local environmental conditions from megafauna presence or absence difficult (Goffredi and Barry, 2002; Grupe et al., 2015). This task is complicated by the fact that dispersal of metabolites like methane and sulfide though sediment porewater is slower than through the benthic water column, which likely leads to benthic organisms having significantly larger spatial niches than the sediment microorganisms providing the geochemical species on which they rely.

Cold methane seeps are also highly dynamic; both the total methane flux as well as the regionality of most intense fluid flow can shift on a scale of weeks to years as a result of tectonic activity and authigenic carbonate formation (Tryon et al., 1999; Torres et al., 2002; Oppo et al., 2020). Regions on the outskirts of a seep are likely the most affected, and these transition zones, referred to as "ecotones," are therefore of particular interest. Macroecological studies have found that ecotone communities are frequently more diverse than the communities on either side of the gradient they separate. This effect may be even more pronounced at the ecotones between chemosynthesis- and photosynthesis-based environments like the transition between a methane seep and background deep sea ecosystem (Meyer-Dombard et al., 2011). Such an ecotone, or a "chemotone," represents the bridge between the energetic seep environment and more oligotrophic background sediment, whether by advection of methane, sulfide, or microbial

biomass away from the seep center (McGinnis et al., 2006; Pohlman et al., 2010). A companion study to ours recently examined the benthic sediment meiofauna and found that the transition zones of methane seeps are distinct, both in terms of infaunal biodiversity and geochemistry (Ashford et al., 2020). Whether the patterns found in meiofauna and megafauna are also observable in microbial community structure remains unexplored, but enhancing our understanding of the connections within the entire methane seep ecosystem will aid our ability to better map the extent and large scale effects of methane seepage.

Here we report the deep sea ecology results from broad sampling across Mound 12, a methane seep on the Costa Rica Pacific Margin. We analyze sediment- and rock-hosted microbial communities and porewater geochemistry and compare against the distribution of animals as measured by AUV mapping in order to construct a framework to understand the levels of activity of a methane seep, especially with respect to the transition zones for both fauna and microbial flora.

Materials and Methods

Site Description:

Mound 12 is a 50 m tall, cone-shaped mud volcano on the Costa Rican Pacific active margin (Hensen et al., 2004; Linke et al., 2005; Mau et al., 2006; Sahling et al., 2008; Tryon et al., 2010; Cortés, 2016). The region of main activity lies to the southwest of the mound itself at ~1000 m depth, where evidence of current or prior seep activity extends ~300 m radially outward from the base of the cone. No methane ebullition has been observed at Mound 12, but the active region has extensive carbonate platforms colonized by myriad chemosynthetic organisms including the Costa Rican yeti crab, *Kiwa puravida* (Thurber et al., 2011; Goffredi et al., 2014). Samples were determined, at the time of collection, to fall into one of three categories: active, transition, or inactive based on visual indicators on the seafloor. Active samples were characterized by carbonate platforms with minimal sediment cover, microbial mat covering visible sediment, and abundant chemosynthetic animals, including bathymodiolin mussels, *K. puravida*, vesicomyid clams, or vestimentiferan tubeworms. Transition sites were characterized as those with a decreased density of bivalves, absence of microbial mat, shell hash of seep bivalves, light sediment cover of visible carbonate, and/or more abundant non-chemosynthetic organisms such as hydroids, galatheid crabs or shrimp. Vesicomyid clams were generally not

observed at transition sites, but hard ground fauna like mussels and tubeworms were still observed. Inactive sites had either mostly buried or absent carbonate and few visible eukaryotes apart from brittle stars, anemones, or fish.

Seafloor Sampling Strategy

Carbonate and sediment pushcore samples were collected using Human Occupied Vessel (HOV) *Alvin* on two R/V *Atlantis* expeditions: AT37-13 (May-June 2017) and AT42-03 (October-November 2018). Upon retrieval, cores were stored shipboard at 4°C until processing within several hours. All cores were extruded upwards and subsampled into depth horizons: 1 cm horizons for the first six cm and 3 cm horizons thereafter. Each horizon was assigned a unique in-house serial number and then subsampled for various downstream analyses. Processing a horizon involved one of two workflows: full geochemical and DNA analysis or DNA analysis alone. For DNA sampling, ~1.5 mL of sediment was flash-frozen in liquid nitrogen until onshore DNA extraction (described below). For full analysis cores, an additional ~0.75 mL of sediment was fixed in 2% electron microscopy-grade paraformaldehyde (PFA) (Electron Microscopy Sciences; Hatfield, PA), and 1 mL sediment was alkalified with 3 mL 5 M NaOH, capped, and stored for methane isotope analysis. PFA-fixed sediment stored at 4°C overnight and was then washed three times with 1.5× phosphate-buffered saline (PBS) the following day and stored at -20°C in 1:1 3× PBS:100% ethanol. Remaining sediment was then squeezed for porewater under Ar into a disposable Luer-lock 30 mL syringe using a Reeburgh-syle squeezer (model 22.200, KC Denmark A/S; Silkeborg, Denmark) (Reeburgh, 1967). The resulting porewater was immediately aliquoted for other analyses detailed under Geochemistry below: Cline Assay (sulfide), Ferrozine Assay (ferrous iron), dissolved inorganic carbon (DIC) concentration and carbon isotope composition, ion chromatography for major and minor anions and cations, and pH.

Carbonate samples were collected with *Alvin* into insulated bioboxes. Using an ethanol-sterilized chisel, subsamples of each rock were collected shipboard. Samples for DNA analysis were placed in sterile Whirl-pak bags (Nasco, Fort Atkinson, Wisconsin) and frozen in liquid nitrogen before storage at -80°C. Rock samples were also fixed in 2% PFA in 5 mL Nalgene containers overnight at 4°C before washing 3 times with 1.5x PBS the following day and stored at -20°C in 1:1 3x PBS:100% ethanol. A list of all samples analyzed herein, with accompanying

coordinates, activity classifications, and measured geochemistry is available in the supplementary data file.

Geochemistry

Sulfide concentrations were measured by onshore Cline Assay after shipboard precipitation with 1:1 0.5 M zinc acetate (Cline, 1969). Ferrous iron concentrations were estimated by shipboard reaction of porewater with ferrozine; reacted samples were stored at 4°C until onshore measurement (Stookey, 1970). Both Cline Assays and Ferrozine assays were measured with a Sunrise™ spectrophotometer (Tecan Group Ltd.; Männedorf, Switzerland), Cline assays at 676 nm wavelength and Ferrozine assays at 562 nm. Porewater aliquots for dissolved inorganic carbon (DIC) analysis were passed through a 0.2 μm filter into He-flushed 12 mL exetainer vials with 100 μL 40% phosphoric acid. DIC concentrations and carbon isotope composition (δ^{13}C-DIC) were measured on a Gasbench II system on a Delta V Plus mass spectrometer (ThermoScientific, Bremen, DE) with reference to VPDB. A 0.2 μm-filtered, 1 mL aliquot of porewater from each horizon was also frozen at -20°C for onshore ion chromatography analysis. Finally, if any porewater remained, the pH was measured using a B-713 LAQUAtwin handheld pH meter (Horiba; Kyoto, Japan).

The concentrations of dissolved anions (F^-, CH_3COO^-, Cl^-, NO_2^-, Br^-, NO_3^-, and SO_4^{2-}) and cations (Na^+, NH_4^+, K^+, Mg^{2+}, and Ca^{2+}) in seawater samples were analyzed by ion chromatography (IC) using a Thermo Scientific Dionex Aquion Ion Chromatograph connected to a Thermo Scientific Dionex AS-DV autosampler at the Dawson lab, Department of Environmental Sciences, Rutgers University (New Brunswick, NJ, USA). Anions were eluted over 30 minutes using a 9 mM $NaCO_3$ eluent with a Dionex IonPac AS11 4 x 50 mm guard column and 4 x 250 mm column coupled to a Dionex AERS 500 carbonate anion suppressor. Cations were eluted over 20 minutes using a 20 mM methanesulfonic acid eluent with a Dionex IonPac CS12a 4 x 40 mm guard column and a 4 x 250 mm column coupled to a Dionex SC-CERS 500 salt converter cation suppressor. For the analyses, the seawater samples were diluted 20-fold with ultrapure water (Thermo Scientific Milli-Q, ~18 MΩ·cm). Six in-house standards of different concentrations, including the elements of interest, were run prior and following the samples and were used to generate a standard curve.

DNA Extraction

DNA was extracted from samples using the Qiagen PowerSoil DNA Extraction Kit (Qiagen; Hilden, Germany; 12888) according to the kit protocol except for the following changes to the lysis step. For sediment samples, following the addition of the detergent to the lysis tubes, the slurries were placed in a bead beater (FastPrep FP120, Thermo Fisher Scientific; Waltham, MA) at 5.5 m/s speed for 45 seconds. The samples were then centrifuged at 10,000 × *g* for 30 s and processed according to the rest of the manufacturer's instructions. Rock samples were processed with the aim of extracting DNA from the endolithic community. The samples were first washed and sonicated to remove external sediment-associated microorganisms according to (Mason et al., 2015). Following the washing, samples were powdered with a sterile mortar and pestle and 0.25 – 0.5 g powder was added to the lysis tubes. The lysis tubes were then flash frozen in liquid nitrogen and thawed in a 25°C water bath. The tubes were then placed in a sonicating water bath for 90 seconds. The detergent was then added and the samples vortexed briefly to mix before incubating the entire sample in a 65°C water bath for 30 minutes. The heated samples were then placed in the beat beater and processed according to the sediments as above.

DNA Sequencing

The V4-V5 region of the 16S rRNA gene was amplified using archaeal/bacterial primers with Illumina (San Diego, CA) adapters on 5' end (515F 5'-TCGTCGGCAGCGTCAGATGTGTATAAGAGACAG-GTGYCAGCMGCCGCGGTAA-3'and 926R 5'-GTCTCGTGGGCTCGGAGATGTGTATAAGAGACAG-CCGYCAATTYMTTTRAGTTT-3'). PCR reaction mix was set up in duplicate for each sample with Q5 Hot Start High-Fidelity 2x Master Mix (New England Biolabs, Ipswich, MA, USA) in a 15 μL reaction volume according to manufacturer's directions with annealing conditions of 54°C for 30 cycles. Duplicate PCR samples were then pooled and barcoded with Illumina Nextera XT index 2 primers that include unique 8-bp barcodes (P5 5'-AATGATACGGCGACCACCGAGATCTACAC-XXXXXXXX-TCGTCGGCAGCGTC-3' and P7 5'-CAAGCAGAAGACGGCATACGAGAT-XXXXXXXX-GTCTCGTGGGCTCGG-3'). Amplification with barcoded primers used Q5 Hot Start PCR

mixture but used 2.5 μL of product in 25 μL of total reaction volume, annealed at 66°C, and cycled only 10 times. Products were purified using Millipore-Sigma (St. Louis, MO, USA) MultiScreen Plate MSNU03010 with vacuum manifold and quantified using ThermoFisher Scientific (Waltham, MA, USA) QuantIT PicoGreen dsDNA Assay Kit P11496 on the BioRad CFX96 Touch Real-Time PCR Detection System. Barcoded samples were combined in equimolar amounts into single tube and purified with Qiagen PCR Purification Kit 28104 before submission to Laragen (Culver City, CA) for 250 bp paired end sequencing on Illumina's MiSeq platform with the addition of 15-20% PhiX control library. Raw read files with accompanying controls were submitted to the NCBI Sequence Read Archive under BioProject Accession Number PRJNA623020.

DNA Sequence Analysis

712 Illumina iTag samples from across the entire set of AT37-13 and AT42-03 expeditions, including no-sample extraction and no-template PCR controls, were processed together in QIIME version 1.8.0 (Caporaso et al., 2010) following a protocol outlined in (Mason et al., 2015). Raw sequence pairs were joined requiring a 50 bp overlap (with a maximum of 4 mismatches in overlapping sequence). Contigs were then quality-trimmed, with minimum Phred quality score of 30 (QIIME default is 4), and any sequences with unknown base call ("N") were removed. Contig sequences were then clustered *de novo* into operational taxonomic units (OTUs) with 99% similarity using UCLUST, and the most abundant sequence was chosen as representative for each *de novo* OTU (Edgar, 2018). Taxonomic identification for each representative sequence was assigned using UCLUST with the Silva-132 database (Quast et al., 2013), requiring minimum similarity of 90% to assign a taxonomy; 9 of the top 10 hits were required to share a taxonomic assignment to assign that taxonomy to a query. In comparison, the QIIME defaults include 90% similarity, but only 2 of 3 database hits must share taxonomy for positive assignment. Our SILVA database is appended with 1,197 in-house high-quality, methane seep-derived bacterial and archaeal clones. Any sequences with pintail values >75 were removed. The modified SILVA database is available upon request from the corresponding authors. Singleton OTUs were removed first, and then any OTU which occurred less than 10 times across all samples (or about 0.000001% of the remaining sequences), were also removed. Known contaminants in PCR reagents and extraction kits as determined by analysis of no-template PCR and no-sample

extraction controls run with each MiSeq set were then removed. After all filtering steps, 66,350 OTUs remained. Samples with fewer than 1,000 sequences recovered from these 66,350 OTUs were removed, resulting in 268 total samples from Mound 12 (other locations from the expeditions not considered here) with an average of 9,097 reads per sample.

We chose not to rarefy our data consistent with several studies indicating that it impedes detection of differential abundance for little apparent benefit (McMurdie and Holmes, 2014; Weiss et al., 2017). These studies indicate that using a fourth-root transformation of relative abundance values is computationally simple, reasonably effective at detecting true differential abundance, and does not require discarding valid data. Accordingly, we used a fourth-root transformation prior to non-metric multidimensional scaling (NMDS) ordinations and for all downstream analyses, conducted in R along with the *vegan* ecological statistics package (R Core Team, 2014; Oksanen et al., 2018). NMDS constructs *de novo* ordinations based on ranked pairwise sample dissimilarities (we used the Bray-Curtis dissimilarity metric), and the fit of the ordination is measured by the stress. Stress values below 0.2 are generally considered acceptable, and all ordinations presented here have stress values < 0.2 with parameter *trymax* = 100. We also conducted analysis of similarity (ANOSIM), similarity percentage (SIMPER), permutational analysis of variance (PERMANOVA) analyses, and correlation analyses with Mantel significance tests, also using *vegan* in R; for ANOSIM, PERMANOVA, and Mantel tests, p-values < 0.05 after 999 permutations were considered significant. OTU and geochemical vectors were calculated for the NMDS ordination using the *vegan envfit* command with 999 permutations. Because of the high number of total OTUs, we used a stricter cutoff to assign significance (p-values < 0.01); in the case of OTU vectors, we considered only vectors that were significant as well as strong contributors to the variance in SIMPER analysis, *i.e.* the top 30 OTUs that were identified in pairwise analysis of the NMDS groupings (Group 1, 2, 3, carbonates) by contribution to the variance.

Seafloor Surveys with Sentry

Seafloor surveys were conducted using WHOI's autonomous underwater vehicle (AUV) Sentry. Sentry is equipped with sidescan sonar, a Reson 7125 multibeam echosounder, and a down-looking digital color camera, enabling bathymetric and photographic data collection. In 2017 and 2018, Sentry was deployed from R/V Atlantis, completing four dives at Mound 12 that were analyzed in this study. In the photo survey portion of each dive, Sentry moved back

and forth on tightly spaced tracks (*i.e.* "mowing the lawn") following a preset navigation plan. Moving at an average speed of 0.57 m/s, Sentry traveled 81.66 km in total across the four dives (#431, 432, 502, 507), at approximately 5m altitude, and took ~ 20 photos per min. Out of a total of 36,612 downward-facing photos, 332 photos were annotated with yeti crabs. For photos with clear visibility, the presence of seep foundational species including bacterial mats, vestimentiferan tubeworms, vesicomyid clams, bathymodiolin mussels, and serpulid tubeworms were noted and used as seep indicators, analogous to (Goffredi et al., 2020). In ArcGIS 10.6.1, these species presences were resampled into 5 m grid cells in the survey area to include only spatially explicit presence points, and they were mapped over multibeam bathymetric data collected by *Sentry* (**Fig. 2.1**). Dive metadata is available in **Table 2.5** and a map of dive tracks and the full ecological map are provided in **Fig. 2.6**.

Spatial Analysis

For spatial analysis of DNA data, we first calculated the approximate radius of the Earth at sea level at Mound 12, *R*, according to:

$$R = \sqrt{(r_1^2 \cos L)^2 + (r_2^2 \sin L)^2 \Big/ (r_1 \cos L)^2 + (r_2 \sin L)^2}$$

where r_1 is the radius of the Earth at the equator, r_2 is the radius of the Earth at the poles, and *L* is the latitude of the Mound 12 area (8.93). We then subtracted 1000 m from *R* since the seep at Mound 12 ranges from 995 m to 1005 m deep, such that R_{depth} = 6,376,626 m. We then estimated the distance between any two points in meters, *D*, according to:

$$D = R_{depth} \cos^{-1}[\sin(\omega lat_1) \sin(\omega lat_2) + \cos(\omega lat_1) \cos(\omega lat_2) \cos(\omega lon_2 - \omega lon_1)]$$

where *lat* and *lon* represent the latitude and longitude of points 1 and 2 and ω is the conversion factor from degrees to radians, $\pi/180$.

When computing the correlation of geographical distance from the seep area to sediment microbial community dissimilarities, we limited our analyses to those sediment cores from the main southwestern seep area and did not consider cores from the southeastern seep area (dubbed the "Little Knoll") or inactive cores. Although cores from the Little Knoll were included for assessing geochemical characteristics of active sites, because the active site is physically separated by ~0.5 km of inactive background sediment, we did not expect the

communities to interact in any significant way. Inactive cores were similarly not included for spatial analysis because our study was focused on the dynamics of the active site and our sampling of background sediment was likely insufficient to meaningfully examine the subtler changes in broader benthic ecology on large scales.

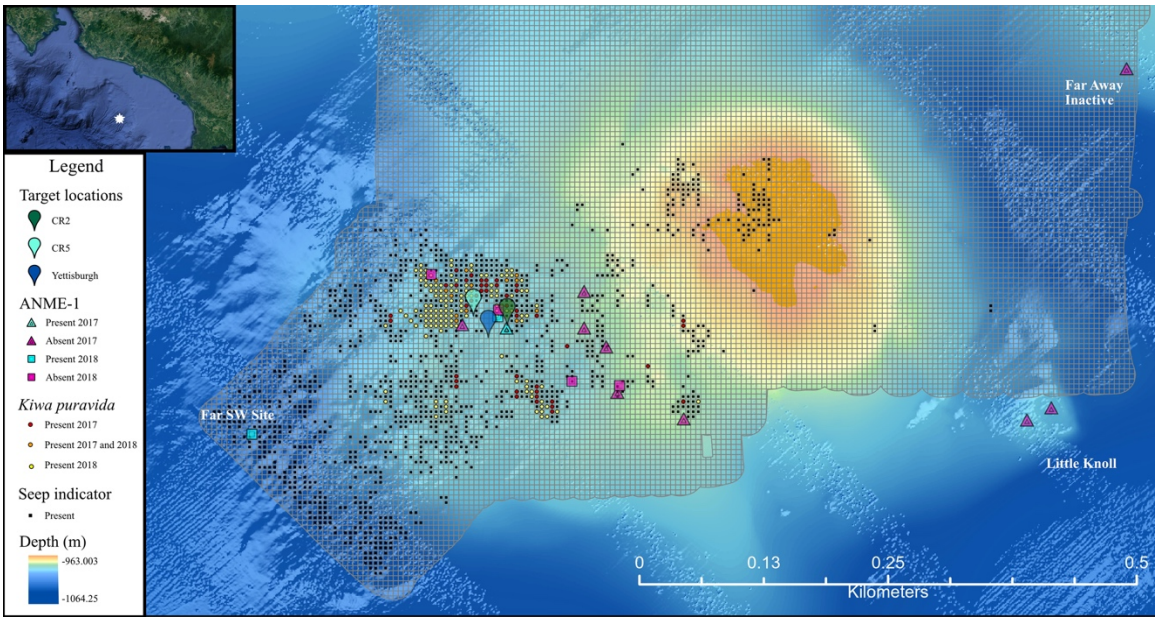

Fig. 2.1: Annotated map of Mound 12. (Inset) Mound 12 is located on the Pacific margin of Costa Rica and marked with a star. The mound itself rises ~50 m above the seafloor, but the main region of seepage is to the southwest. Seafloor photos from *Sentry* were analyzed for evidence of active seepage and resampled into a 5x5 m grid overlaid on top of bathymetry also obtained by *Sentry*. Evidence of general seep activity in the form of known chemosynthetic fauna is indicated by markers in the grid, with *K. puravida* specifically noted. Seafloor markers placed in 2009 are similarly noted, which indicated areas of high activity at that time. 8-9 years later, *K. puravida* populations appear to have migrated ~20 m W-SW. Sediment cores are also noted and colored specifically according to the presence of abundant ANME-1 organisms in the upper 4 cm. Auxiliary sites, including the far southwest site, Little Knoll, and distant inactive site are noted.

Results

AUV *Sentry* maps and *K. puravida* presence

Geotagged photos obtained by AUV *Sentry* were manually flagged for the evidence of Costa Rican yeti crabs (*Kiwa puravida*) as well as general expressions of seep activity (bacterial mats, etc.) and then used to create an overall distribution map (**Fig. 2.1**) This exercise revealed that the predominant area of seepage activity was in the southwest of Mound 12. The majority

of the *K. puravida* clustered in a ~30 m radius area. Comparing photomosaics from cruises in 2017 and 2018 revealed that the *K. puravida* population moved ~15 m west-southwest in the 16 months between the two cruises, perhaps in response to changing geochemical conditions. Additionally, the markers for "Yettisburgh," Site CR2, and Site CR5 (which were placed in 2009 as indicators for abundant *K. puravida*) had few proximal *K. puravida*, further supporting the observation that the majority of the yeti crab population had shifted westward. *Sentry* dive 507 mapped a region further to the southwest than previous dives and provided evidence of previously unknown methane seep activity. Using *Alvin,* we were able to specifically target this area (AD4987) and take several additional cores for comparison with the main site (discussed below).

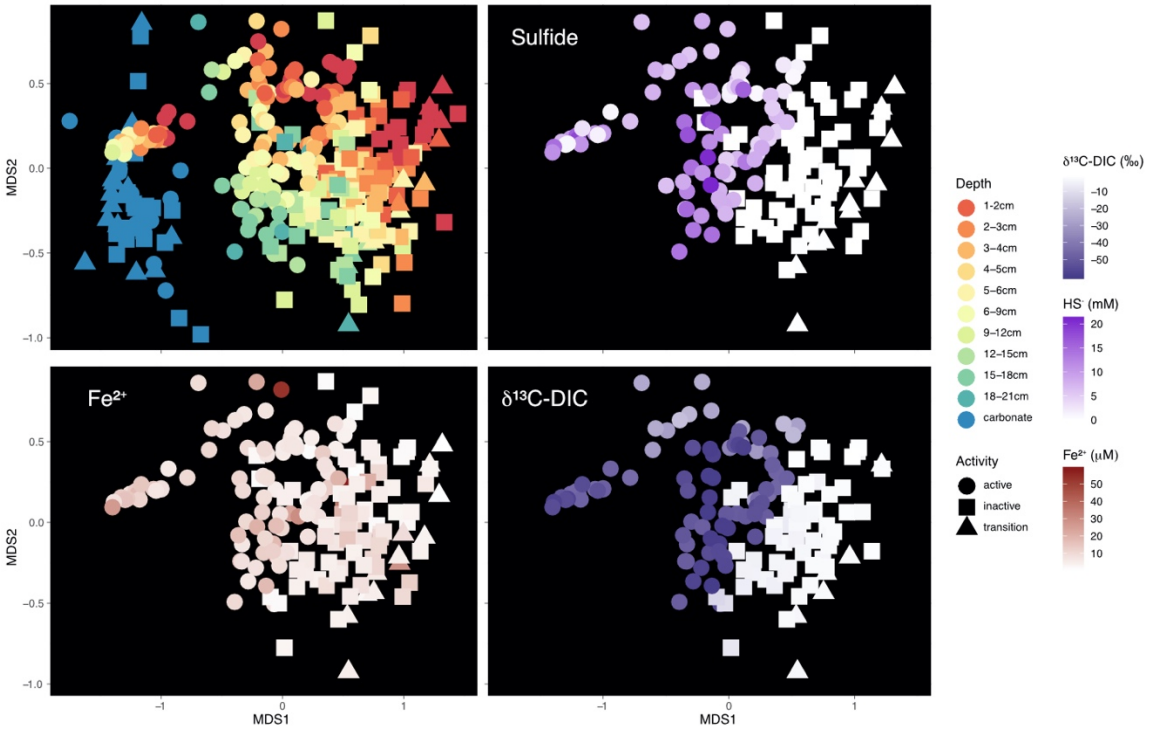

Fig. 2.2: NMDS of all samples analyzed, using Bray-Curtis dissimilarities of fourth-root transformed relative abundance data (Stress = 0.137). All panels utilize the same ordination. **A:** NMDS of all samples, including carbonates. Samples are colored by depth horizon for sediment samples, treating all carbonates as one depth bin. **B, C, D:** Geochemical data of the sediment porewater was overlaid on the sample points in the NMDS for $\delta^{13}C\text{-}CO_2$, sulfide concentrations, and ferrous iron concentrations, respectively. Active samples showed universally higher sulfide and ferrous iron and more negative $\delta^{13}C\text{-}CO_2$ than transition or inactive samples.

Microbial community diversity and ordination

To characterize the microbial community structure and assess similarities between sample sites, substrates (carbonate versus sediment), and methane activity venting level (active, transition, inactive), we used an NMDS ordination of each sample in this study, where the distance between any two points is related to the dissimilarity of their microbial community composition (**Fig. 2.2a**). The ordination illustrates several broad patterns that emerged within this ecosystem-wide dataset. The microbial assemblages of carbonate samples were generally similar to each other, independent of whether those carbonates were collected from an active, transition, or inactive sampling site, whereas sediment communities were clustered into three broad groups (simply called Group 1, Group 2, Group 3). We observed strong spatial auto-correlation within the sediment samples; identifiers demarcating samples from unique pushcores were the best predictor for variance (ANOSIM R Value = 0.6917, p-value = 0.001). In fact, even GPS coordinates were not as correlated with variance as individual pushcore identifiers (R Value = 0.4839, p-value = 0.001), indicating that paired cores, which are taken within a ~1 m^2 area (and assigned the same GPS coordinates) are measurably different from one another.

Sediment samples also varied strongly with activity classification (R Value = 0.4443, p-value = 0.001), which was a better predictor for community composition within sediments than depth, which was significant but a comparatively small contributor to overall variance (R Value = 0.1056, p-value = 0.001). Three groupings of sediment samples emerged from the ordination corresponding to: four active cores from Yettisburgh, so-named in 2009 for the abundant *K. puravida* in the area (Group 1), sixteen cores from active seeps elsewhere at Mound 12 (Group 2), and a group comprised of eleven transition and inactive core samples (Group 3). Group 1 cores ordinated closest to the carbonates, highlighting the community similarity between these samples. Group 1 cores were also unusual in that they displayed very little variance with depth, indicating that the community composition was similar throughout the length of the sediment core. Group 1 sediment cores were also shorter than average, no more than 12 cm deep, because coring attempts at that location frequently hit hard pavement at depth.

Group 2 cores were collected from seep areas characterized by vestimentiferan tubeworms, vesicomyid clams, and bathymodiolin mussels, but rarely near *K. puravida*. Unlike Group 1 samples, the community composition of these cores did vary significantly with depth, and Group 2 cores had the highest dissimilarities between their shallowest and deepest horizons.

Group 1 and 2 cores did not have significantly different Shannon diversities, however, as assessed by a Welch's *t* test on the average of the diversity of each horizon (6.616 vs 6.555), although the variance of Group 2 diversities was significantly higher (0.0355 vs 0.7786, F-test p-value = 0.046).

Group 3 samples, which consisted of transition and inactive area sediments had an average Shannon diversity of 7.284, which was significantly higher than both Group 1 and Group 2 (p-values both < 0.001). The shallower horizons of AD4908-PC8 and AD4909-PC9 contained even higher relative abundances of *Anaerolinea* than other Group 3 cores in the shallower sediment horizons, but followed the trend of the other transition and inactive cores at depth. These two cores were also processed shipboard the morning after their retrieval, and it is possible that the delay in processing affected the communities closest to the sediment-water interface.

Dominant sediment species by ordination group

Examining the dominant microbial OTUs in each ordination group revealed the taxa which characterized each sediment community and were responsible for driving the variance between them (**Fig. 2.3, Fig. 2.7**). In general, carbonates and active cores from both Group 1 and 2 are dominated by ANME, polyphyletic anaerobic methanotrophic archaea within the *Euryarchaeota*. Although these organisms perform the same overall metabolism, they are distinct phylogenetically: ANME-1 comprise their own family-level division, whereas ANME-2 comprise two groups that lie within the *Methanosarcinales* (Knittel and Boetius, 2009; Chadwick et al., 2020). The specific subgroups of ANME that are abundant in each individual change ordination group are different and are the highest contributors to the variance between them.

The microbial diversity recovered from all carbonates (n = 49) had abundant endolithic ANME organisms, specifically ANME-1, which comprised 43.1% of the community on average. Carbonates were the only sample group to contain a higher proportion of sequences belonging to ANME-1 than ANME-2, which were dominant in active sediments, consistent with other seep carbonate studies (Marlow et al., 2014a; Case et al., 2015; Mason et al., 2015). Archaeal OTUs made up the largest proportion of sequences when binned by genus-level taxonomy; 8 of the top 10 OTUs were archaea, including one Lokiarchaeota OTU. Abundant bacterial OTUs were affiliated with *Thiohalophilus* (2.5%), a Gammaproteobacterium, and the SEEP-SRB-1 clade (1.4%), belonging to the *Desulfosarcinaceae* that is a common syntrophic SRB

partner to ANME (Orphan et al., 2001a; Schreiber et al., 2010; Ruff et al., 2015). Notably, carbonates contained the lowest relative abundance of SEEP-SRB-1, even lower than Group 3 samples. Although other groups of deltaproteobacterial SRB were still detected in carbonates, the total abundance of SRB in carbonates was still lower than in active seep area sediments, consistent with other studies of endolithic seep communities (Marlow et al., 2014a; Case et al., 2015).

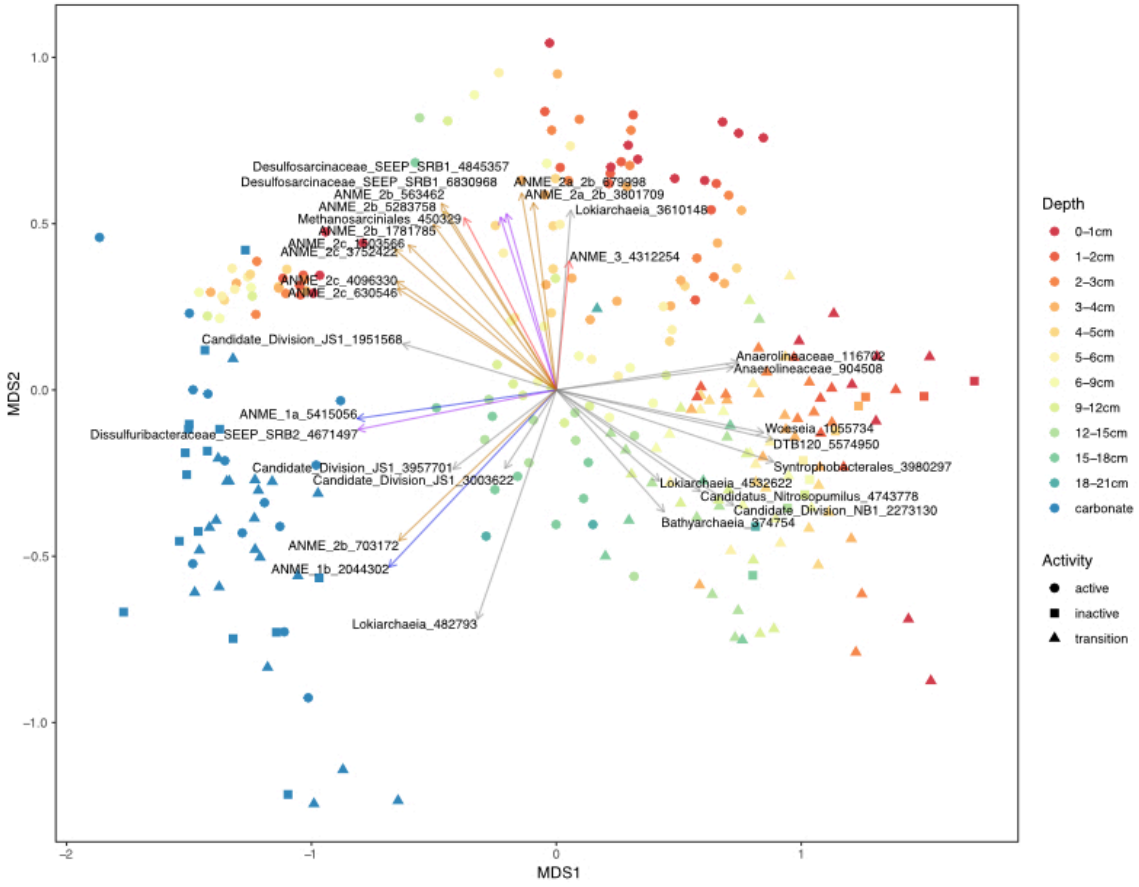

Fig. 2.3: NMDS ordination of all Mound 12 samples with fitted vectors for OTUs responsible for driving differences between ordination groups. Each OTU was fitted to the ordination using *envfit* and assigned a p-value. The top 30 OTUs with p-value = 0.001 that also appeared in pairwise SIMPER analysis by ordination Group (carbonates, 1, 2, 3) are displayed here. Vectors corresponding to ANME-1 OTUs are colored blue, ANME-2 vectors are colored orange, and other possible ANME OTUs are colored red. OTUs for SRB are colored purple. The remaining OTUs correspond to putative heterotrophs or nitrogen-metabolizing organisms.

Group 1 sediment samples, from active seepage areas within the Yettisburgh site, cluster close to the carbonate samples and similarly contained high relative abundances of ANME-1 organisms in addition to ANME-2c. *Desulfosarcinaceae* genera were more abundant in Group 1 sediments than in carbonates (5.6%), and SEEP-SRB-2 organisms, a known partner of ANME-1 from family *Dissulfuribacteraceae*, were also in the top 10 OTUs at 2.9% relative abundance. As noted above, the contribution of depth to variance within the Group 1 samples was small (ANOSIM R Value = 0.1876, p-value = 0.005). Relative abundance changes in two taxa were most responsible for driving variance with depth: decreasing abundance of ANME-2 and increasing abundance of Candidate Division JS1, a class within phylum Caldatribacteria that has been implicated in fermentation and syntrophy metabolisms (Lee et al., 2018).

Group 2 samples, composed of sediments from other seep locations aside from Yettisburgh, were characterized by high relative abundance of ANME-2a and 2b in all depth horizons. Group 2 displayed the highest depth-related variance (R Value = 0.2617, p = 0.001), however, and the primary OTUs driving differences by depth were assigned to different ANME-2 lineages (SIMPER analysis). Specifically, OTUs dominating shallow depth horizons were identified as belonging to the ANME-2a-2b subdivision, while deeper horizons contain more abundant ANME-2c. This depth-related variation in ANME clades points to niche differentiation among methanotrophic archaea observed in the sediment, consistent with other studies that have examined ANME lineage differentiation in the sediment (Roalkvam et al., 2011; Roalkvam et al., 2012). Other organisms that became more abundant with depth included Deltaproteobacteria members of the SEEP-SRB-1 group as well as OTUs identified as Candidate Division JS-1 organisms (a class of Candidate Phylum Caldatribacteria). Notably, the second most abundant group genus-level taxonomic bin in Group 2 belonged to *Anaerolineaceae* (9.0%), which was only exceed in relative abundance by Group 3 samples (14.0%; Groups 1 and 2 were 1.1% and 1.6%).

Group 3 sediment samples, standing in contrast to carbonates and Groups 1 and 2, had very low abundances ANME OTUs. No genus-level bin of ANME exceeded 1% average relative abundance. In 6 samples, 0 reads were detected from any of the 14,796 ANME-identified OTUs. Instead, Group 3 sediments were dominated by Deltaproteobacteria OTUs from order Syntrophobacterales and uncultured members of *Anaerolineaceae*, a family within the phylum Chloroflexi believed to primarily act as fermenters and syntrophic heterotrophs

(Sekiguchi et al., 2003; Sewell et al., 2017). The most abundant OTU across all Group 3 samples belonged to Syntrophobacterales and 25 of the top 50 OTUs within Group 3 samples were identified as belonging to *Anaerolineaceae*. These organisms are abundant in marine sediments and likely play a role in the oxidation of complex organic matter as it is buried. Other abundant OTUs in Group 3 were associated with Bathyarchaeota (formerly Miscellaneous Crenarchaeotal Group), Lokiarchaeota (formerly Marine Benthic Group B), bacterial Candidate Phylum DTB-120, *Candidatus* Nitrosopumilus (formerly Marine Crenarchaeota Group 1, and the SG8-4 family of planctomycetes. Despite the large number of OTUs putatively associated with syntrophic lineages in our samples, conventional syntrophic partners like methanogens were rare; *Methanococcoides* was the most abundant, making up 0.07% of the Group 3 community on average.

Spatial analysis

We used spatial statistics to identify which sediment samples collected at Mound 12 were taken closest to the center of the seepage area. Because accurate *in situ* methane concentrations are difficult to measure in deep sea seeps, we focused on using the sediment microbial community of a pushcore as an indicator for the local geochemistry and correlating Bray-Curtis dissimilarity of two sites with their distance from one another. Under this framework, our first step was to find the correlation between the pairwise dissimilarity and distance of all active sites. We excepted transition and inactive samples outside the ~150 m radius active area, as well as those active pushcores that were taken at the smaller mud mound to the southeast of Mound 12 (the "Little Knoll") in order to focus on the main seepage area to the southwest and to avoid confounding our analysis with separated areas. The Spearman correlation coefficient for the generalized distance vs. dissimilarity comparison was 0.4015 (Mantel test p-value = 0.001). This analysis assumes that the active area has a central point, and that activity shifts concurrently with distance outward from that point in any direction. We expect any two communities to increase in community dissimilarity with increasing distance, but substituting the generalized distance matrix for one predicated on distance from the correct central core should provide a higher correlation than the generalized distance. Using a central point as the basis for the distance calculation allows for cores along opposing radii from the center to nevertheless contribute positively to the correlation if they are biologically similar, or negatively if not. After comparing the Spearman correlation coefficients of dissimilarity with distance, treating each active core as

a potential center, the highest Spearman correlation coefficient was obtained using the Group 1 cores close to Yettisburgh as the central point (0.5845, p-value = 0.001).

Geochemistry

The porewater from a subset of sediment cores was analyzed for anions and cations, DIC, and δ^{13}C-DIC and δ^{18}O (see supplementary data file); a subset of the chemical species are presented in **Figure 2.2** as a color saturation for each sample in the ordination. Comparing this data with community composition, sulfide and ferrous iron were higher in Group 1 and 2 active cores versus Group 3 (transition and inactive cores), and δ^{13}C-DIC was lower on average (11.6 vs. 6.0 μM Fe^{2+}; 8.32 vs 0.06 mM HS^-; -47.50 vs. -2.19‰ δ^{13}C-DIC), consistent with the classification of active seep cores and supporting 16S diversity data. Each of the differences were significant, as assessed by a Welch's unpaired *t* test (each p-value < 0.001). The increased sulfide and more negative δ^{13}C-DIC within active seep cores are consistent with the dominance of ANME archaea identified in the 16S rRNA survey that mediate sulfate-coupled anaerobic oxidation of methane with syntrophic SRB. The presence of ferrous iron may be the result of deep fluid advection, overall increased microbial respiration deriving from higher rates of carbon cycling in this region, or even iron-mediated AOM (Sivan et al., 2011; Levin et al., 2016).

Although the microbial community differences between Group 1 and Group 2 active cores were significant, the porewater geochemistry was more similar. Overall, the average values for sulfide and ferrous iron concentrations, and δ^{13}C-DIC were not significantly different between the two groups of samples, as assessed by a Welch's unpaired *t* test. However, the variance of the δ^{13}C-DIC in Group 1, Yettisburgh samples was indeed significantly lower than Group 2 seep samples (23 vs. 58‰, p = 0.029) as assessed by a two-sample F test. The primary source for the difference in variance is among the shallowest sediment horizons, which are more typically 20-25‰ higher than rest of the core, indicating that the porewater mixes with the overlying seawater. In Group 1 cores, the shallowest horizons are only 2-4‰ higher on average instead, indicating that more of the DIC in those horizons' porewater is sourced from methane oxidation. Additionally, although cation data from these cores is limited, one Group 1 and one Group 2 core were measured (AD4906-PC8 and AD4907-PC3, respectively). Notably, the Group 1 core showed significantly higher calcium concentrations, on average, than the Group 2 core (18.71 vs. 6.11 mM, p-value < 0.001) as well as higher than the typical Ca concentration

in seawater of ~10 mM. Fitting the vectors for sulfide, iron (by ferrozine assay) and δ^{13}C-DIC onto the microbial community ordination of the sediments was also performed; each of those geochemical parameters was significant and similarly indicated that samples from Groups 1 and 2 had higher iron, higher sulfide, and lower δ^{13}C-DIC than those from Group 3 (**Fig. 2.9**).

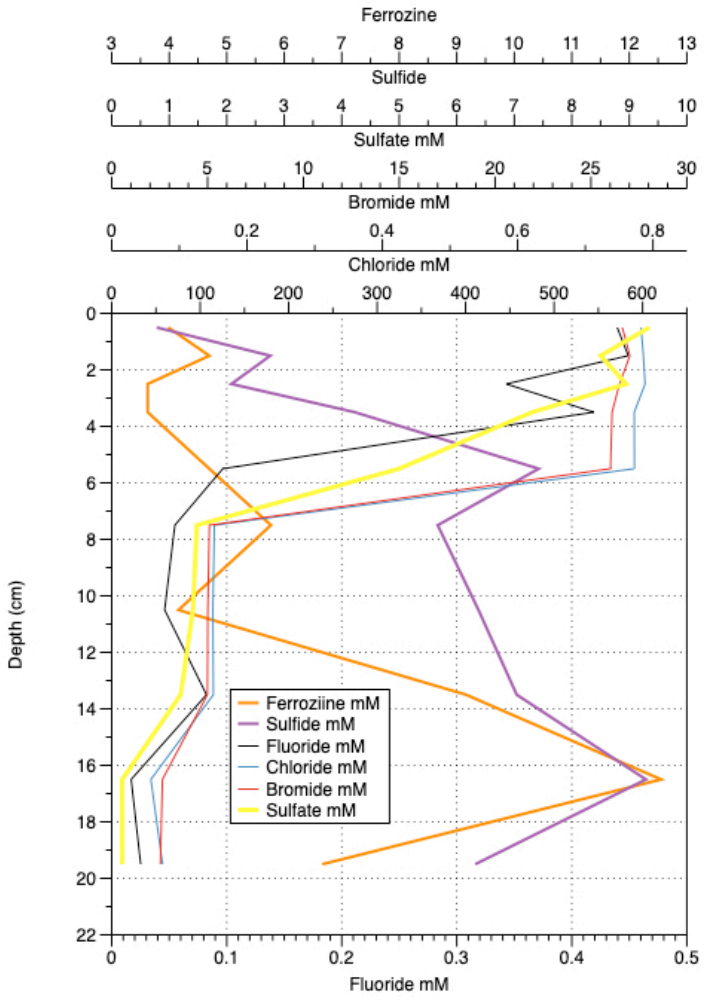

Fig. 2.4: Geochemical depth profile of AD4987-PC7. This core was taken to the southwest of the main active site. Notably, concentrations of fluoride, bromide, and chloride decreased dramatically starting at about 4 cm depth, a trend observed in no other Mound 12 core we analyzed, indicating significant freshwater input, likely from deeper hydrothermal fluids.

The additional core taken from a seep area to the southwest of the main site (bottom left of **Fig. 2.1**) had a unique geochemical profile for this site (**Fig. 2.4**). At this site, porewater concentrations of iron and sulfide were consistent with the other Group 1 and 2 cores (maximum values 12.6 μM and 9.29 mM respectively). The concentrations of bromide, chloride, and fluoride, however, which typically change very little with depth in other Mound 12 cores and reflect background seawater values, changed significantly in this core from seawater values in the upper 4 cm near the seabed to a minimum at the lowest horizons recovered (18-21 cm). Each species decreased by at least an order of magnitude: bromide from 0.7658 mM to 0.0719 mM, chloride from 602.83 mM to 44.26 mM, and fluoride from 0.449 mM to 0.017 mM. No other core we analyzed at

Mound 12 had a similar variation in conservative tracers, and our results may indicate that this core was taken in a direct flowpath of deeply-sourced hydrothermal fluids.

Discussion

Assessing the center of the methane seepage region

Mound 12 is a 50 m tall mud volcano with the primary region of methane seepage oxidation to the southwest. Although we observed some evidence of a seep activity at the top of the mound and at a smaller mound to the southeast, the region to the southwest contained the most extensive carbonate platforms and highest density of seep-associated fauna (**Fig. 2.1**). During *Alvin* observation, samples taken in locations with fewer observable seep fauna were labeled as "transition." These samples typically had observable bathymodiolin mussels and vestimentiferan tubeworms, but they were less abundant and often overgrown with hydroids or other non-seep fauna. Transition sites were not significantly different microbially or geochemically from "inactive" samples, indicating that within the sediment, methane oxidation is highly localized. Few clams were observed at transition sites, supporting the lack of sulfide we measured in sediment porewater. Other studies have similarly indicated that the anaerobic methane oxidizing microbial community is highly localized, often limited to locations with visible microbial mat at the sediment-water interface (Lloyd et al., 2010; Green-Saxena et al., 2014). The transects performed in this prior studies are typically limited to the immediate edge bacterial mats overlaying abundant ANME in the sediments, but they also observed low abundances of ANME deeper in the sediment. We also detected low abundances of ANME (1-3%) in the lower portions of transition cores (typically below the 6-9 cm horizon), whereas inactive cores contained virtually no ANME, but these differences were not enough to distinguish the cores statistically. The seep animals that live in transition sites are unlikely to survive based on the sulfide generated by these deep ANME, and more likely rely on small amounts of sulfide or other energy-rich chemicals carried by benthic currents away from the active areas or perhaps AOM carried out by ANME in the carbonates (Marlow et al., 2014b).

Our results indicate that Group 1 cores, all of which were taken at a marker labeled as "Yettisburgh," represent the sediment cores closest to the center of methane seepage. Firstly, the average microbial community of Group 1 cores are most similar to the endolithic community of authigenic seep carbonates (**Fig. 2.2, Fig. 2.7**), with high relative abundances of ANME

lineages present even at the shallowest depth horizons, especially from the ANME-1 subclade. The carbonates themselves form as a result of sulfate-coupled AOM, and evidence suggests that although endolithic communities are still active and are not simply fossilized, the carbonates support similar archaeal and bacterial taxa as occurs in the seeps (Marlow et al., 2014b; Mason et al., 2015). The Yettisburgh sediment cores were also the most internally consistent, and displayed the lowest community differentiation along the length of the core, indicating that methane concentrations were sufficiently high to support anaerobic methane oxidation throughout.

The geochemistry of Group 1 cores was similar to other active cores with respect to maximum sulfide and ferrous iron concentrations, but notably had very low δ^{13}C-DIC values even in the shallowest sediment horizons, indicating high rates of AOM and an overall upward flow path of porewater that limited mixing with overlying seawater. Prior studies of the geochemistry at Mound 12 indicates that the methane-rich fluids are deeply sourced from the subduction channel and pass through a serpentinizing zone, which would enrich them in calcium, although because calcium is also consumed during authigenic carbonate formation, porewater concentrations can sometimes fall below seawater values (Hensen et al., 2004; Tivey, 2007; Lilley and Von Damm, 2008; Tryon et al., 2010; Joseph, 2017). The Group 1 core measured for dissolved cations showed significantly higher Ca concentrations than the Group 2 core (18.71 vs. 6.11 mM on average) and was almost double the typical seawater value of ~10 mM, further supporting the hypothesis that Group 1 cores had higher influx of enriched fluids. Additionally, our spatial analysis indicated that the change in microbial community composition of our cores is strongly correlated with their distance from the Yettisburgh cores specifically, with a higher correlation coefficient for this site than using any other active core as the reference point and higher than a no-reference comparison. Mantel tests used to test the significance of spatial correlation in this way are subject to increased Type I (false positive) error rates, especially if they are performed on community distances with unknown heteroscedasticity (Guillot et al., 2013; Legendre et al., 2015). For this reason, we used Bray-Curtis dissimilarities to calculate pairwise sample comparisons and calculated the correlation coefficients for each core in the sampling area (not just the cores of interest) to ensure that the correlation with distance for Yettisburgh sediment cores was not only significant (which was true of many of our tests) but

the highest of our sampled locations. When considered together, our microbial community, geochemical, and spatial analyses provided strong support for the hypothesis that sediment cores at Yettisburgh were the closest to the center of the area of methane seepage.

Temporal dynamics of Mound 12

Our photomosaics of the Mound 12 seafloor obtained by *Sentry* in 2017 and 2018 indicated that the *K. puravida* population had shifted towards the southwest by 5-15 m in the intervening 16 months between the *Sentry* scans. Additionally, the markers for Yettisburgh, CR2, and CR5 were placed in 2009 on a previous expedition to denote high populations of *K. puravida*. The sediments and carbonates surrounding these markers did not have high local populations of *K. puravida* in either 2017 or 2018, further supporting the observation that population of *K. puravida* at Mound 12 had migrated westward over time. Unique among chemosynthetic seep fauna, *K. puravida* are highly mobile, and it is likely these crabs migrated in response to changing local benthic sulfide concentrations to fuel their symbiotic microorganisms. Although little is known about the migratory behavioral patterns of *K. puravida*, specimens of the related species, *Kiwa tyleri*, were reported in areas away from the hydrothermal vents that sustain them (Thatje et al., 2015). Still, that behavior has been limited to brooding females presumably seeking milder conditions for embryogenesis and would not explain the population-level migration we observed at Mound 12.

Notably, sediment cores that contained abundant ANME-1 microorganisms (Group 1 in the NMDS ordination) did not follow the same spatial as the *K. puravida*. Instead, these cores from were taken in nearly the same location in both 2017 and 2018, close to the Yettisburgh and Site CR5 markers (**Fig. 2.1**). If *K. puravida* is indeed responding dynamically to changing geochemical conditions, the photomosaic analysis and the spatial analysis of sediment cores (above) are not in agreement, since Group 1 cores were found from within the same ~25 m^2 area in both 2017 and 2018. There are several possibilities that would explain the discrepancy. First, although we did not collect data benthic currents or flowpaths, it is possible that they carry sediment-derived sulfide westward through the benthic water column. If so, the *K. puravida* population would likely shift in tandem with the current dynamics, which may be seasonal or follow some other dynamic pattern. Second, even if *K. puravida* does respond dynamically to geochemical conditions, it is possible that the concentrations of sulfide, methane, or oxygen are not suitable in the center of the seep and that they prefer to be somewhat removed. Although

the specifics of chemotaxis and sulfide tolerance of *K. puravida* is unknown, another hairy crab with sulfide-oxidizing symbiotes, *Shinkaia crosnieri*, has been observed to survive aqueous sulfide concentrations up to 0.53 mM *ex situ* and the sulfide oxidation rate was measured at 5 μM/min/individual (Watsuji et al., 2017). Since *S. crosnieri* individuals are roughly half the size of *K. puravida,* it is likely that *K. puravida* has an even higher sulfide tolerance and is able to safely live anywhere in the Mound 12 benthos. Third, *K. puravida* appears to prefer to take refuge on a rocky carbonate substrate, and all of the associated geochemistry is associated with sediment cores, often 15 meters away from the closest yeti crab. See **Fig. 2.8** for an image of a party of *K. puravida* grouped together on a carbonate immediately adjacent to a bacterial mat that was discovered to contain abundant ANME-1. It is possible, therefore, that the center of methane seepage has indeed shifted towards the southwest, but because that area was uncoreable, the change was not appropriately reflected in the sediment samples we collected.

The unusual sediment core taken in a bacterial mat ~0.25 km southwest of Yettisburgh may provide some insight into the question posed above. Although young vesicomyid clams (**Fig. 2.8**) were observed adjacent to the bacterial mat, no nearby carbonate or *K. puravida* were observed with *Alvin* or *Sentry*. The core analyzed from this area contained abundant ANME-1 organisms, similar to Group 1 cores from Yettisburgh, but the bromide, fluoride, and chloride concentrations decreased dramatically starting in the 4-5 cm horizon. This signal may indicate that the far southwestern core, AD4987-PC7, had significant input from deeply-sourced fluids. As part of the formation of a hydrothermal seep, seawater within the ocean sediment interacts with heat from the underlying subducting slab. As the seawater does so, it interacts geochemically, frequently leaching metals like iron and manganese while depositing others like magnesium. Dewatering of the deep smectite clays also occurs with the increased temperature (estimated ~100 ºC) and pressure, and the fresher fluids, now enriched in dissolved metals and gasses, return to the surface and suffuse the seafloor sediment (Tivey, 2007; Lilley and Von Damm, 2008; Tryon et al., 2010). The lack of nearby *K. puravida* would seem to contraindicate the possibility that benthic currents are primarily responsible for *K. puravida* distribution, since the paths connecting Yettisburgh to the southwestern ANME-1-containing core and Yettisburgh to the bulk of the *K. puravida* population are not aligned. The presence of vesicomyid clams at AD4987-PC7, which dig into the sediment to access sulfide, also implies that geochemical conditions alone are not preventing colonization by *K. puravida.* The clams at this

location were small, only about ~4 cm long (**Fig. 2.8D**). Although the specific clams at this site were not collected for identification and the growth rates of many vesicomyids are not well quantified, *Calyptogena kilmeri*, a seep-associated species, grows up to approximately 10 cm in length, and reaches an average length of 4 cm after about 2 years (Barry et al., 2007). Considering the potentially young clams and the lack of visible carbonates or other seep fauna in the vicinity, it seems likely that the seepage in this area is relatively new. The lack of carbonate may be a primary driver for the lack of *K. puravida* presence. Other studies have indicated that marine invertebrates that live in the sediment, such as dorvilleid polychaetes or clams, act as primary colonizers, and hard ground-preferring fauna, including yeti crabs, mussels, and tubeworms may colonize these new seepage areas more slowly (Giovannoni and Cary, 1993; Van Dover, 1994; Hilario et al., 2005; Levin et al., 2006).

Comparison of Mound 12 to other seep environments

A recent meta-analysis of the global microbiome revealed that many methane seeps worldwide are colonized by similar taxonomic classes of organisms, though the exact genera or species change from region to region (Ruff et al., 2015). Halobacterota, the ANME-containing archaeal phylum (formerly Methanomicrobia) was the dominant taxon of archaea, with lower relative abundance of Bathyarchaeota and Thermoplasmata. The top three classes of bacteria belonged to the Candidate Division JS-1, heterotrophic Gammaproteobacteria, and Deltaproteobacteria, which includes many of the sulfate-reducing partners of ANME. The sediment microbial community in the active area of Mound 12 is mostly consistent with these results. The analysis by Ruff, et al. indicated that ANME from the 2ab subgroup were, on average, the most common within active seeps. ANME distribution and diversity at Mound 12 was variable across seep sites and with depth. ANME-2ab clades were common within Group 2 cores, however, ANME-1 and ANME-2c organisms were more abundant within Group 1 cores. Since Group 2 cores were more common in our exploration of Mound 12, however, the results still agree with the Ruff, et al. analysis. Although sediment cores from Mound 12 did contain abundant Deltaproteobacteria (primarily *Desulfobacterales*) and Candidate Division JS-1, Gammaproteobacteria were markedly less abundant than at other sites analyzed by Ruff, et al. Instead, *Anaerolinea* were more common in our analysis, especially in Group 2 and Group 3. Since *Anaerolinea* are also typically chemoheterotrophs, it seems likely that Mound 12 simply has a different suite of carbon-degrading heterotrophs than other similar sites (Sekiguchi et al., 2003).

One of the key findings of our study was that ANME-1 archaea were more abundant in the four sediment cores close to Yettisburgh, which we identified as the center of the area of elevated methane fluid advection. ANME-1 are frequently observed deeper in the sediments than ANME-2a-2b, although the specific ecological and environmental forces influencing this partitioning are not well understood (Roalkvam et al., 2012). Past studies have proposed conflicting interpretations of whether ANME-1 or ANME-2 archaea are better adapted to higher methane concentrations. A study at Black Sea "reefs" indicated that ANME-2 dominated in locations with observable methane ebullition, but *in vitro* studies have indicated that ANME-1 can outcompete ANME-2 in high-methane environments (Blumenberg et al., 2004; Girguis et al., 2005). At Hydrate Ridge, sediment samples with high ANME-1 relative abundance were found to contain more total ANME aggregates than those with only ANME-2, perhaps indicating ANME-1 colonize locations with higher methane concentrations (Marlow et al., 2014a).

Some ANME-1 have been observed as single cells or segmented rods without closely associated bacteria, raising the question of whether they grow loosely associated with SRB or are capable of oxidizing methane without a syntrophic partner (Orphan et al., 2002; Knittel et al., 2005; House et al., 2009). Recently, some studies have suggested some ANME-1 not only perform anaerobic methane oxidation but also methanogenesis, which has made assigning ecological functionality to this group even more difficult (Lloyd et al., 2011; Beulig et al., 2019). Crystal structures and phylogenetic trees of the methyl-coenzyme M reductase (MCR) enzyme, which catalyzes methane generation in methanogens or methane activation in ANME, indicate that the ANME-1 version of the protein is the most similar to that of true methanogens (Shima et al., 2011). Nevertheless, the sulfide concentration and δ^{13}C-DIC signal in Group 1 samples indicate that the ANME-1 at these sites are performing methane oxidation, and ANME-1 are often found in net methane-oxidizing environments, including in some areas where no other methanotrophic taxa were detected (Teske et al., 2002; Lloyd et al., 2006; Harrison et al., 2009; Stokke et al., 2012; Gründger et al., 2019). In particular, a recent study at a gas hydrate pingo (a type of gas mound) observed ANME-1-dominated sediment microbial communities similar to the Yettisburgh sediment assemblage and enriched in Candidate Division JS-1, *Anaerolinea*, and *Desulfobacteraceae* bacteria (Gründger et al., 2019).

Implications for seep habitats

Our finding that the microbial communities of transition zone sediments and inactive sediments are indistinguishable has implications for seep habitats in general. Although transition sites did host chemosynthetic fauna, there was no evidence that methane oxidation sufficient to support them was occurring in the proximal sediments. Other studies, which have examined areas surrounding seep bacterial mats, have found the microbial community is indeed highly localized to the mat area, and our study expands that finding further into the seep periphery (Lloyd et al., 2010; Green-Saxena et al., 2014). The chemosynthetic animals at transition sites are likely relying on the less traditional sources of sulfide, including distribution through the benthic water column or low fluxes of sulfide out of carbonates from endolithic ANME assemblages (Marlow et al., 2014b). This finding highlights that the presentation of methane seeps as viewed by observers in remotely operated vehicles or submersibles may not precisely reflect where the bedrock metabolism of these seeps, anaerobic methane oxidation, is occurring. The "transition" in the sediments may be occurring even in places where chemosynthetic seep fauna are abundant and active, as evidenced by the decreased relative abundance of methanotrophs and increased abundance of heterotrophs like *Anaerolinea* in our Group 2 sediment cores, as well as the increased variance in the Group 2 diversity.

These findings warrant additional caution be exercised in the field of deep seabed mining. Seeps and vents have recently been targeted by mining companies because of their comparative richness in hydrocarbons and metals, including massive polymetallic nodules and rare earth elements (Baker et al., 2010; Ramirez-Llodra et al., 2011; Miller et al., 2018). Benthic communities, however, have been shown to be highly sensitive to disruption, with communities slow to recover; a simulated abyssal mining experiment in the Peru Basin had decreased diversity and heterogeneity even 26 years after the fact (Simon-Lledo et al., 2019). Considering the localization of the active site we observed at Mound 12, it is likely that the disruption of mining activities in the most active seepage areas would extend significantly beyond the range of the mining itself.

Conclusion

By combining the analysis of 268 sediment and carbonate microbial communities with geochemistry and spatial analysis, we have constructed a broad model for the interactions and

nature of the methane seep at Mound 12. By comparing our sediment cores against background sediment samples, we found that the niche for seep-associated microorganisms was smaller than that for fauna. Spatial correlation analysis also suggested that the seepage site to the southwest of the mud volcano has its functional center at Yettisburgh, an extensive carbonate platform with abundant nearby *Kiwa puravida,* where the sediments contained higher relative abundance ANME-1 subgroup organisms than at other active sites. *K. puravida* was also found to have shifted to the southwest in the 16 months between expeditions, indicating that the primary area of seepage may have changed, and a subsequent dive did discover a region southwest of the main site with apparently new seep activity. Altogether, our data highlighted the potential correlation geochemistry, seep fauna, and ANME lineages. The narrow range of ANME-1 in the sediments also suggested that caution should be exercised when disrupting methane seep sediments, since destabilizing the center of the seep could have far-reaching effects on benthic life.

Supplemental Figures

Dive	Date	Latitude (Survey Start)	Longitude (Survey Start)	Survey Time	Mean Survey Depth	Mean Survey Altitude	Photo Transect Speed	Photo Transect Distance
Sentry 431	5/24/17	8.9379	-84.4166	12.9 hrs	969 m	25m	0.56 m/s	17.47 km
Sentry 432	5/25/17	8.9367	-84.3068	10.2 hrs	992 m	6m	0.60 m/s	21.79 km
Sentry 502	10/21/18	8.9320	-84.3069	10.5 hrs	981 m	9 m	0.58 m/s	20.77 km
Sentry 507	10/30/18	8.9284	-84.3153	11.3 hrs	988 m	7 m	0.54 m/s	21.63 km

Table 2.5: Dive metadata for all AUV *Sentry* dives at Mound 12, which were used to construct the maps for Figure 1.

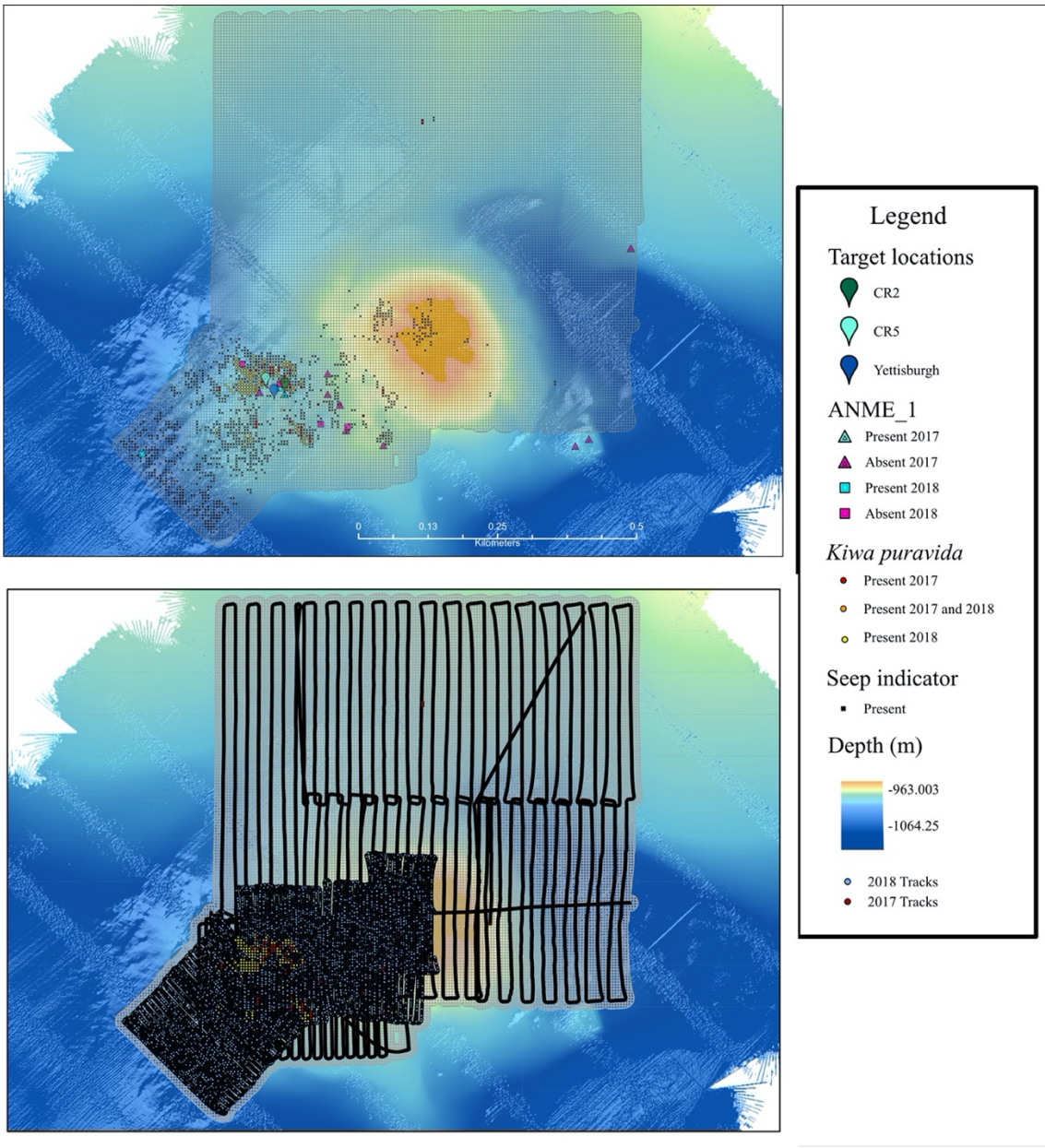

Fig. 2.6: **Top:** Extended map of *Sentry* photomosaics at Mound 12, which indicates the presence of a small number of *K. puravida* north of Mound 12. **Bottom:** Dive Tracks of the 4 AUV *Sentry* dives at Mound 12. These dives were used to construct the map of yeti crab and general seep fauna presence. The primary site of seepage was covered by dives in both 2017 and 2018.

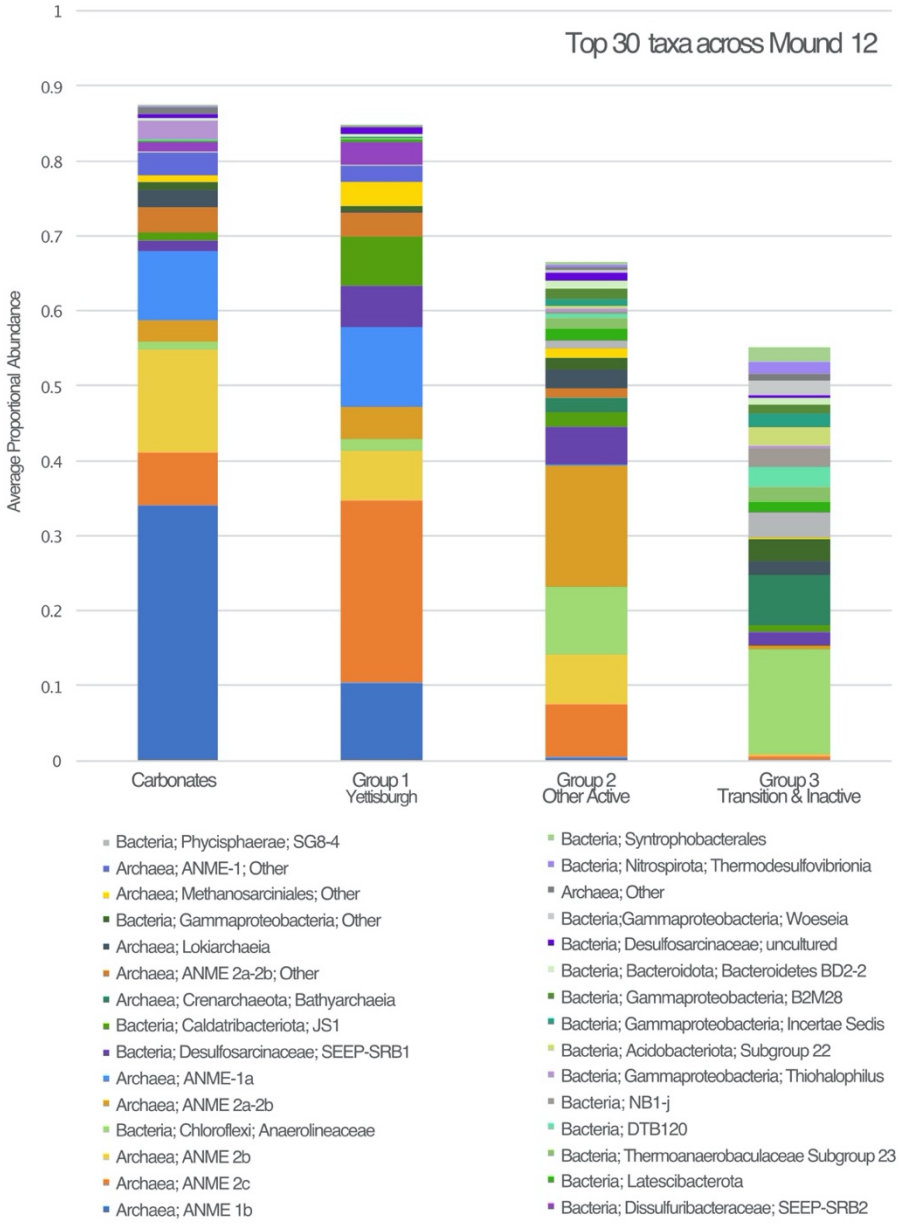

Fig. 2.7: Stacked bar chart of the average relative abundance top 30 taxonomic groups present in all Mound 12 samples, divided by their ecology. OTUs belonging to each taxonomic division are binned together. The top groups were identified by summing the average relative abundance of each taxonomic division across each group. Each division is annotated with the most specific identity possible. ANME-1 organisms are in blue tones, ANME-2 organisms in orange and yellow, SRB are in purple, other putative heterotrophs are in green and organisms with unknown metabolisms in gray. Remaining taxonomic groups are represented by the white box at the top.

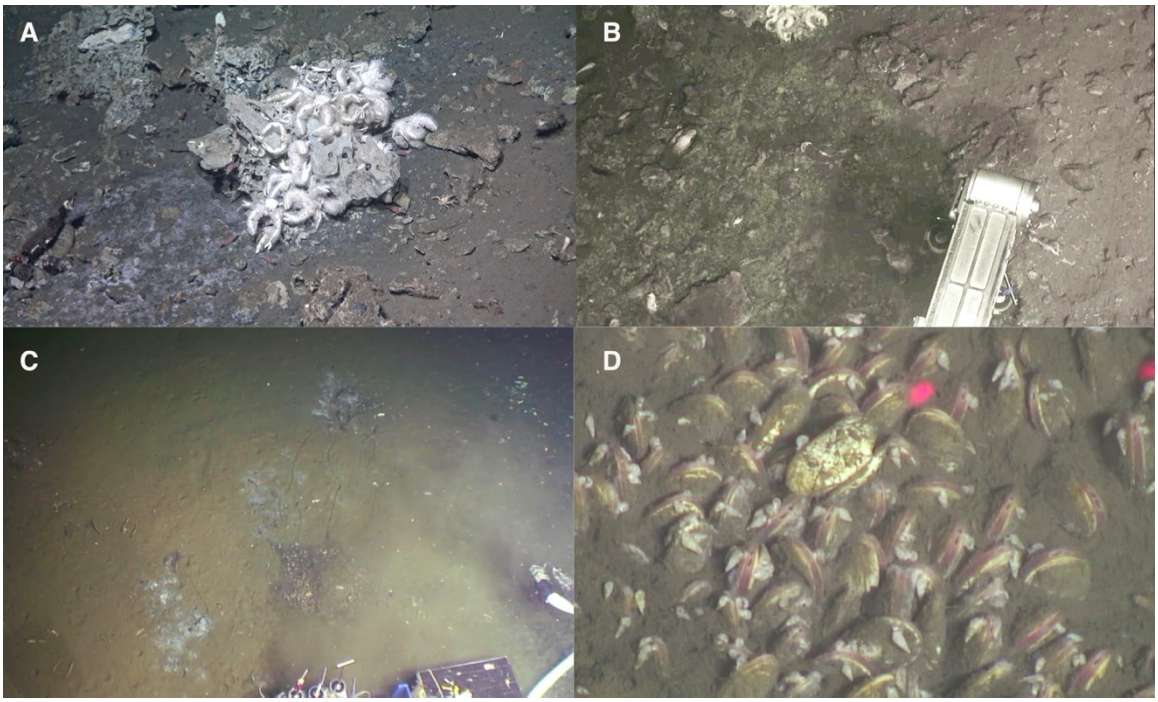

Fig. 2.8: Images of variance bacterial mats and the nearby chemosynthetic fauna. **A:** *K. puravida* clustered on a carbonate rock adjacent to a gray-white bacterial mat on dive AD4984. PC8 was taken at this location, which did not contain high relative abundance of ANME-1 organisms. **B:** Group 1 sediment core PC11 from AD4975, taken within a gray bacterial mat close to marker CR2 and Yettisburgh. A small party of 6-8 *K. puravida* is visible at the top, perched on a small carbonate rock. This sediment core did contain abundant ANME-1 organisms. **C, D:** Images from the newly active site to the southwest of Yettisburgh taken on AD4987. **C:** An overview image, showing three gray and white bacterial mats. PC7, which contained abundant ANME-1 organisms and showed a marked decrease in bromine, fluoride, and chloride concentrations, was taken in the bacterial mat on the bottom left. **D:** A patch of juvenile clams, visible between the bottom two bacterial mats in C. The two laser points act as a scale bar, and are separated by approximately 10 cm, indicating that the clams in this area are ~4 cm in length.

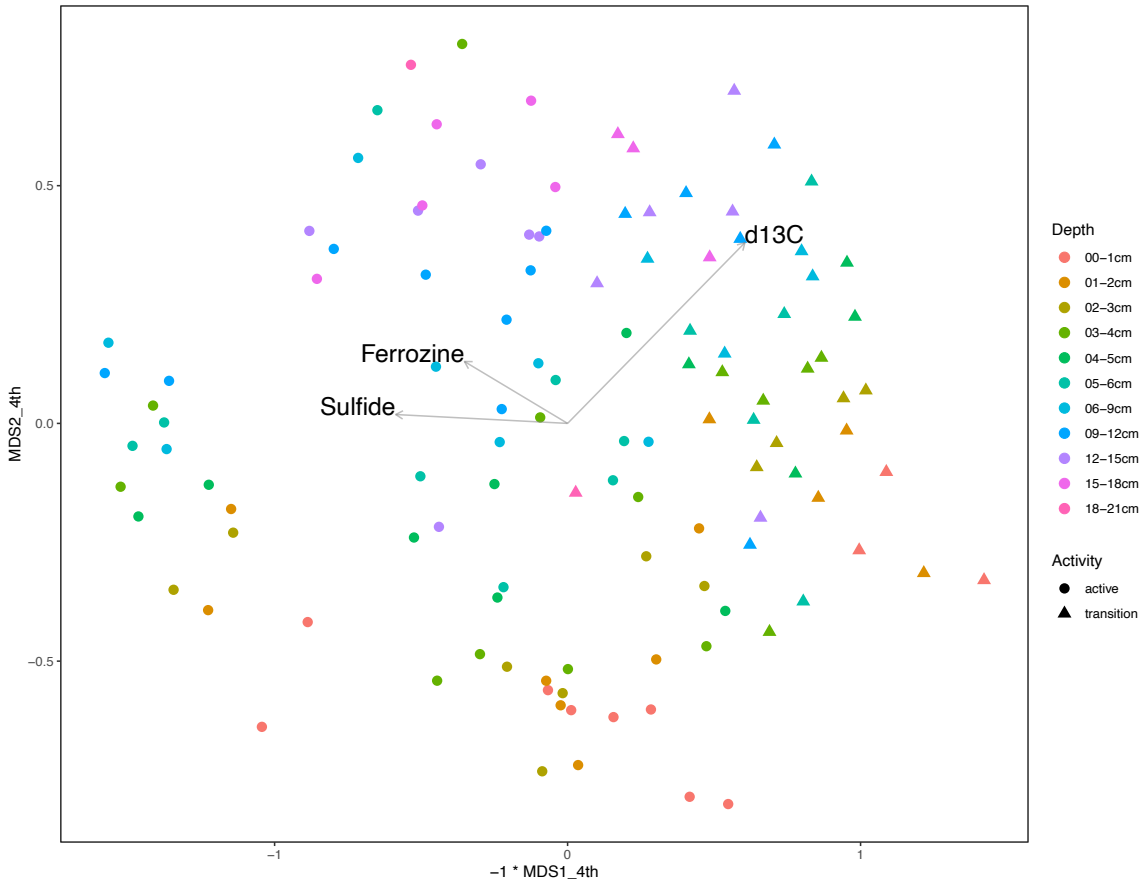

Fig. 2.9: NMDS of all sediment samples that were measured for sulfide and ferrous iron concentrations and $\delta^{13}C\text{-}CO_2$ in the porewater (Stress = 0.140). The horizontal axis was flipped to better correspond to the earlier NMDS of all samples; this does not change the relationships in the ordination. The *envfit* function in *vegan* was performed on the ordination and found that all three geochemical parameters were significant (p-value < 0.01). The corresponding vectors are plotted on top here.

Table 2.10: Abbreviated metadata of analyzed samples

CruiseID	SN	DiveNumber	Depth	Pushcore	Activity	Site	Lat	Long	Group
AT37-13	9709	AD4906	carbonate	R12	inactive		8.93109	-84.31292	carbonate
AT37-13	9710	AD4906	carbonate	R18	active		8.93062	-84.312752	carbonate
AT37-13	9714	AD4907	carbonate	R13	active		8.930347	-84.312463	carbonate
AT37-13	9715	AD4907	carbonate	Natural	transition		8.930363	-84.312589	carbonate
AT37-13	9720	AD4907	carbonate	Natural	transition		8.930363	-84.312589	carbonate
AT37-13	9720	AD4907	carbonate	Natural	transition		8.930363	-84.312589	carbonate
AT37-13	9723	AD4908	carbonate	R1	active		8.930762	-84.31261	carbonate
AT37-13	9724	AD4908	carbonate	R5	active		8.93089	-84.31299	carbonate
AT37-13	9725	AD4908	carbonate	R11	inactive		8.93137	-84.3118	carbonate
AT37-13	9726	AD4908	carbonate	R3	inactive		8.930445	-84.313353	carbonate
AT37-13	9727	AD4908	carbonate	R7	transition		8.93133	-84.31248	carbonate
AT37-13	9728	AD4909	carbonate	Natural	active		8.930783	-84.3126	carbonate
AT37-13	9729	AD4910	carbonate	R2	active		8.93035	-84.31243	carbonate
AT37-13	9730	AD4910	carbonate	R1	active		8.93035	-84.31243	carbonate
AT37-13	9731	AD4910	carbonate	R4	inactive		8.930074	-84.31135	carbonate
AT37-13	9732	AD4910	carbonate	R3	inactive		8.930074	-84.31135	carbonate
AT42-03	10928	AD4974	carbonate	R10	transition		8.92977	-84.3079	carbonate
AT42-03	10929	AD4974	carbonate	R11	transition		8.92977	-84.3079	carbonate
AT42-03	10930	AD4974	carbonate		transition		8.92977	-84.3079	carbonate
AT42-03	10931	AD4974	carbonate	R13	transition		8.92977	-84.3079	carbonate
AT42-03	10932	AD4974	carbonate	R14	transition		8.92977	-84.3079	carbonate
AT42-03	10933	AD4974	carbonate	R5	transition		8.92967	-84.30789	carbonate
AT42-03	10934	AD4974	carbonate	R6	transition		8.92967	-84.30789	carbonate
AT42-03	10935	AD4974	carbonate	R7	transition		8.92967	-84.30789	carbonate
AT42-03	10936	AD4974	carbonate		transition		8.92967	-84.307885	carbonate
AT42-03	10937	AD4974	carbonate	R9	transition		8.92967	-84.30789	carbonate
AT42-03	10953	AD4974	carbonate	R3	transition		8.93047	-84.31324	carbonate
AT42-03	10954	AD4974	carbonate		active		8.93037	-84.313185	carbonate
AT42-03	10999	AD4974	carbonate	R1	inactive		8.9337	-84.30672	carbonate
AT42-03	11000	AD4975	carbonate	R2	inactive		8.9337	-84.30672	carbonate
AT42-03	11001	AD4975	carbonate	R3	inactive		8.9337	-84.30672	carbonate
AT42-03	11002	AD4975	carbonate	R4	inactive		8.9337	-84.30672	carbonate
AT42-03	11003	AD4975	carbonate		inactive		8.9337	-84.30672	carbonate
AT42-03	11005	AD4975	carbonate	R1	inactive		8.93278	-84.30673	carbonate
AT42-03	11006	AD4975	carbonate	R2	inactive		8.93278	-84.30673	carbonate

AT42-03	11007	AD4975	carbonate	R3	inactive		8.93278	-84.30673	carbonate
AT42-03	11008	AD4975	carbonate	R4	inactive		8.93278	-84.30673	carbonate
AT42-03	11009	AD4975	carbonate		inactive		8.93278	-84.30673	carbonate
AT42-03	11026	AD4975	carbonate	R6	transition		8.93135	-84.31245	carbonate
AT42-03	11027	AD4975	carbonate	R10	transition		8.93148	-84.31192	carbonate
AT42-03	11128	AD4978	carbonate		active		8.93087	-84.31291	carbonate
AT42-03	11140	AD4978	carbonate		transition		8.93048	-84.31329	carbonate
AT42-03	11152	AD4978	carbonate		active		8.93081	-84.31264	carbonate
AT42-03	11153	AD4978	carbonate		active		8.93067	-84.31253	carbonate
AT42-03	11380	AD4985	carbonate		active		8.9304	-84.31249	carbonate
AT42-03	11381	AD4985	carbonate		active		8.9304	-84.31249	carbonate
AT42-03	11384	AD4985	carbonate		transition		8.93112	-84.31405	carbonate
AT42-03	11385	AD4985	carbonate		transition		8.92605	-84.31277	carbonate
AT42-03	11386	AD4985	carbonate		transition		8.92605	-84.31277	carbonate
AT37-13	9111	AD4908	00-1cm	PC2	active	Yetisburg	8.9304	-84.3125	1
AT37-13	9112	AD4908	01-2cm	PC2	active	Yetisburg	8.9304	-84.3125	1
AT37-13	9113	AD4908	02-3cm	PC2	active	Yetisburg	8.9304	-84.3125	1
AT37-13	9114	AD4908	03-4cm	PC2	active	Yetisburg	8.9304	-84.3125	1
AT37-13	9115	AD4908	04-5cm	PC2	active	Yetisburg	8.9304	-84.3125	1
AT37-13	9116	AD4908	05-6cm	PC2	active	Yetisburg	8.9304	-84.3125	1
AT37-13	9117	AD4908	06-9cm	PC2	active	Yetisburg	8.9304	-84.3125	1
AT37-13	9118	AD4908	09-12cm	PC2	active	Yetisburg	8.9304	-84.3125	1
AT37-13	9133	AD4908	00-1cm	PC3	active	Yetisburg	8.9304	-84.3125	1
AT37-13	9134	AD4908	01-2cm	PC3	active	Yetisburg	8.9304	-84.3125	1
AT37-13	9135	AD4908	02-3cm	PC3	active	Yetisburg	8.9304	-84.3125	1
AT37-13	9136	AD4908	03-4cm	PC3	active	Yetisburg	8.9304	-84.3125	1
AT37-13	9137	AD4908	04-5cm	PC3	active	Yetisburg	8.9304	-84.3125	1
AT37-13	9138	AD4908	05-6cm	PC3	active	Yetisburg	8.9304	-84.3125	1
AT37-13	9144	AD4908	00-1cm	PC1	active	Yetisburg	8.9304	-84.3125	1
AT37-13	9145	AD4908	01-2cm	PC1	active	Yetisburg	8.9304	-84.3125	1
AT37-13	9146	AD4908	02-3cm	PC1	active	Yetisburg	8.9304	-84.3125	1
AT37-13	9147	AD4908	03-4cm	PC1	active	Yetisburg	8.9304	-84.3125	1
AT37-13	9148	AD4908	04-5cm	PC1	active	Yetisburg	8.9304	-84.3125	1
AT37-13	9149	AD4908	05-6cm	PC1	active	Yetisburg	8.9304	-84.3125	1
AT37-13	9150	AD4908	06-9cm	PC1	active	Yetisburg	8.9304	-84.3125	1
AT37-13	9155	AD4908	00-1cm	PC14	active	Yetisburg	8.9304	-84.3125	1
AT37-13	9156	AD4908	01-2cm	PC14	active	Yetisburg	8.9304	-84.3125	1
AT37-13	9157	AD4908	02-3cm	PC14	active	Yetisburg	8.9304	-84.3125	1

AT37-13	9158	AD4908	03-4cm	PC14	active	Yetisburg	8.9304	-84.3125	1
AT37-13	9159	AD4908	04-5cm	PC14	active	Yetisburg	8.9304	-84.3125	1
AT37-13	9160	AD4908	05-6cm	PC14	active	Yetisburg	8.9304	-84.3125	1
AT37-13	9161	AD4908	06-9cm	PC14	active	Yetisburg	8.9304	-84.3125	1
AT37-13	9162	AD4908	09-12cm	PC14	active	Yetisburg	8.9304	-84.3125	1
AT37-13	9033	AD4907	00-1cm	PC4	active	Mussel_Beach	8.9307	-84.3118	2
AT37-13	9034	AD4907	01-2cm	PC4	active	Mussel_Beach	8.9307	-84.3118	2
AT37-13	9035	AD4907	02-3cm	PC4	active	Mussel_Beach	8.9307	-84.3118	2
AT37-13	9036	AD4907	03-4cm	PC4	active	Mussel_Beach	8.9307	-84.3118	2
AT37-13	9037	AD4907	04-5cm	PC4	active	Mussel_Beach	8.9307	-84.3118	2
AT37-13	9038	AD4907	05-6cm	PC4	active	Mussel_Beach	8.9307	-84.3118	2
AT37-13	9039	AD4907	06-9cm	PC4	active	Mussel_Beach	8.9307	-84.3118	2
AT37-13	9040	AD4907	09-12cm	PC4	active	Mussel_Beach	8.9307	-84.3118	2
AT37-13	9041	AD4907	12-15cm	PC4	active	Mussel_Beach	8.9307	-84.3118	2
AT37-13	9042	AD4907	15-18cm	PC4	active	Mussel_Beach	8.9307	-84.3118	2
AT37-13	9055	AD4907	00-1cm	PC8	active	Mussel_Beach	8.9307	-84.3118	2
AT37-13	9056	AD4907	01-2cm	PC8	active	Mussel_Beach	8.9307	-84.3118	2
AT37-13	9057	AD4907	02-3cm	PC8	active	Mussel_Beach	8.9307	-84.3118	2
AT37-13	9058	AD4907	03-4cm	PC8	active	Mussel_Beach	8.9307	-84.3118	2
AT37-13	9059	AD4907	04-5cm	PC8	active	Mussel_Beach	8.9307	-84.3118	2
AT37-13	9060	AD4907	05-6cm	PC8	active	Mussel_Beach	8.9307	-84.3118	2
AT37-13	9061	AD4907	06-9cm	PC8	active	Mussel_Beach	8.9307	-84.3118	2
AT37-13	9062	AD4907	09-12cm	PC8	active	Mussel_Beach	8.9307	-84.3118	2
AT37-13	9063	AD4907	12-15cm	PC8	active	Mussel_Beach	8.9307	-84.3118	2
AT37-13	9064	AD4907	15-18cm	PC8	active	Mussel_Beach	8.9307	-84.3118	2
AT37-13	9066	AD4907	00-1cm	PC3	active	Mussel_Beach	8.9307	-84.3118	2
AT37-13	9067	AD4907	01-2cm	PC3	active	Mussel_Beach	8.9307	-84.3118	2
AT37-13	9068	AD4907	02-3cm	PC3	active	Mussel_Beach	8.9307	-84.3118	2
AT37-13	9069	AD4907	03-4cm	PC3	active	Mussel_Beach	8.9307	-84.3118	2
AT37-13	9070	AD4907	04-5cm	PC3	active	Mussel_Beach	8.9307	-84.3118	2
AT37-13	9071	AD4907	05-6cm	PC3	active	Mussel_Beach	8.9307	-84.3118	2
AT37-13	9072	AD4907	06-9cm	PC3	active	Mussel_Beach	8.9307	-84.3118	2
AT37-13	9073	AD4907	09-12cm	PC3	active	Mussel_Beach	8.9307	-84.3118	2
AT37-13	9074	AD4907	12-15cm	PC3	active	Mussel_Beach	8.9307	-84.3118	2
AT37-13	9075	AD4907	15-18cm	PC3	active	Mussel_Beach	8.9307	-84.3118	2
AT37-13	9233	AD4910	00-1cm	PC1	active	Mussel_Beach	8.9297	-84.3115	2
AT37-13	9234	AD4910	01-2cm	PC1	active	Mussel_Beach	8.9297	-84.3115	2
AT37-13	9235	AD4910	02-3cm	PC1	active	Mussel_Beach	8.9297	-84.3115	2

AT37-13	9236	AD4910	03-4cm	PC1	active	Mussel_Beach	8.9297	-84.3115	2
AT37-13	9237	AD4910	04-5cm	PC1	active	Mussel_Beach	8.9297	-84.3115	2
AT37-13	9238	AD4910	05-6cm	PC1	active	Mussel_Beach	8.9297	-84.3115	2
AT37-13	9239	AD4910	06-9cm	PC1	active	Mussel_Beach	8.9297	-84.3115	2
AT37-13	9240	AD4910	09-12cm	PC1	active	Mussel_Beach	8.9297	-84.3115	2
AT37-13	9241	AD4910	12-15cm	PC1	active	Mussel_Beach	8.9297	-84.3115	2
AT37-13	9242	AD4910	15-18cm	PC1	active	Mussel_Beach	8.9297	-84.3115	2
AT37-13	9333	AD4917	00-1cm	PC3	active	Little_Knoll	8.9296	-84.3076	2
AT37-13	9334	AD4917	01-2cm	PC3	active	Little_Knoll	8.9296	-84.3076	2
AT37-13	9335	AD4917	02-3cm	PC3	active	Little_Knoll	8.9296	-84.3076	2
AT37-13	9336	AD4917	03-4cm	PC3	active	Little_Knoll	8.9296	-84.3076	2
AT37-13	9337	AD4917	04-5cm	PC3	active	Little_Knoll	8.9296	-84.3076	2
AT37-13	9338	AD4917	05-6cm	PC3	active	Little_Knoll	8.9296	-84.3076	2
AT37-13	9339	AD4917	06-9cm	PC3	active	Little_Knoll	8.9296	-84.3076	2
AT37-13	9340	AD4917	09-12cm	PC3	active	Little_Knoll	8.9296	-84.3076	2
AT37-13	9341	AD4917	12-15cm	PC3	active	Little_Knoll	8.9296	-84.3076	2
AT37-13	9342	AD4917	15-18cm	PC3	active	Little_Knoll	8.9296	-84.3076	2
AT37-13	9343	AD4917	18-21cm	PC3	active	Little_Knoll	8.9296	-84.3076	2
AT37-13	9420	AD4922	15-18cm	PC11	transition	transition	8.9296	-84.3078	2
AT37-13	9421	AD4922	18-21cm	PC11	transition	transition	8.9296	-84.3078	2
AT37-13	10000	AD4909	00-1cm	PC5	active	Mussel_Beach	8.9302	-84.3116	2
AT37-13	10001	AD4909	01-2cm	PC5	active	Mussel_Beach	8.9302	-84.3116	2
AT37-13	10002	AD4909	02-3cm	PC5	active	Mussel_Beach	8.9302	-84.3116	2
AT37-13	10003	AD4909	03-4cm	PC5	active	Mussel_Beach	8.9302	-84.3116	2
AT37-13	10004	AD4909	04-5cm	PC5	active	Mussel_Beach	8.9302	-84.3116	2
AT37-13	10005	AD4909	05-6cm	PC5	active	Mussel_Beach	8.9302	-84.3116	2
AT37-13	10006	AD4909	06-9cm	PC5	active	Mussel_Beach	8.9302	-84.3116	2
AT37-13	10007	AD4909	09-12cm	PC5	active	Mussel_Beach	8.9302	-84.3116	2
AT37-13	10008	AD4909	12-15cm	PC5	active	Mussel_Beach	8.9302	-84.3116	2
AT37-13	10030	AD4910	00-1cm	PC8	active	Mussel_Beach	8.9297	-84.3115	2
AT37-13	10031	AD4910	01-2cm	PC8	active	Mussel_Beach	8.9297	-84.3115	2
AT37-13	10032	AD4910	02-3cm	PC8	active	Mussel_Beach	8.9297	-84.3115	2
AT37-13	10033	AD4910	03-4cm	PC8	active	Mussel_Beach	8.9297	-84.3115	2
AT37-13	10034	AD4910	04-5cm	PC8	active	Mussel_Beach	8.9297	-84.3115	2
AT37-13	10035	AD4910	05-6cm	PC8	active	Mussel_Beach	8.9297	-84.3115	2
AT37-13	10036	AD4910	06-9cm	PC8	active	Mussel_Beach	8.9297	-84.3115	2
AT37-13	10037	AD4910	09-12cm	PC8	active	Mussel_Beach	8.9297	-84.3115	2
AT37-13	10038	AD4910	12-15cm	PC8	active	Mussel_Beach	8.9297	-84.3115	2

AT37-13	10039	AD4910	15-18cm	PC8	active	Mussel_Beach	8.9297	-84.3115	2
AT37-13	10040	AD4910	18-21cm	PC8	active	Mussel_Beach	8.9297	-84.3115	2
AT42-03	10940	AD4974	00-1cm	PC7	active	active_other	8.9298	-84.3115	2
AT42-03	10941	AD4974	01-2cm	PC7	active	active_other	8.9298	-84.3115	2
AT42-03	10942	AD4974	02-3cm	PC7	active	active_other	8.9298	-84.3115	2
AT42-03	10943	AD4974	03-4cm	PC7	active	active_other	8.9298	-84.3115	2
AT42-03	10944	AD4974	04-5cm	PC7	active	active_other	8.9298	-84.3115	2
AT42-03	10945	AD4974	05-6cm	PC7	active	active_other	8.9298	-84.3115	2
AT42-03	10946	AD4974	06-9cm	PC7	active	active_other	8.9298	-84.3115	2
AT42-03	10947	AD4974	09-12cm	PC7	active	active_other	8.9298	-84.3115	2
AT42-03	10948	AD4974	12-15cm	PC7	active	active_other	8.9298	-84.3115	2
AT42-03	10949	AD4974	15-18cm	PC7	active	active_other	8.9298	-84.3115	2
AT42-03	10950	AD4974	18-21cm	PC7	active	active_other	8.9298	-84.3115	2
AT42-03	10995	AD4974	12-15cm	PC9	transition	outer transition	8.92968	-84.30785	2
AT42-03	11018	AD4975	03-4cm	PC11	active	active_other	8.9305	-84.3126	2
AT42-03	11114	AD4978	03-4cm	PC8	active	active_other	8.9299	-84.3119	2
AT42-03	11322	AD4984	00-1cm	PC9	active	active_other	8.93062	-84.31233	2
AT42-03	11323	AD4984	01-2cm	PC9	active	active_other	8.93062	-84.31233	2
AT42-03	11324	AD4984	02-3cm	PC9	active	active_other	8.93062	-84.31233	2
AT42-03	11325	AD4984	03-4cm	PC9	active	active_other	8.93062	-84.31233	2
AT42-03	11326	AD4984	04-5cm	PC9	active	active_other	8.93062	-84.31233	2
AT42-03	11327	AD4984	05-6cm	PC9	active	active_other	8.93062	-84.31233	2
AT42-03	11328	AD4984	06-9cm	PC9	active	active_other	8.93062	-84.31233	2
AT42-03	11329	AD4984	09-12cm	PC9	active	active_other	8.93062	-84.31233	2
AT42-03	11330	AD4984	12-15cm	PC9	active	active_other	8.93062	-84.31233	2
AT42-03	11331	AD4984	15-18cm	PC9	active	active_other	8.93062	-84.31233	2
AT42-03	11345	AD4984	03-4cm	PC4	active	active_other	8.9306	-84.3123	2
AT42-03	11374	AD4984	03-4cm	PC8	active	active_other	8.9305	-84.3126	2
AT42-03	11395	AD4985	03-4cm	PC5	active	active_other	8.9305	-84.3125	2
AT37-13	9000	AD4906	00-1cm	PC2	transition	transition	8.9304	-84.3129	3
AT37-13	9001	AD4906	01-2cm	PC2	transition	transition	8.9304	-84.3129	3
AT37-13	9002	AD4906	02-3cm	PC2	transition	transition	8.9304	-84.3129	3
AT37-13	9003	AD4906	03-4cm	PC2	transition	transition	8.9304	-84.3129	3
AT37-13	9004	AD4906	04-5cm	PC2	transition	transition	8.9304	-84.3129	3
AT37-13	9005	AD4906	05-6cm	PC2	transition	transition	8.9304	-84.3129	3
AT37-13	9006	AD4906	06-9cm	PC2	transition	transition	8.9304	-84.3129	3
AT37-13	9007	AD4906	09-12cm	PC2	transition	transition	8.9304	-84.3129	3
AT37-13	9008	AD4906	12-15cm	PC2	transition	transition	8.9304	-84.3129	3

AT37-13	9009	AD4906	15-18cm	PC2	transition	transition	8.9304	-84.3129	3
AT37-13	9011	AD4906	00-1cm	PC8	transition	transition	8.9304	-84.3129	3
AT37-13	9012	AD4906	01-2cm	PC8	transition	transition	8.9304	-84.3129	3
AT37-13	9013	AD4906	02-3cm	PC8	transition	transition	8.9304	-84.3129	3
AT37-13	9014	AD4906	03-4cm	PC8	transition	transition	8.9304	-84.3129	3
AT37-13	9015	AD4906	04-5cm	PC8	transition	transition	8.9304	-84.3129	3
AT37-13	9016	AD4906	05-6cm	PC8	transition	transition	8.9304	-84.3129	3
AT37-13	9017	AD4906	06-9cm	PC8	transition	transition	8.9304	-84.3129	3
AT37-13	9018	AD4906	09-12cm	PC8	transition	transition	8.9304	-84.3129	3
AT37-13	9019	AD4906	12-15cm	PC8	transition	transition	8.9304	-84.3129	3
AT37-13	9022	AD4906	00-1cm	PC3	transition	transition	8.9304	-84.3129	3
AT37-13	9023	AD4906	01-2cm	PC3	transition	transition	8.9304	-84.3129	3
AT37-13	9024	AD4906	02-3cm	PC3	transition	transition	8.9304	-84.3129	3
AT37-13	9025	AD4906	03-4cm	PC3	transition	transition	8.9304	-84.3129	3
AT37-13	9026	AD4906	04-5cm	PC3	transition	transition	8.9304	-84.3129	3
AT37-13	9027	AD4906	05-6cm	PC3	transition	transition	8.9304	-84.3129	3
AT37-13	9028	AD4906	06-9cm	PC3	transition	transition	8.9304	-84.3129	3
AT37-13	9029	AD4906	09-12cm	PC3	transition	transition	8.9304	-84.3129	3
AT37-13	9030	AD4906	12-15cm	PC3	transition	transition	8.9304	-84.3129	3
AT37-13	9044	AD4907	00-1cm	PC1	transition	transition	8.9296	-84.3109	3
AT37-13	9045	AD4907	01-2cm	PC1	transition	transition	8.9296	-84.3109	3
AT37-13	9046	AD4907	02-3cm	PC1	transition	transition	8.9296	-84.3109	3
AT37-13	9047	AD4907	03-4cm	PC1	transition	transition	8.9296	-84.3109	3
AT37-13	9048	AD4907	04-5cm	PC1	transition	transition	8.9296	-84.3109	3
AT37-13	9049	AD4907	05-6cm	PC1	transition	transition	8.9296	-84.3109	3
AT37-13	9050	AD4907	06-9cm	PC1	transition	transition	8.9296	-84.3109	3
AT37-13	9051	AD4907	09-12cm	PC1	transition	transition	8.9296	-84.3109	3
AT37-13	9052	AD4907	12-15cm	PC1	transition	transition	8.9296	-84.3109	3
AT37-13	9053	AD4907	15-18cm	PC1	transition	transition	8.9296	-84.3109	3
AT37-13	9088	AD4907	00-1cm	PC14	transition	transition	8.9296	-84.3109	3
AT37-13	9089	AD4907	01-2cm	PC14	transition	transition	8.9296	-84.3109	3
AT37-13	9090	AD4907	02-3cm	PC14	transition	transition	8.9296	-84.3109	3
AT37-13	9091	AD4907	03-4cm	PC14	transition	transition	8.9296	-84.3109	3
AT37-13	9092	AD4907	04-5cm	PC14	transition	transition	8.9296	-84.3109	3
AT37-13	9093	AD4907	05-6cm	PC14	transition	transition	8.9296	-84.3109	3
AT37-13	9094	AD4907	06-9cm	PC14	transition	transition	8.9296	-84.3109	3
AT37-13	9095	AD4907	09-12cm	PC14	transition	transition	8.9296	-84.3109	3
AT37-13	9096	AD4907	12-15cm	PC14	transition	transition	8.9296	-84.3109	3

AT37-13	9097	AD4907	15-18cm	PC14	transition	transition	8.9296	-84.3109	3
AT37-13	9100	AD4907	00-1cm	PC15	transition	transition	8.9296	-84.3109	3
AT37-13	9101	AD4907	01-2cm	PC15	transition	transition	8.9296	-84.3109	3
AT37-13	9102	AD4907	02-3cm	PC15	transition	transition	8.9296	-84.3109	3
AT37-13	9103	AD4907	03-4cm	PC15	transition	transition	8.9296	-84.3109	3
AT37-13	9104	AD4907	04-5cm	PC15	transition	transition	8.9296	-84.3109	3
AT37-13	9105	AD4907	05-6cm	PC15	transition	transition	8.9296	-84.3109	3
AT37-13	9106	AD4907	06-9cm	PC15	transition	transition	8.9296	-84.3109	3
AT37-13	9107	AD4907	09-12cm	PC15	transition	transition	8.9296	-84.3109	3
AT37-13	9108	AD4907	12-15cm	PC15	transition	transition	8.9296	-84.3109	3
AT37-13	9122	AD4908	00-1cm	PC4	transition	transition	8.9314	-84.3118	3
AT37-13	9123	AD4908	01-2cm	PC4	transition	transition	8.9314	-84.3118	3
AT37-13	9124	AD4908	02-3cm	PC4	transition	transition	8.9314	-84.3118	3
AT37-13	9125	AD4908	03-4cm	PC4	transition	transition	8.9314	-84.3118	3
AT37-13	9126	AD4908	04-5cm	PC4	transition	transition	8.9314	-84.3118	3
AT37-13	9127	AD4908	05-6cm	PC4	transition	transition	8.9314	-84.3118	3
AT37-13	9128	AD4908	06-9cm	PC4	transition	transition	8.9314	-84.3118	3
AT37-13	9129	AD4908	09-12cm	PC4	transition	transition	8.9314	-84.3118	3
AT37-13	9130	AD4908	12-15cm	PC4	transition	transition	8.9314	-84.3118	3
AT37-13	9166	AD4908	00-1cm	PC8	transition	transition	8.9314	-84.3118	3
AT37-13	9167	AD4908	01-2cm	PC8	transition	transition	8.9314	-84.3118	3
AT37-13	9168	AD4908	02-3cm	PC8	transition	transition	8.9314	-84.3118	3
AT37-13	9169	AD4908	03-4cm	PC8	transition	transition	8.9314	-84.3118	3
AT37-13	9170	AD4908	04-5cm	PC8	transition	transition	8.9314	-84.3118	3
AT37-13	9171	AD4908	05-6cm	PC8	transition	transition	8.9314	-84.3118	3
AT37-13	9172	AD4908	06-9cm	PC8	transition	transition	8.9314	-84.3118	3
AT37-13	9173	AD4908	09-12cm	PC8	transition	transition	8.9314	-84.3118	3
AT37-13	9174	AD4908	12-15cm	PC8	transition	transition	8.9314	-84.3118	3
AT37-13	9177	AD4908	00-1cm	PC9	transition	transition	8.9314	-84.3118	3
AT37-13	9178	AD4908	01-2cm	PC9	transition	transition	8.9314	-84.3118	3
AT37-13	9179	AD4908	02-3cm	PC9	transition	transition	8.9314	-84.3118	3
AT37-13	9180	AD4908	03-4cm	PC9	transition	transition	8.9314	-84.3118	3
AT37-13	9181	AD4908	04-5cm	PC9	transition	transition	8.9314	-84.3118	3
AT37-13	9182	AD4908	05-6cm	PC9	transition	transition	8.9314	-84.3118	3
AT37-13	9183	AD4908	06-9cm	PC9	transition	transition	8.9314	-84.3118	3
AT37-13	9184	AD4908	09-12cm	PC9	transition	transition	8.9314	-84.3118	3
AT37-13	9185	AD4908	12-15cm	PC9	transition	transition	8.9314	-84.3118	3
AT37-13	9186	AD4908	15-18cm	PC9	transition	transition	8.9314	-84.3118	3

AT37-13	9411	AD4922	00-1cm	PC11	transition	transition	8.9296	-84.3078	3
AT37-13	9412	AD4922	01-2cm	PC11	transition	transition	8.9296	-84.3078	3
AT37-13	9413	AD4922	02-3cm	PC11	transition	transition	8.9296	-84.3078	3
AT37-13	9414	AD4922	03-4cm	PC11	transition	transition	8.9296	-84.3078	3
AT37-13	9415	AD4922	04-5cm	PC11	transition	transition	8.9296	-84.3078	3
AT37-13	9416	AD4922	05-6cm	PC11	transition	transition	8.9296	-84.3078	3
AT37-13	9417	AD4922	06-9cm	PC11	transition	transition	8.9296	-84.3078	3
AT37-13	9418	AD4922	09-12cm	PC11	transition	transition	8.9296	-84.3078	3
AT37-13	9419	AD4922	12-15cm	PC11	transition	transition	8.9296	-84.3078	3
AT37-13	10251	AD4922	00-1cm	PC3	inactive	far_away	8.9327	-84.307	3
AT37-13	10252	AD4922	01-2cm	PC3	inactive	far_away	8.9327	-84.307	3
AT37-13	10253	AD4922	02-3cm	PC3	inactive	far_away	8.9327	-84.307	3
AT37-13	10254	AD4922	03-4cm	PC3	inactive	far_away	8.9327	-84.307	3
AT37-13	10255	AD4922	04-5cm	PC3	inactive	far_away	8.9327	-84.307	3
AT37-13	10256	AD4922	05-6cm	PC3	inactive	far_away	8.9327	-84.307	3
AT37-13	10257	AD4922	06-9cm	PC3	inactive	far_away	8.9327	-84.307	3
AT37-13	10258	AD4922	09-12cm	PC3	inactive	far_away	8.9327	-84.307	3
AT37-13	10259	AD4922	12-15cm	PC3	inactive	far_away	8.9327	-84.307	3
AT37-13	10260	AD4922	15-18cm	PC3	inactive	far_away	8.9327	-84.307	3
AT37-13	10261	AD4922	18-21cm	PC3	inactive	far_away	8.9327	-84.307	3

Chapter 3

MICROBIAL COMMUNITY DYNAMICS AND SUCCESSION IN METHANE SEEP CARBONATES

Abstract

Methane seeps are unique features on the seafloor where methane and reduced fluids permeate the sediment, providing an energy-rich habitat for endemic marine fauna. Extensive authigenic carbonate slabs are a common feature of seeps, and fossil seep carbonates offer a window into the ecology of the ancient seafloor. Recent studies have demonstrated that microorganisms inhabiting these seep carbonates, called endoliths, remain metabolically active even after being encrusted, and a more thorough understanding of the community dynamics of these systems is needed before the ecological history of fossil seeps can be correctly inferred from the rock record. We analyzed the bacterial and archaeal communities of 20 native carbonates from zones of differing activity and 28 carbonates transplanted between those zones at Mound 12, a methane seep on the Pacific active margin of Costa Rica, along with 15 incubations deployed over a period of 16 months to provide context to understand anaerobic methanotroph (ANME) niche differentiation and fossil seep histories. Our results demonstrated the prevalence of the ANME subgroup 1 within native and transplanted Mound 12 carbonates but not within the incubated experiments, indicating that ANME endoliths are the result of self-entombment rather than preferential attachment. We also demonstrated that the response of carbonate endolithic communities to transplantation was complex. The relative proportion of ANME-1 significantly increased in carbonates transplanted to a low-activity zone, whereas the community of samples transplanted to inactive zones did not significantly change. These results provide insight into how seep carbonates are formed and how the communities change over time, providing a framework for interpreting fossil seep biomarkers.

Introduction

Methane seeps are marine regions where methane-rich fluids permeate the seafloor and stand out from the rest of the benthos by virtue of their geochemistry, richness and diversity of life, and abundance of carbonate-rich rocks that vary in size, ranging from microcrystalline precipitates to square kilometer-size pavements (Levin, 2005; Naehr et al., 2007; Joseph, 2017; Georgieva et al., 2019). Thousands of methane seeps and hydrothermal vents have been identified on the seafloor, often the result of tectonically-driven seawater advection that is re-emitted enriched in dissolved nutrients and gasses (Tivey, 2007; Beaulieu et al., 2013; Beaulieu et al., 2015). The bedrock metabolism of these communities is the anaerobic oxidation of methane (AOM) with sulfate, mediated by a partnership of sulfate-reducing bacteria (SRB) and

anaerobic methanotrophic (ANME) archaea (Boetius et al., 2000; Orphan et al., 2001a; Orphan et al., 2009; Ruff et al., 2015). AOM consumes 50-80% of sediment methane, preventing its escape to the benthic hydrosphere or, ultimately, the atmosphere (Reeburgh, 2007a; Boetius and Wenzhöfer, 2013; Levin et al., 2016). The sulfide that results from AOM is also captured as a chemical substrate by a variety of unique or endemic organisms with sulfide-oxidizing bacterial symbiotes, including species of mussels, clams, crabs, and tubeworms (Levin, 2005; Cordes et al., 2010; Bowden et al., 2013; Goffredi et al., 2014; Levin et al., 2015; Amon et al., 2017; Ashford et al., 2020; Soares Pereira, 2020).

The coupling of sulfate reduction with methane oxidation by this microbial partnership produces alkalinity and promotes the formation of a variety of authigenic carbonate minerals up to millions of cubic feet in volume (Aloisi et al., 2002; Klaucke et al., 2008; Mason et al., 2015). The carbonates themselves continue to act as a substrate for some ANME, which live within the rock matrix as endoliths (Marlow et al., 2014a; Case et al., 2015; Mason et al., 2015). Although many endoliths gain nutrients and metabolites from their host rock, ANME endoliths are unusual in that the formation of authigenic carbonate presumably restricts the diffusion of methane and sulfate into the rock (Hovland, 2002; Walker and Pace, 2007). Nevertheless, endolithic ANME have been shown to continue to oxidize methane, indicating that the often-vuggy and micritic carbonate matrix is porous enough to permit methane diffusion (Marlow et al., 2014a; Marlow et al., 2014b).

Any organism that embeds itself in rock represents a potential candidate for fossilization and biomarker preservation, and fossil seeps are not uncommon in the geologic record (Blumenberg et al., 2004; Stadnitskaia et al., 2008b; Bailey et al., 2010; Georgieva et al., 2019). Several archaea-derived lipids, including crocetane, archaeol, *sn*-2 hydroxyarchaeol, and glycerol dialkyl glycerol tetraethers (GDGT) have been detected in multiple fossil authigenic seep carbonate mounds, and the relative proportions of these lipids can be analyzed to compute the composition of the endolithic community at the time of fossilization (Blumenberg et al., 2004; Stadnitskaia et al., 2008a; Stadnitskaia et al., 2008b). Methane seeps are dynamic, however, with seepage flux changing or shifting spatially on scales from days to years to centuries (Tryon et al., 1999; Torres et al., 2002). Little data exists that reveals how the endolithic communities of methane seep carbonates respond to these changes, but an understanding of the community dynamics is essential for interpreting the historical record of these seeps. Biomarkers that are

extracted from seep carbonates are not derived from buried, dead organisms but from a community that can continue to grow and change long after the carbonate crust is formed. Biomarker studies of seeps, particularly those seeking to understand seep evolution, must be undertaken with caution.

Here, we analyze the endolithic communities of carbonate rocks from Mound 12, a methane seep west of Costa Rica, as well as describe the results of a 16-month transplant experiment that mimics changing seep conditions, in order to better understand methane seep endolithic community dynamics. We find that seep endolithic communities are broadly similar regardless of age, but that these communities may subtly shift as the center of methane flux changes.

Materials and Methods

Site description

Mound 12 is a 50 m tall, cone-shaped mud volcano on the Costa Rican Pacific active margin (Linke et al., 2005; Mau et al., 2006; Sahling et al., 2008; Cortés, 2016). The region of main activity lies to the southwest of the mound itself, where evidence of current or prior seep activity extends ~300 m radially outward from the base of the cone. No methane ebullition has been observed at Mound 12, but the active region has extensive carbonate platforms colonized by myriad chemosynthetic organisms including the Costa Rican yeti crab, *Kiwa puravida* (Thurber et al., 2011; Goffredi et al., 2014). Samples were determined, at the time of collection, to fall into one of three categories: active, transition, or inactive. Transition sites were further divided into inner transition and outer transition by reviewing video footage. Active sites were characterized by exposed carbonate platforms with minimal sediment cover, microbial mat covering visible sediment, and abundant chemosynthetic animals, including bathymodiolin mussels, *K. puravida*, vesicomyid clams, or vestimentiferan tubeworms. Inner transition (IT) sites were characterized as those with a decreased density of bivalves, absence of microbial mat, shell hash of seep bivalves, light sediment cover of visible carbonate, and/or more abundant non-chemosynthetic organisms such as hydroids, galatheid crabs, or shrimp. Outer transition (OT) sites were characterized by mostly buried carbonate, no visible chemosynthetic organisms, and more abundant non-chemosynthetic organisms such as hydroids or corals. Inactive sites had nearly

entirely buried or absent carbonate and few visible eukaryotes outside of brittle stars, anemones, or fish.

Sampling

All samples were collected using Human Occupied Vessel (HOV) *Alvin* on two R/V *Atlantis* expeditions: AT37-13 (May-June 2017) and AT42-03 (October-November 2018). Carbonate rock samples were collected with *Alvin* into bioboxes made from thick Delrin plastic. Using a sterile chisel, pieces of each rock were chipped off. Samples for DNA analysis were placed in sterile Whirl-pak bags (Nasco, Fort Atkinson, Wisconsin) and frozen in liquid nitrogen before storage at -80°C. Additional rock samples were fixed in 2% PFA in 5 mL Nalgene containers overnight at 4°C before washing 3 times with 1.5× PBS the following day and stored at -20°C in 1:1 3× PBS:100% ethanol. The water sample was taken with a Niskin bottle fitted onto *Alvin* at the Yettisburgh active site on dive A4985 in 2018. After returning to the surface, the water was filtered through an inline 0.22 μm Sterivex™ filter (MilliporeSigma; Burlington, MA) using a Masterflex L/S peristaltic pump (Model 7528-30, Cole-Parmer; Vernon Hills, IL) at 60 rpm. Tygon peristaltic pump tubing (Saint Gobain; Courbevoie, France) used with the pump was acid-washed in 4% HCl prior to the expedition and flushed with ultrapure water in between uses. ~40 mL of sample was also flushed through the tubing before attaching the filter.

Sample Description

A list of all samples analyzed herein, with accompanying coordinates, activity classifications, is found in the supplementary data file. Twenty natural carbonates were collected from Mound 12: 10 from active sites, 7 from the inner transition (IT) and 3 from the outer transition (OT). We also conducted 28 carbonate transplant experiments. Each transplanted carbonate was collected by *Alvin* and moved to a zone of differing activity on the same dive. In some cases, natural carbonates were collected alongside transplanted rocks to serve as controls. Six different types of transplants were conducted: active to IT (n = 4), active to OT (n = 5), active to inactive (n = 5), IT to active (n = 4), IT to OT (n = 5), and IT to inactive (n = 5). These names are shortened with arrows in the following sections, *e.g.* active→IT. Due to the lack of carbonates in OT or inactive sites (by definition), we were unable to find sufficient samples to conduct transplants from those zones. Two additional carbonates were collected on AT37-13 that were part of long-term incubations on the seafloor. These carbonates were originally

collected from the Costa Rica active margin in 2009 on AT15-44, left to dry for two months, and then replaced on the seafloor in 2010 on AT15-59 in Active areas at Mound 12. Metadata from these samples is sparse, so while these samples were similar to other native active rocks in our analysis, we have considered them separately so as not to confound our analysis.

To test mineralogy-based variation of carbonate microbial communities and to test whether endolithic communities were the result of preferential colonization of a mineral or self-entombment, sterile carbonate chips were also incubated on the seafloor in three locations designated active, transition, and inactive. Each incubation package contained four carbonate types, selected to represent the range of common carbonate mineralogy in the environment: Iceland spar calcite (Ward's Science #470025-522; Rochester, NY), coarse-grained crystalline dolomite (Ward's Science #470025-558), crystalline aragonite from Morocco (Jewel Tunnel Imports; Baldwin Park, CA), and a donut-shaped hydrothermal vent carbonate collected at the Eel River Basin (44.66996, -125.09828) by the Monterey Bay Aquarium Research Institute Remotely Operated Vehicle *Tiburon* dive 870 in 2005. This donut-shaped rock sample had been kept dry since its collection in 2005. Each of the carbonates were cut into ~1 cm^2 chips using a water-cooled low-speed diamond saw. The chips were then dried and any surficial reduced carbon removed with a vacuum plasma cleaner (PE-25; Plasma Etch; Carson City, NV) for 20 minutes; surface cleaning was followed by autoclaving for 30 minutes. Four chips of each mineral type were placed into a 1 mm nylon mesh bag along with 2 autoclaved polyurethane sponges (after (Imachi et al., 2011). Each bag was deployed on the seafloor during AT37-13 in 2017 and recovered during AT42-03 in 2018, resulting in a total incubation time of ~16 months.

DNA Extraction

Natural and transplanted rock samples were processed with the aim of extracting DNA from the endolithic community with minimized contribution from the sediment microbial community. The samples were first washed and sonicated at 8W (Branson Sonifier 150D, Branson Ultrasonics Corp.; Danbury CT) to remove external sediment-associated microorganisms following (Mason et al., 2015). Following the washing, samples were powdered with a sterile mortar and pestle and 0.25 – 0.5 g powder was added to the lysis tubes of the PowerSoil DNA extraction kit (Qiagen; Hilden, Germany). We also performed several additional steps to separate cells from the minerals and lyse them. First, the lysis tubes with powdered

sample were flash frozen in liquid nitrogen and thawed in a 25°C water bath. The thawed tubes were then placed in a sonicating water bath for 90 seconds. The C1 detergent was then added and the samples vortexed briefly to mix before incubating the entire sample in a 65°C water bath for 30 minutes. The heated samples were then placed in a bead beater (FastPrep FP120, Thermo Fisher Scientific; Waltham, MA) at 5.5 m/s speed for 45 seconds. The samples were then centrifuged at 10,000 × *g* for 30 s and processed according to the rest of the manufacturer's instructions. Our contamination controls included no-sample extraction kit controls as well as a sterilized, unincubated calcite chip that was crushed and extracted in the same manner above.

Since seafloor-incubated sterile carbonates were not expected to contain significant endolithic populations after just 16 months, we did not sonicate those samples before crushing the rock. Instead, those samples were washed with filtered seawater during shipboard recovery to remove sediment and frozen. Upon thawing them in lab, they were placed directly into the sterile mortar and pestle, crushed, and then extracted following the lysis and purification steps outlined above.

DNA Sequencing

The V4-V5 region of the 16S rRNA gene was amplified using archaeal/bacterial primers with Illumina (San Diego, CA) adapters on the 5' end (515F 5'-TCGTCGGCAGCGTCAGATGTGTATAAGAGACAG-GTGYCAGCMGCCGCGGTAA-3' and 926R 5'-GTCTCGTGGGCTCGGAGATGTGTATAAGAGACAG-CCGYCAATTYMTTTRAGTTT-3'). PCR reaction mix was set up in duplicate for each sample with Q5 Hot Start High-Fidelity 2x Master Mix (New England Biolabs, Ipswich, MA, USA) in a 15 μL reaction volume according to manufacturer's directions with annealing conditions of 54°C for 30 cycles. Template-free controls were also included for each sequencing run. Duplicate PCR samples were then pooled and barcoded with Illumina Nextera XT index 2 primers that include unique 8-bp barcodes (P5 5'-AATGATACGGCGACCACCGAGATCTACAC-XXXXXXXX-TCGTCGGCAGCGTC-3' and P7 5'-CAAGCAGAAGACGGCATACGAGAT-XXXXXXXX-GTCTCGTGGGCTCGG-3'). Amplification with barcoded primers used Q5 Hot Start PCR mixture but used 2.5 μL of product in 25 μL of total reaction volume, annealed at 66°C, and cycled only 10 times. Products

were purified using Millipore-Sigma (St. Louis, MO, USA) MultiScreen Plate MSNU03010 with vacuum manifold and quantified using ThermoFisher Scientific (Waltham, MA, USA) QuantIT PicoGreen dsDNA Assay Kit P11496 on the BioRad CFX96 Touch Real-Time PCR Detection System. Barcoded samples were combined in equimolar amounts into a single tube and purified with Qiagen PCR Purification Kit 28104 before submission to Laragen (Culver City, CA) for 250 bp paired end sequencing on Illumina's MiSeq platform with the addition of 15-20% PhiX control library. Raw read files with accompanying controls were submitted to the NCBI Sequence Read Archive under BioProject Accession Number PRJNA623020.

DNA sequence analysis

712 sequenced samples from across the entire set of AT37-13 and AT42-03 expeditions, including sample-free extraction controls and template-free PCR controls, were processed together in QIIME version 1.8.0 (Caporaso et al., 2010) following a recently published protocol (Mason et al., 2015). Raw sequence pairs were joined requiring a 50 bp overlap (with a maximum of 4 mismatches in overlapping sequence). Contigs were then quality-trimmed, with minimum Phred quality score of 30 (QIIME default is 4), and any sequences with unknown base call ("N") were removed. Contig sequences were then clustered *de novo* into operational taxonomic units (OTUs) with 99% similarity using UCLUST, and the most abundant sequence was chosen as representative for each *de novo* OTU (Edgar, 2018). Taxonomic identification for each representative sequence was assigned using UCLUST with the Silva-132 database (Quast et al., 2013), requiring minimum similarity of 90% to assign a taxonomy; 9 of the top 10 hits were required to share a taxonomic assignment to assign that identification to a query. By comparison, the QIIME defaults include 90% similarity, but only 2 of 3 database hits must share taxonomy for positive assignment. Our SILVA database is appended with 1,197 in-house high-quality, methane seep-derived bacterial and archaeal clones. Any sequences with pintail values >75 were removed. The modified SILVA database is available upon request from the corresponding authors. Singleton OTUs were removed first, and then any OTU which occurred less than 10 times across all samples (or about 0.000001% of the remaining sequences, were also removed. Known contaminants in PCR reagents and extraction kits as determined by analysis of no-template PCR and no-sample extraction controls run with each MiSeq set were then removed. After all filtering steps, 66,350 OTUs remained. Samples with fewer than 1,000 sequences recovered from these 66,350 OTUs were removed. In Chapter 2, 268 sediments and carbonates

from Mound 12 were considered; in this study, we analyzed 66 total samples: fifty natural and transplanted carbonates from Mound 12, fifteen sterile substrates incubated at Mound 12 (3 bags of 5 substrates each), and one filtered benthic water sample.

We chose not to rarefy our data consistent with several studies indicating that it impedes detection of differential abundance for little apparent benefit (McMurdie and Holmes, 2014; Weiss et al., 2017). These studies indicate that using a fourth-root transformation of relative abundance values is computationally simple, reasonably effective at detecting true differential abundance, and does not require discarding valid data. Accordingly, we used a fourth-root transformation prior to non-metric multidimensional scaling (NMDS) ordinations and all downstream analyses, conducted in R along with the *vegan* ecological statistics package (R Core Team, 2014; Oksanen et al., 2018). NMDS constructs *de novo* ordinations based on ranked pairwise sample dissimilarities (we used the Bray-Curtis dissimilarity metric), and the fit of the ordination is measured by the stress. Stress values below 0.2 are generally considered acceptable, and all ordinations presented here have stress values < 0.2 with parameter *trymax* = 100. We also conducted analysis of similarity (ANOSIM), similarity percentage (SIMPER), permutational analysis of variance (PERMANOVA) analyses, and homogeneity of dispersion (PERMDISP), also using *vegan* in R; p-values < 0.05 after 999 permutations (alpha value) were considered significant. OTU vectors were calculated for the NMDS ordination using the *vegan envfit* command with 999 permutations. In **Fig. 3.3**, we included only the most significant vectors (p-values = 0.001) that were also indicated as strong contributors to the variance in SIMPER analysis, *i.e.* the top 50 OTUs that were identified in pairwise analysis of the transplant treatment identifier (active→inactive, IT (native), IT→active, etc.) by contribution to the variance.

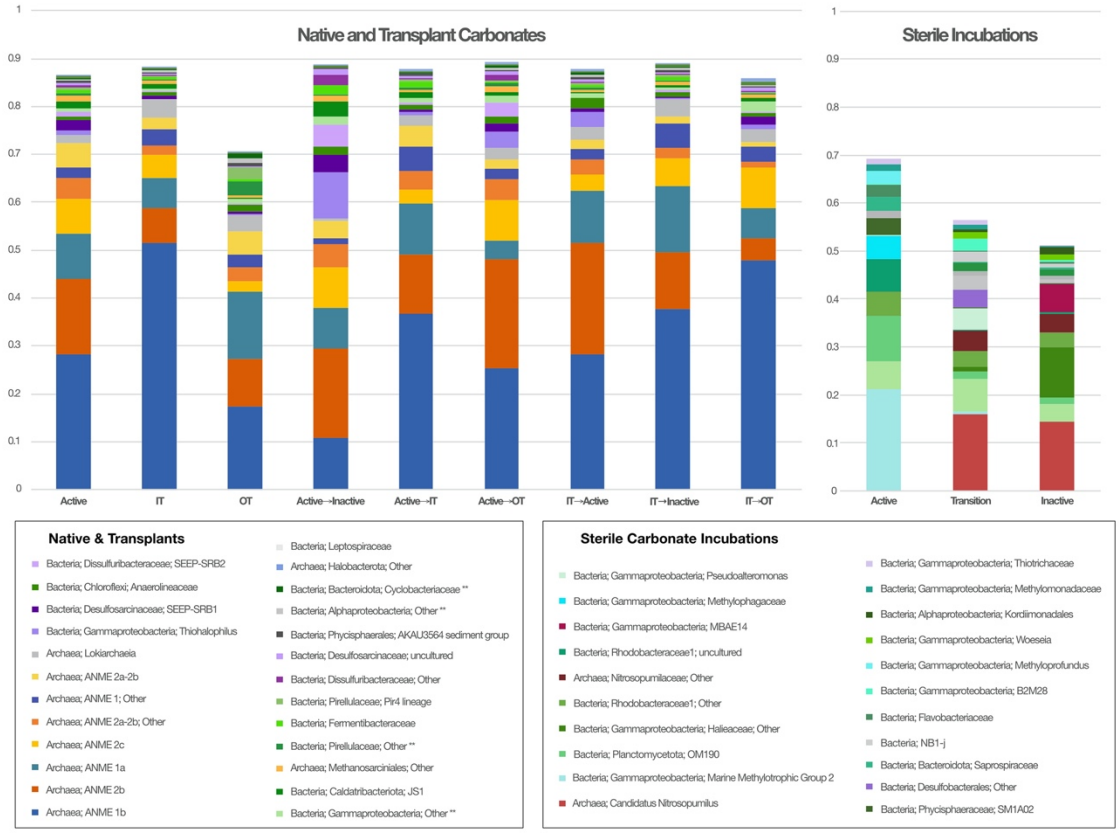

Fig. 3.1: Average microbial community of each treatment by relative abundance. 99%-similar OTUs were binned together by shared taxonomic assignment. The top 25 most abundant taxonomy bins for native and transplant carbonates and sterile carbonate incubations are presented here. ANME-1 bins are colored in dark blue tones, ANME-2 bins are in yellow and orange, sulfur-metabolizing organisms (including SRB and sulfide-oxidizers) are colored in purple tones, methylotrophs and aerobic methanotrophs are in light blue, other heterotrophs are in green, and nitrogen-metabolizing organisms (including ammonium-oxidizers and nitrate-reducers) are in red. Bins with no putative function are colored in gray. Most bins were not shared between the two charts; the three shared bins are marked with **. All of the native and transplanted samples contained high proportions of ANME-1 and ANME-2 subgroup organisms, but almost no ANME sequences were detected in incubated carbonate chips. Instead, those samples were dominated by methylotrophic organisms (active area) or ammonium-oxidizing *Nitrosopumilis* (transition and inactive area).

Results

Native carbonates versus sterile incubations

In our analysis of the colonizing microbial communities, the starkest difference between groups of samples lay between native carbonates (including both natural and transplanted

samples) and the sterile carbonate incubations (**Fig. 3.1, Fig. 3.4**). Native carbonates were characterized by high relative abundances of anaerobic methanotrophic archaea (ANME) from subclades 1 and 2. In every category of native carbonates, ANME organisms comprised >50% of the total endolithic microbial community; within IT non-transplanted carbonates, ANME-identified OTUs comprised 77.6% of the community, on average (the maximum). By contrast, no ANME subgroup exceeded 1% average relative abundance in any of the sterile carbonate incubations, even when binning OTUs of the same subgroup together (**Fig. 3.1)**. Instead, sterile incubations from the active site were dominated by organisms from the Marine Methylotrophic Group 2 of Gammaproteobacteria, which are aerobic methylotrophs (Ruff et al., 2013), as well as other possibly methylotrophic organisms from the Rhodobacteraceae and Methylophagaceae families. Transition and inactive sterile incubations were dominated by ammonium-oxidizing archaeal genus *Nitrosopumilus* (Walker et al., 2010; Qin et al., 2017), and also showed abundant putatively aerobic or sulfate-reducing heterotrophs. The transition and inactive carbonates samples were also the solid substrates that were most similar to the microbial community recovered from the Mound 12 benthic water sample, which was dominated by organisms from order Alteromonadales, including *Alteromonas*, *Pseudoalteromonas*, and *Marinobacter*.

Native carbonate differences by activity

Among the natural and transplant carbonates (excluding the two samples deployed in 2010 for lack of metadata), the treatment identifier (*e.g.* active, IT, OT, active → IT, etc.) was significant, but did not strongly correlate with the sample variance (ANOSIM R Value = 0.1453, p-value = 0.015). Our NMDS of the samples, however, indicated that the low correlation may have been the result of a difference in response amongst the groups, and we subsequently conducted pairwise ANOSIM between each treatment identifier. **Fig. 2** highlights these differences in the NMDS and **Table 3.5** contains the p-values for each ANOSIM and dispersion of each group. Among the native, non-transplanted samples, each pairwise combination of active, IT, and OT was significantly different (**Fig. 3.2a**); the one-way ANOSIM of all native, non-incubated carbonates also indicated significant difference (R Value = 0.2823, p-value = 0.004). Active samples were by far the most diverse group (although also the most deeply sampled), and much of the residual variation lay within that group.

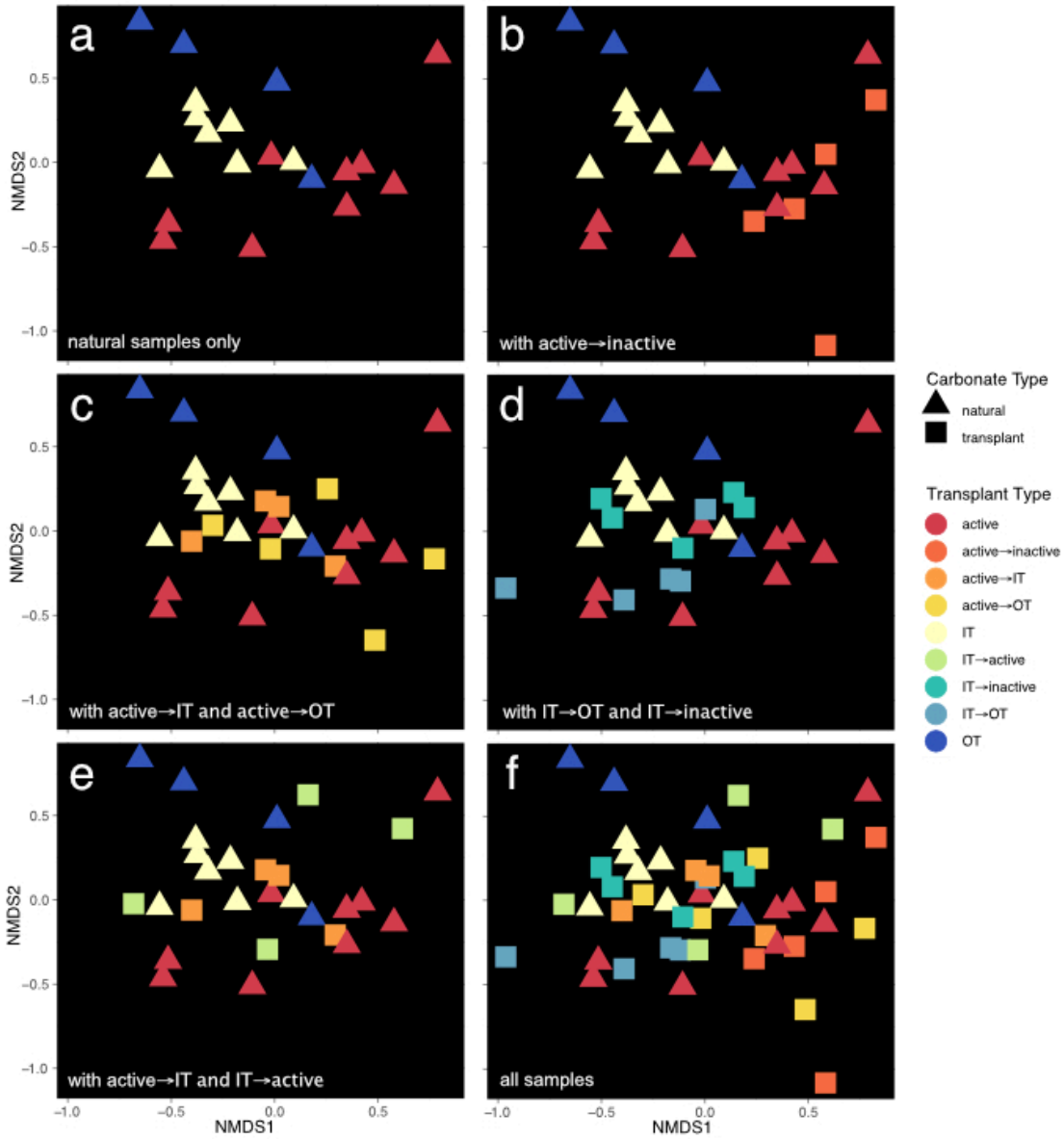

Fig. 3.2: Faceted NMDS of ordination of native and transplanted carbonates. The ordination of all samples is bottom right; all other displayed ordinations are derived from the full-sample ordination and subset for easier visualization. Distance between any two points is indicative of their community dissimilarity. The stress of the full ordination was 0.174.

Because the communities of all the native carbonates analyzed, both natural and incubated, were fundamentally similar, assessing the differences between different treatment identifiers primarily involved identifying differential abundance of the major taxa and changes in the ancillary taxa. The major differences between active and IT carbonates lay with abundance

differences in ANME-1b taxa. Of the top 100 OTUs identified by SIMPER analysis as contributing to the variance between these sample groups, 41 were annotated as ANME-1b. Of those 41, 34 were more abundant, on average, in IT samples, and 7 were more abundant in active samples. **Fig. 3.3** displays vectors most responsible for differences in ordination space substantiated by group-wide differential abundance analysis with SIMPER. OTUs annotated as ANME-2 were more uniform in their patterns of colonization. 26 of the top 100 OTUs contributing to variance were annotated as belong to one of the ANME-2 subgroups (17 from 2b, 6 from 2a-2b, and 3 from 2c); all 26 showed higher abundance in active samples than IT samples. IT samples also contained higher relative abundances of several non-ANME organisms, including organisms from orders Thalassobaculales, Leptospirales, Bacteroidales, and Caldatribacteriales, all of which are putative heterotrophs.

The main differences in active and OT carbonates were universally higher abundances of ammonium-oxidizing and nitrite-oxidizing organisms in the latter. 26 of the top 100 OTUs contributing to active versus OT carbonate difference were identified as belonging to ammonium-oxidizing family Nitrosopumilaceae, including *Nitrosopumilus maritimus* (Walker et al., 2010; Qin et al., 2017). Two additional OTUs annotated as *Nitrosomonas*, an ammonium-oxidizing Gammaproteobacterium, and six OTUs identified as *Nitrospina*, putative nitrite-oxidizers, were also in the top 100 variant OTUs. Each of these putative nitrogen-cycling OTUs were more abundant in OT versus active carbonates. Interestingly, although the sum of ANME-1b OTUs had lower overall abundance in OT carbonates versus active carbonates, individual OTUs of ANME-1b that were detected had higher average relative abundance, indicating that OT carbonates contained a less diverse guild of anaerobic methanotrophs overall. As was the case in the active versus IT comparison, ANME-2 group organisms were more abundant in active samples.

The comparison between IT and OT carbonates was largely reflective of the differences discussed above. Although IT and OT carbonates both contained more OTUs identified as *Nitrosopumilus* than Active samples, OT carbonates still contained the most. Similarly, IT carbonates were characterized by high relative abundances of ANME organisms, especially the ANME-1b subclade.

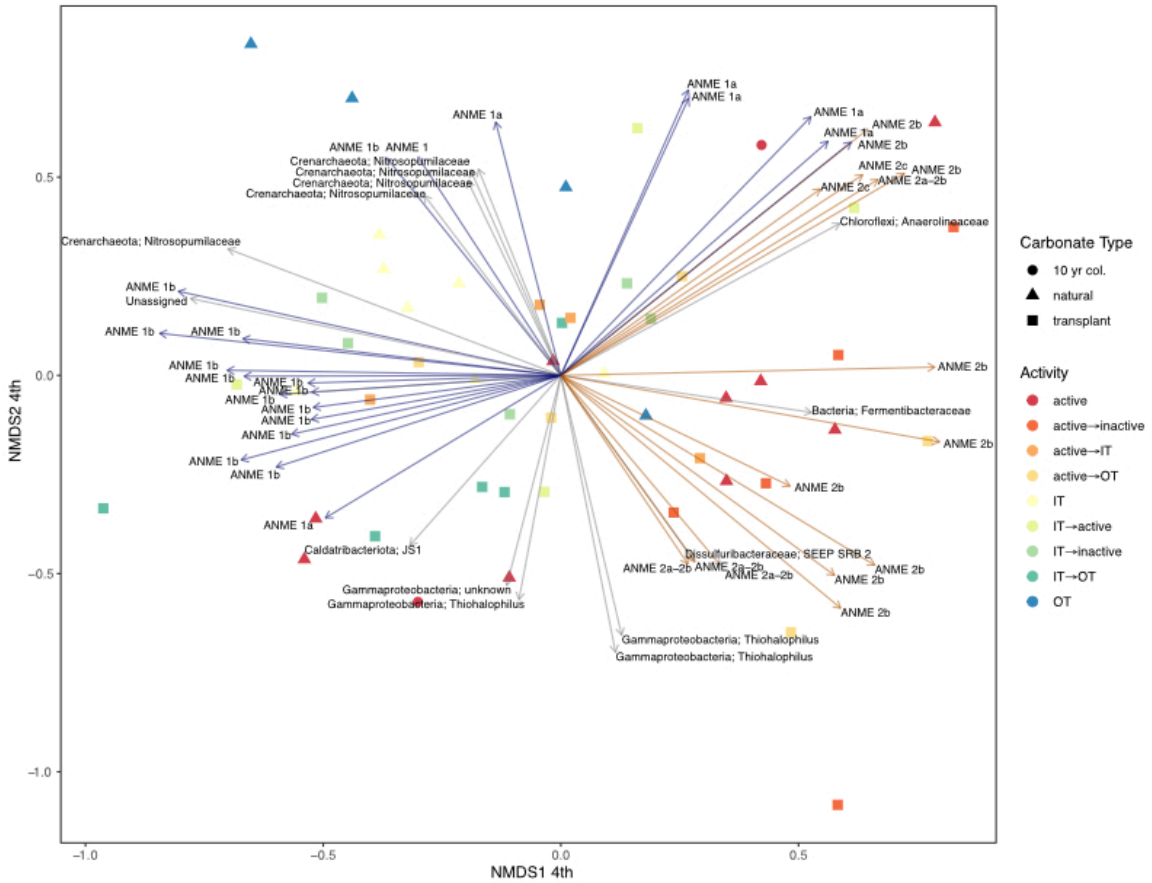

Fig. 3.3: NMDS ordination of all native and transplant carbonates with the top 50 OTUs that contributed to the variance between samples (identified by SIMPER) and were the most significant contributors to ordination distances (*envfit* p-value 0.001). ANME-1 vectors are colored in blue, and ANME-2 vectors are colored orange. Native active samples displayed the greatest dispersion of any sample group and had greater abundances of ANME-2 subgroup organisms than other treatments, whereas IT samples, including active→IT transplants, contained higher relative abundances of ANME-1 organisms. 7-year colonization samples (described in Methods) are included here as well and group with native active samples, but were not included in statistical analyses. Stress = 0.174.

Transplant-related changes in microbial community

As evidenced by the NMDS plot of carbonate samples and pairwise-ANOSIM analysis of transplant types, the response of microbial communities within transplanted rocks was complex (**Fig. 3.2**, **Table 3.5**). Interestingly, the endolithic communities of active→inactive (**Fig. 3.2b**), IT→inactive (**Fig. 3.2d**), active→OT (**Fig. 3.2c**), and IT→OT (**Fig. 3.2d**) transplants were not significantly different from the communities of their respective baseline

carbonates, indicating the endolithic communities of both groups of transplants remained broadly similar even after ~16 months in a presumably low-methane environment. Although the communities between active samples and active→OT or active→inactive transplants were not significantly different from the whole-community perspective, we did note that organisms from genus *Thiohalophilus*, putative sulfide-oxidizing Gammaproteobacteria were more abundant in the transplants than the baseline samples.

In contrast to transplants to the OT or inactive area, which were mostly unchanged from their original environment, the microbial community of active→IT transplants took on some of the characteristics of their destination (**Fig. 3.2c**). Specifically, the active→IT transplants showed increased relative abundance of ANME-1b organisms, and decreased abundance of ANME-2b organisms relative to the active baseline, trending towards the community structure of IT carbonates (**Fig. 3.1**). Active→IT transplants were not significantly different from either Active or IT baseline carbonates (even though the Active and IT baselines were significantly different) and instead bridged these two different communities.

IT→active transplants, notably, were not simply the inverse of active→IT transplants (**Fig. 3.2e**). Out of these 4 transplants, 1 was similar to the IT baseline (10954), 2 were similar to the active samples (11128, 11152), and the last (11153) actually clustered closest to the OT baseline carbonates. Although this group of transplants was highly varied, the average community of these samples was similar to that of the active baseline samples, and significantly different from the IT baseline samples (p-value = 0.031).

Discussion

Microbial community of native carbonates versus incubations

As mentioned in Chapter 2, the endolithic communities of seafloor carbonates from Mound 12 are broadly similar. Over 50% of all the recovered sequenced belonged to OTUs identified as ANME, clades of archaea that perform anaerobic methane oxidation in conjunction with a bacterial partner, commonly a sulfate-reducing deltaproteobacterium from the Seep SRB-1 or Seep SRB-2 subgroups (Orphan et al., 2001a; Orphan et al., 2001b; Orphan et al., 2004; Orphan et al., 2009; Ruff et al., 2015; Metcalfe et al., 2020). In fact, the formation of the carbonates themselves is intrinsically linked to the activity of ANME archaea, since methane

oxidations generates alkalinity. ANME are frequently found in high abundance within the endolithic community of these carbonates, and have been found to continue oxidizing methane (Marlow et al., 2014b). Many organisms are known to preferentially attach to solid substrates, however, especially in sediment communities (Orcutt et al., 2010; McMahon and Parnell, 2014; Bar-On et al., 2018; Mullin et al., 2020). Discerning whether high ANME abundance in methane seep carbonates is due solely to self-entombment versus preferential attachment has not been well-quantified (Case et al., 2015). In our incubations of four sterile carbonate lithologies in the active, IT, and inactive zone, we detected very few sequences belonging to ANME-annotated OTUs. No subclade of ANME (all OTUs from that clade binned together) even reached 1% of the recovered community from any sterile carbonate sample. Other groups of sediment organisms, including *Nitrosopumilus,* methylotrophic lineages of Gammaproteobacteria (MMG-2), and *Anaerolinea* were much more abundant on these carbonates, up to ~15% relative abundance for *Nitrosopumilus*, and ~20% abundance of MMG-2. Our results indicate that virtually all of the ANME presence in methane seep carbonates is a result of self-entombment.

Because so few ANME were found on our sterile carbonate incubations, the organisms that were found can also be compared with the sediment microbial community. Precisely because organisms belonging to *Nitrosopumilus* and MMG-2 were found even in the absence of ANME, we infer that they preferentially colonize these carbonates. In native carbonates, it is possible that the sequences we detected from these organisms were remnants of organisms trapped in the carbonate matrix during formation rather than true endolithic microorganisms. The increasing abundance of some organisms in carbonates with decreasing activity, including *Nitrosopumilus*, indicates that these organisms may actually migrate into the carbonate matrix.

Microbial community of native carbonates

The endolithic microbial community of our native carbonates was consistent with the results of previous studies on endolithic communities from (Marlow et al., 2014b; Case et al., 2015). Those studies also examined the microbial communities from carbonates in the less active area (labeled IT or OT in this study) and also found that they contained higher relative abundances of ANME-1 organisms. As is visible in **Fig. 3.3**, IT and OT carbonate ordination position was due to more abundant OTUs identified as ANME-1a and ANME-1b. Native OT carbonates were also distinguished from active and IT carbonates by the relative abundance of

Nitrosopumilus organisms, detected roughly twice as often as in active or IT carbonates on average, though still at low total relative abundance (0.7% ± 0.4 vs. 0.3% ± 0.8).

Native active carbonates showed higher relative abundances of ANME-2 subgroup organisms than IT or OT carbonates. This result was consistent with samples analyzed by Case, et al., despite studying seep carbonates from a different area. Active carbonates, however, were also the most varied, as assessed by PERMDISP, and the dispersion of active samples was largely due to which ANME-2 OTU was dominant. It may be that, as was true for sediments analyzed in Chapter 2, methane seep carbonates demonstrate a sharply defined zone of highest activity. However, even a pair of active samples taken from the same location (serial numbers 9729 and 9730) did not cluster together in our ordination, which indicates that the conditions governing the endolithic microbial community structure may be very complex, perhaps related to microscale heterogeneity in the mineralogy of the rocks, pore space, or some other factor (Edwards and Rutenberg, 2001; Sylvan et al., 2013; Toner et al., 2013).

Pairwise ANOSIM results

In assessing the changes in the carbonate endolithic community wrought by transplantation, we primarily relied on the results of pairwise ANOSIM analyses to assess whether transplants were significantly different from rocks from either their origin or destination (**Fig. 3.5**). ANOSIM compares dissimilarity rankings within and between sample groupings, and then permutes the data to compute a p-value. Because the data is thus twice removed from raw abundance, by transformation into pairwise dissimilarity metrics and then a simple ranking of those dissimilarities, ANOSIM makes virtually no assumptions about the underlying structure or distribution of the data (Clarke, 1993). Also, since the methodology between ANOSIM analysis and NMDS ordination are similar, ANOSIM is well-suited to assess the significance of clusters observed in the ordination. Whenever multiple significance tests are conducted, however, the likelihood of a Type-1 error (false positive in determining significant difference) increases, and it is critical, therefore, to assess where an error is most likely to have occurred. When presented with an unbalanced experiment (groups with different sample sizes) as is the case here, virtually all resemblance tests (*e.g.* ANOSIM, PERMANOVA, MANOVA) are overly conservative with assigning significant difference if the larger group is also the most heterogeneous (Anderson and Walsh, 2013). In our study, carbonates from the active site were

both the largest group and the most heterogeneous, and it is likely, therefore, that our designation of significantly different samples is also conservative. In addition to the pairwise-ANOSIM analyses, we also ran the *envfit* function to fit OTU vectors onto the NMDS, an analysis that is blind to sample groupings, to better visualize changes amongst groups (**Fig. 3.3**).

Carbonate microbial community shifts with transplants

Case, et al. conducted a limited number (total $n = 6$) of transplant experiments between active and IT-type regions (Case et al., 2015). Those transplants also indicated that the microbial community of transplants from active to low activity were not distinguishable from active samples, similar to active→OT and active→inactive transplants in this study. The two transplants that Case, et al. conducted from the low activity region to the active region were found to contain microbial communities similar to carbonates from the active site. IT→active transplants in this study indicated that the microbial community in IT rocks did not respond in a predictable fashion; those transplants showed the second highest dispersion of any sample group after active samples (**Table 3.5**). IT→active transplant communities were found to be significantly different from the native IT baseline carbonates and not significantly different from active samples, consistent with the findings of Case, et al., although the inherent biases of dispersion tests like ANOSIM are typically too liberal in assigning significance when the more heterogeneous group is also the smaller (Anderson and Walsh, 2013).

The same factors that make active samples more broadly dispersed taxonomically than other groups may also make transplants back into the active zone more complex. If, for example, fluid flow through the carbonate is a strong organizational force for endolithic communities, transplants to the active area are likely to demonstrate varied response rates as communities within different areas of that rock might respond to the surrounding environment at different rates.

Ecological implications

Our transplant experiments revealed that the changes in the endolithic community of a carbonate wrought by moving the rock from one site to another were not straightforward. The difference between moving a carbonate to the IT versus to the OT or inactive area was particularly striking. When both active and IT carbonates were moved to areas of low or absent dissolved methane (OT and inactive areas), the endolithic communities were not significantly

different from the native rocks of the original zone. By contrast, the community of active→IT transplants did shift towards a more IT-like composition, with increased relative abundance of ANME-1b. One possible reason for this shift is that the IT area, while lower in activity, likely still has some dissolved methane in the benthic water column that sustains the local chemosynthetic fauna. The lower dissolved methane may act as a selective pressure, providing sufficient energy for organisms that are better adapted to the endolithic lifestyle, possibly including ANME-1 subgroup organisms, but not others. Seep carbonates are also known to trap small amounts of methane within the rock matrix, and it is possible that ANME-1 are better able to extract and utilize preserved methane (Miyajima et al., 2018). A handful of previous studies have indicated that ANME-1 are more abundant than any other ANME subclade in methane seep carbonates and nodules (Marlow et al., 2014b; Case et al., 2015; Mason et al., 2015). ANME-1 also tend to partner with a distinct subgroup of SRB, HotSeep-1, or SEEP-SRB2, which they share with ANME-2c, pointing to a unique life strategy (Krukenberg et al., 2018; Metcalfe et al., 2020). Although the precise metabolic mechanism for the symbiosis between any subgroup of ANME and SRB remain unknown, some studies have suggested that ANME-1 are less reliant on their SRB partner than other ANME subgroups (Knittel et al., 2005). Previous studies examining lipid biomarkers at fossil seeps have been predicated on the notion that ANME-2 are better adapted than ANME-1 to high methane environments and have constructed models of carbonate formation using those assumptions (Blumenberg et al., 2004; Stadnitskaia et al., 2008a; Stadnitskaia et al., 2008b). Elucidating the link between ANME-1 and seep carbonates promises to dramatically aid with the interpretation and reevaluation of fossil seeps biomarkers, but ultimately, more research the specific adaptations of ANME-1 to an endolithic lifestyle is necessary.

One of the findings in Chapter 2 was that ANME-1 group organisms were only present in a specific subset of sediment cores at Mound 12; those cores also appeared to serve as the center of the active zone geochemically and ecologically. ANME-1 group organisms have also been found to outcompete ANME-2 group organisms in high-methane enrichment cultures (Girguis et al., 2005). Although ANME-1 were present in all carbonates, both native and transplants, they were highest in the native IT carbonates, rather than in active samples, a pattern that has been observed in other carbonate studies (Marlow et al., 2014b; Case et al., 2015).

Notably, however, Marlow, et al. demonstrated higher carbonate content in the sediment of active sites with high ANME-1 versus those without (Marlow et al., 2014a). That study examined just two sediment samples, but the results were consistent with our findings here and in Chapter 2. If ANME-1 organisms are indeed better adapted to an endolithic lifestyle, that might explain the mismatch between activity levels of samples with high ANME-1. Measuring the relative abundance of ANME-1 would then serve as a useful proxy for carbonate formation rates in the sediment and aid in describing the ecology of future seep communities.

Conclusion

We compared the endolithic communities of native seep carbonates from different zones of activity with a set of transplant experiments between those zones. We found that when carbonates were transplanted to areas with slightly lower methane, the endolithic community experienced a selective pressure and reliably shifted to a more ANME-1-dominated composition. Community composition of samples transplanted to areas with dramatically lower methane did not change significantly, implying that the endolithic community was affected equally. These results provide context to understand the ecological niches of the different ANME subgroups and, when combined with biomarker studies of fossil seeps, provide evidence to help interpret the temporal dynamics of ancient seeps.

Supplemental Figures

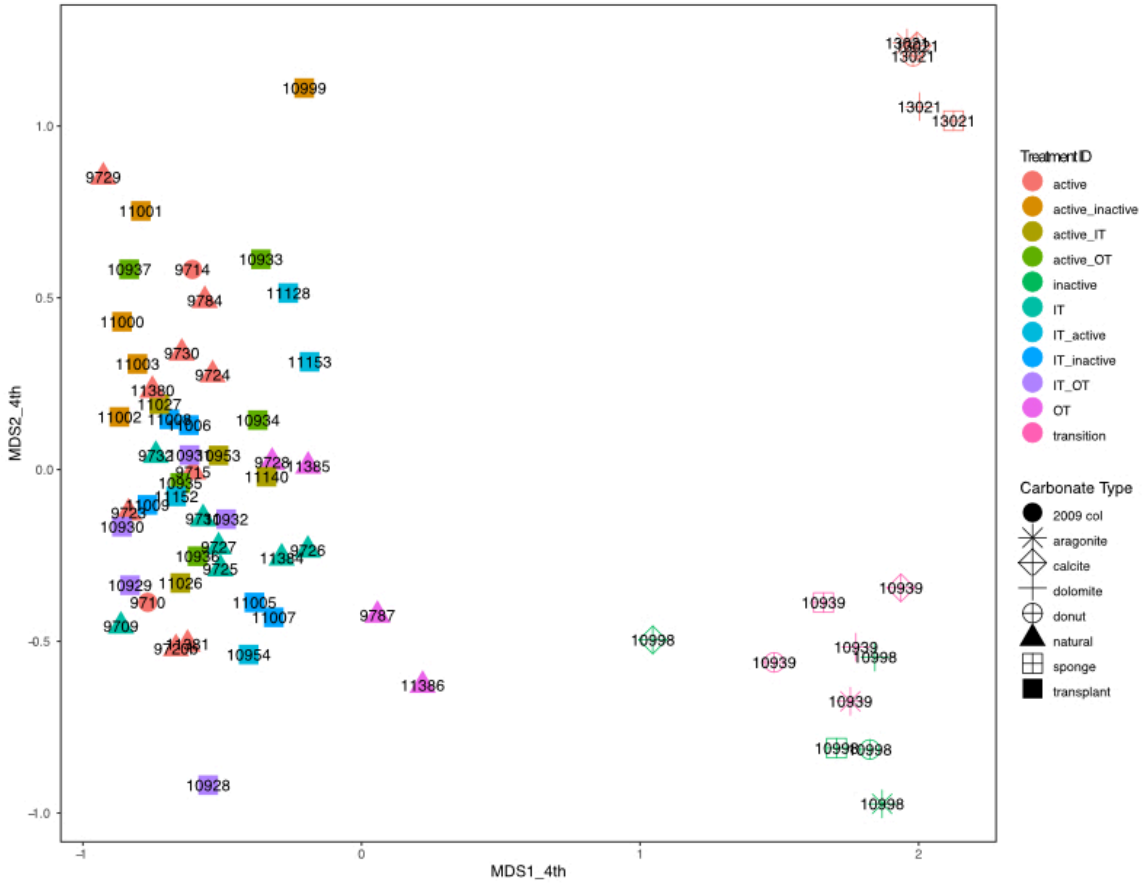

Fig. 3.4: NMDS ordination of all samples, including native and transplanted carbonates, and sterile incubations. Sterile carbonate incubation samples were all significantly different from Mound 12 carbonates, with transition and inactive area sterile incubations were also significantly different from active area sterile incubations. Stress = 0.111

Pairwise ANOSIM p-values

	Dispersion	active	IT	OT	A→IT	A→OT	active→ inactive	IT→A	IT→OT	IT→inactive
active	0.5104									
IT	0.4570	0.022								
OT	0.4453	0.034	0.011							
A→IT	0.4189	0.776	0.188	0.038						
A→OT	0.4838	0.574	0.022	0.034	0.401					
active→inactive	0.4785	0.285	0.003	0.016	0.035	0.336				
IT→A	0.4985	0.275	0.031	0.274	0.614	0.684	0.145			
IT→OT	0.4721	0.285	0.056	0.011	0.379	0.424	0.007	0.255		
IT→inactive	0.4164	0.196	0.351	0.037	0.190	0.121	0.009	0.136	0.29	

Table 3.5: ANOSIM p-values of pairwise analysis of each carbonate treatment. If the p-value was lower than our alpha value cutoff (0.05), the cell is colored green. The dispersion of each sample group (measured as distance from group mean by PERMDISP) is also shown.

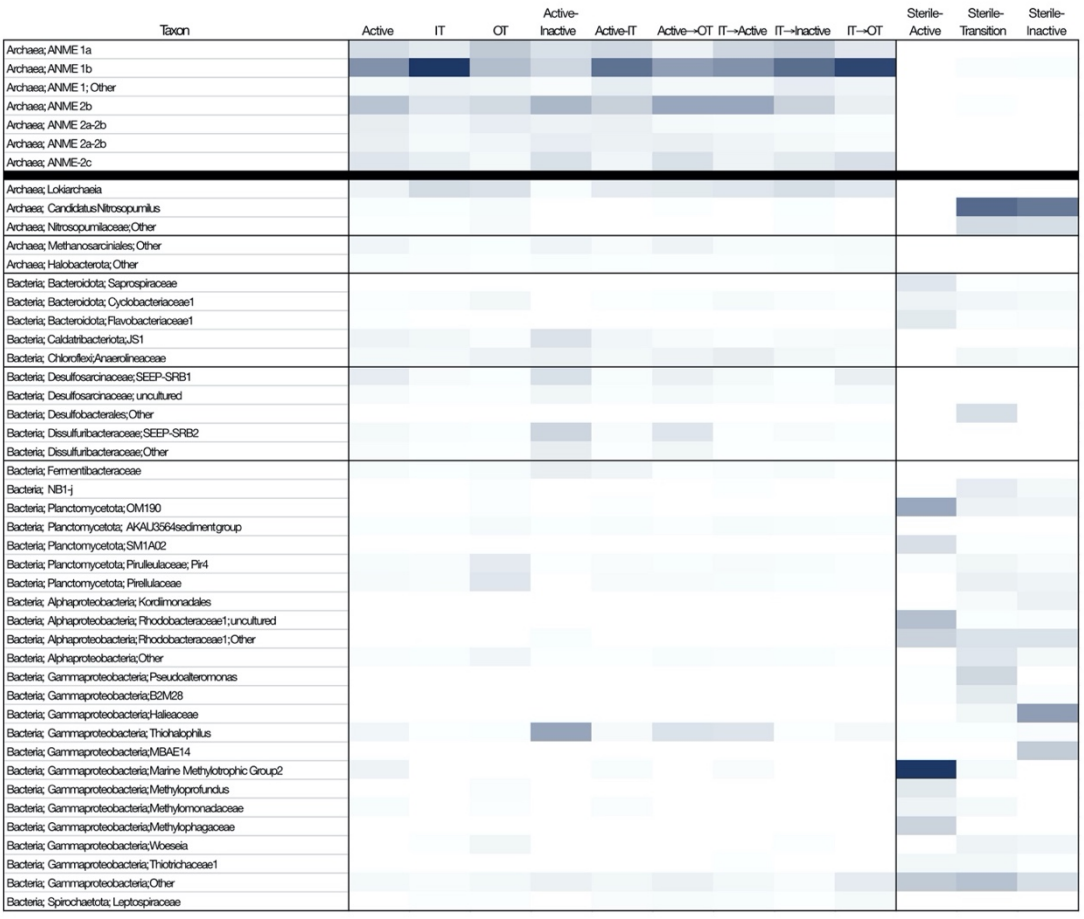

Fig. 3.6: Heat map version of the stacked bar chart in Fig. 1. ANME bins and other bins are scaled separately according to the ranges listed on the right.

Conclusion

Although the deep biosphere contains roughly 14% of the global biomass, the nature and extent to which this biome interacts with broader global biogeochemical cycles still evades scientific consensus (Bar-On et al., 2018). Considering that the density and activity of microorganisms in the deep biosphere are generally low, some observers have gone so far as to suggest that fundamental principles of evolution, including selection and competition, are virtually nonexistent in this environment and that the microorganisms detected therein are not so much adapted to the unique challenges of the environment but merely on a slow march to death (Starnawski et al., 2017). Preliminary evidence suggests that much of this life is located in fracture zones or along plate boundaries — locations where energy is more readily available whether by way of groundwater transport or the grinding and shearing of the host rock itself (Biddle et al., 2011). Experiments that do not explicitly target areas likely to be along these steep energy gradients (which describes the majority of deep biosphere experiments to date) are therefore less likely to recover microbial diversity or activity rates that are reflective of the bulk of the biomass. Careful experiments that attempt to understand the pore space and hydrology of the region, though difficult, have been attempted and found that highly deformed and fractured regions within an individual well were more active than other depths (Riedinger et al., 2015). Practically, these experiments are difficult to carry out and require a highly interdisciplinary team to understand not only the local geology and hydrology, perhaps even drilling a new well in an interesting area, but also the microbiology. In the experiments presented here, we mostly tried to circumvent this particular challenge by examining the community along a pre-existing well in a known fracture zone (Chapter 1) or by working on the seafloor (Chapters 2 & 3), an environment that mimics the steep energy gradient without requiring subsurface access.

Ultimately, the experiments that will be most beneficial in assessing the possibility of a boom-bust lifestyle in the deep biosphere will be those that are able to capture a tectonic event in real time and observe whether there is a corresponding increase in microbial biomass or activity. This seemingly daunting task is nevertheless becoming more possible with ever-improving technology, including apparatus to drill the wells themselves as well as sampling and

sample analysis. The extant mines that have historically been used for deep biosphere experiments likely will not be good experimental targets, since mines are not typically located in regions of high tectonic activity. Instead, these experiments will rely on boreholes into fractured rock zones along fault lines (such as those currently being drilled by Alexis Templeton and collaborators in Oman), with frequent or even continuous monitoring of both microbial community composition and geochemistry (analogous to the Rifle, CO field monitoring site) (Wrighton et al., 2014; Rempfert et al., 2017). The experiments conducted in Chapter 1 serve as one early attempt at continuous monitoring, and even included an energy influx in the form of organic sponges. In retrospect, we neglected to collect cell count data, both on the mineral surfaces and in the water itself, in part because counting cells on mineral surfaces is very difficult. A more robust monitoring system, with reliable discrete water sampling, would help mitigate that issue, as would the addition of confocal FISH or deep UV microscopy to examine cells attached to mineral substrates. As these instruments continue to improve, I am confident that this dream of a project will become more and more attainable and that observing deep biosphere microbial community changes in direct response to tectonic activity will be possible, finally allowing the scientific community to remedy this oversight in our global biogeochemical budgets.

Chapters 2 and 3 serve as an alternative method to observe a similarly steep environmental gradient at a significantly easier study site, analogous to studying adaptations of microorganisms inhabiting the Atacama Desert in order to better hypothesize about life on Mars (Navarro-Gonzalez et al., 2003; Schulze-Makuch et al., 2018). The Orphan Lab has diverse interests at methane seeps, ranging from the ecological dynamics of seep ecotones to the physiology of ANME, and many unresolved questions remain for those that continue to study these areas. One of the most challenging is to observe these sites on longer timescales. Our study at Mound 12, which included dives at the site in 2017 and 2018, made it clear that these sites are not static but instead change on relatively rapid timescales. Of course, diving consistently at the same sites is not particularly feasible; first, much of the ocean floor remains completely unexplored and must therefore be a priority, and second, the cost of consistent observation by the same team would be astronomical. However, more consistent use of the photomapping

techniques we employed would enable scientists across multiple expeditions to share data in a program like ArcGIS and observe how the same site changes through time.

As additional data beyond the photomapping is collected, it could also be layered onto the maps to provide comprehensive views of the seafloor. This past summer, the Orphan Lab not only collaborated with a programming team to produce a sediment core viewing program ("Opal"), complete with geochemical parameters and microbial diversity smoothing algorithms, but I personally oversaw and helped create a megafauna map in ArcGIS, using bathymetry and photomapping data obtained by an MBARI team. The data is stunning to observe this way and enables us microbiologists to truly get a sense for the habitat of particular sediment cores without the need for sifting through hundreds of hours of ROV video footage. Especially as folks like me move on from the lab, these data products will be invaluable for new lab members to immediately immerse themselves in the ecology of our field sites.

Chapters 2 and 3 also raised interesting questions as to the niche and habitat differentiation of the various ANME strains. The ecological, evolutionary, and physiological questions of relating to the differentiation ANME-1 and ANME-2a-2b have been particularly compelling. ANME-1 are frequently found deeper in our sediment cores, closer to the region where true methanogens are present. Grayson Chadwick's review covered what is known regarding the physiological distinction between these clades (Chadwick et al., 2020) and made it clear that ANME-1 consistently lack the F_{420}-dependent methylenetetrahydromethanopterin (Mer), the protein which serves to shuttle electrons onto the F_{420} cofactor. Instead, Chadwick theorizes, ANME-1 may be using methylenetetrahydrofolate reductase (MetF), which would require substituting NADP+ for cofactor F_{420}. If true, this switch would imply that ANME-1 dump electrons onto an electron carrier with higher electron potential (-320 versus -360 mV), and this subtle change in energetics may explain why some studies hypothesized that certain lineages of ANME-1 may be capable of performing methanogenesis in addition to methane oxidation (Lloyd et al., 2011; Beulig et al., 2019). The lower energetic barrier would aid in making the reactions more reversible. It may also help explain why some studies have observed that ANME-1 are capable of rapid growth in high methane partial pressures (Girguis et al., 2005). The higher methane would increase overall throughput through the reaction and make up for

the lower energetic yield, analogous to how cytochrome *c* oxidase has a lower affinity for oxygen but nevertheless works faster in high oxygen environments (Giuffrè et al., 2014).

Still to be explained is the puzzling connection between ANME-1 and carbonates. I suspect strongly that sediments at Mound 12 (Group 1 cores) that contained high relative abundance of ANME-1 also contained abundant grain-sized particles of carbonate. As I described in Chapter 3, numerous other studies have also found high abundance of ANME-1 in the endolithic communities of these rocks (Marlow et al., 2014a; Case et al., 2015). Jeff Marlow, a former lab member, also found higher carbonate values in the sediment composition of high-ANME-1 sediments (Marlow et al., 2014a). It is not particularly clear what physiological feature would enable ANME-1 to outcompete other ANME lineages inside the rock matrix. As I noted in Chapter 3, several previous studies have imaged ANME-1 organisms in only a very loose association with sulfate-reducing bacteria, contrary to the tight aggregates typically observed (Orphan et al., 2002; Knittel et al., 2005; House et al., 2009). Perhaps this loose association is sufficient to survive inside carbonates, where pore space may limit the more classic aggregates, which are commonly tens of microns across. It stands to reason, then, that ANME-1 either use a soluble electron carrier as a shuttle or that they are able to dump electrons into the rock matrix somehow, making them grow independently of sulfate-reducers, analogous to well-studied iron-reducing bacteria. To my knowledge, efforts to cultivate or isolate ANME-1 have not been particularly successful, but perhaps attempting to isolate them with sterilized, powdered carbonate would find some success.

I want to close by simply saying that Caltech has truly been an incredible place to do this work. The opportunities that I have provided have stimulated me intellectually and kept the flame of my curiosity alight; I am confident I will hold those memories close throughout my life. Putting this thesis together has been a good way to revisit some of those memories and re-evaluate the science with the addition all the knowledge I have gained through my time at Caltech. For any future Orphan lab members who have made it this far, I offer a small piece of advice: enjoy the journey. We work on wonders.

BIBLIOGRAPHY

Aloisi, G., Bouloubassi, I., Heijs, S.K., Pancost, R.D., Pierre, C., Sinninghe Damsté, J.S., et al. (2002). CH4-consuming microorganisms and the formation of carbonate crusts at cold seeps. *Earth and Planetary Science Letters* 203**,** 195-203. doi: 10.1016/S0012-821X(02)00878-6.

Amon, D.J., Gobin, J., Van Dover, C.L., Levin, L.A., Marsh, L., and Raineault, N.A. (2017). Characterization of Methane-Seep Communities in a Deep-Sea Area Designated for Oil and Natural Gas Exploitation Off Trinidad and Tobago. *Frontiers in Marine Science* 4. doi: 10.3389/fmars.2017.00342.

Anderson, M.J., and Walsh, D.C.I. (2013). PERMANOVA, ANOSIM, and the Mantel test in the face of heterogeneous dispersions: Whall null hypothesis are you testing? *Ecological Monographs* 83**,** 557-574.

Arndt, S., Jørgensen, B.B., LaRowe, D.E., Middelburg, J.J., Pancost, R.D., and Regnier, P. (2013). Quantifying the degradation of organic matter in marine sediments: A review and synthesis. *Earth-Science Reviews* 123**,** 53-86. doi: 10.1016/j.earscirev.2013.02.008.

Ashford, O.S., Guan, S., Capone, D., Rigney, K., Rowley, K., Orphan, V.J., et al. (2020). A chemosynthetic ecotone — 'chemotone' — in the sediments surrounding deep-sea methane seeps. *Limnology and Oceanography* (accepted).

Aüllo, T., Ranchou-Peyruse, A., Ollivier, B., and Magot, M. (2013). *Desulfotomaculum* spp. and related gram-positive sulfate-reducing bacteria in deep subsurface environments. *Front Microbiol* 4(362). doi: 10.3389/fmicb.2013.00362.

Baas Becking, L.G.M., and Canfield, D.E. (2015). *Baas Becking's Geobiology: Or Introduction to Environmental Science*. John Wiley & Sons, Ltd.

Bailey, J.V., Raub, T.D., Meckler, A.N., Harrison, B.K., Raub, T.M.D., Green, A.M., et al. (2010). Pseudofossils in relict methane seep carbonates resemble endemic microbial consortia. *Palaeogeography, Palaeoclimatology, Palaeoecology* 285(1-2)**,** 131-142. doi: 10.1016/j.palaeo.2009.11.002.

Baker, M.C., Ramirez-Llodra, E.Z., Tyler, P.A., German, C.R., Boetius, A., Cordes, E.E., et al. (2010). "Biogeography, Ecology, and Vulnerability of Chemosynthetic Ecosystems in the Deep Sea," in *Life in the World's Oceans: Diversity, Distribution, and Abundance,* ed. A.D. Mcintyre. Blackwell Publishing Ltd), 161-182.

Bar-On, Y.M., Phillips, R., and Milo, R. (2018). The biomass distribution on Earth. *Proceedings of the National Academy of Sciences* 115(25)**,** 6506-6511. doi: 10.1073/pnas.1711842115.

Barry, J.P., Whaling, P.J., and Kochevar, R.K. (2007). Growth, production, and mortality of the chemosynthetic vesicomyid bivalve, Calyptogena kilmeri from cold seeps off central California. *Marine Ecology* 28(1)**,** 169-182. doi: 10.1111/j.1439-0485.2007.00119.x.

Battin, T.J., Luyssaert, S., Kaplan, L.A., Aufdenkampe, A.K., Richter, A., and Tranvik, L.J. (2009). The boundless carbon cycle. *Nature Geoscience* 2(9)**,** 598-600. doi: 10.1038/ngeo618.

Beaulieu, S.E., Baker, E.T., and German, C.R. (2015). Where are the undiscovered hydrothermal vents on oceanic spreading ridges? *Deep Sea Research Part II: Topical Studies in Oceanography* 121**,** 202-212. doi: 10.1016/j.dsr2.2015.05.001.

Beaulieu, S.E., Baker, E.T., German, C.R., and Maffei, A. (2013). An authoritative global database for active submarine hydrothermal vent fields. *Geochemistry, Geophysics, Geosystems* 14(11)**,** 4892-4905. doi: 10.1002/2013gc004998.

Belcher, W.R., Bedinger, M.S., Back, J.T., and Sweetkind, D.S. (2009). Interbasin flow in the Great Basin with special reference to the southern Funeral Mountains and the source of Furnace Creek springs, Death Valley, California, U.S. *Journal of Hydrology* 369(1-2)**,** 30-43. doi: 10.1016/j.jhydrol.2009.02.048.

Belcher, W.R., Elliott, P.E., and Geldon, A.L. (2001). Hydraulic-Property Estimates for Use with a Transient Ground-Water Flow Model of the Death Valley Regional Ground-Water Flow System, Nevada and California. *Water-Resources Investigations Report* 01(4210).

Beulig, F., Roy, H., McGlynn, S.E., and Jorgensen, B.B. (2019). Cryptic CH4 cycling in the sulfate-methane transition of marine sediments apparently mediated by ANME-1 archaea. *ISME J* 13(2)**,** 250-262. doi: 10.1038/s41396-018-0273-z.

Biddle, J.F., Sylvan, J.B., Brazelton, W.J., Tully, B.J., Edwards, K.J., Moyer, C.L., et al. (2011). Prospects for the study of evolution in the deep biosphere. *Front Microbiol* 2**,** 285. doi: 10.3389/fmicb.2011.00285.

Blazewicz, S.J., Barnard, R.L., Daly, R.A., and Firestone, M.K. (2013). Evaluating rRNA as an indicator of microbial activity in environmental communities: limitations and uses. *ISME J* 7**,** 2061-2068. doi: 10.1038/ismej.2013.102.

Blumenberg, M., Seifert, R., Reitner, J., Pape, T., and Michaelis, W. (2004). Membrane lipid patterns typify distinct anaerobic methanotrophic consortia. *Proc Natl Acad Sci U S A* 101(30)**,** 11111-11116. doi: 10.1073/pnas.0401188101.

Boetius, A., Ravenschlag, K., Schubert, C.J., Rickert, D., Widdel, F., Gieseke, A., et al. (2000). A marine microbial consortium apparently mediating anaerobic oxidation of methane. *Nature* 407**,** 623-626.

Boetius, A., and Wenzhöfer, F. (2013). Seafloor oxygen consumption fuelled by methane from cold seeps. *Nature Geoscience* 6(9)**,** 725-734. doi: 10.1038/ngeo1926.

Bowden, D.A., Rowden, A.A., Thurber, A.R., Baco, A.R., Levin, L.A., and Smith, C.R. (2013). Cold seep epifaunal communities on the Hikurangi margin, New Zealand: composition, succession, and vulnerability to human activities. *PLoS One* 8(10)**,** e76869. doi: 10.1371/journal.pone.0076869.

Braby, C.E., Rouse, G., Johnson, S.B., Jones, W.J., and Vrijenhoek, R.C. (2007). Bathymetric and temporal variation among Osedax boneworms and associated megafauna on whale-falls in Monterey Bay, California. *Deep Sea Research Part I: Oceanographic Research Papers* 54(10)**,** 1773-17791. doi: 10.1016/j.dsr.2007.05.014.

Bradley, J.A., Amend, J.P., and LaRowe, D.E. (2018). Bioenergetic Controls on Microbial Ecophysiology in Marine Sediments. *Front Microbiol* 9**,** 180. doi: 10.3389/fmicb.2018.00180.

Bradley, J.A., Arndt, S., Amend, J.P., Burwicz, E., Dale, A.W., Egger, M., et al. (2020). Widespread energy limitation to life in global subseafloor sediments. *Science Advances* 6**,** eaba0697. doi: 10.1126/sciadv.aba0697.

Braun, S., Mhatre, S.S., Jaussi, M., Roy, H., Kjeldsen, K.U., Pearce, C., et al. (2017). Microbial turnover times in the deep seabed studied by amino acid racemization modelling. *Sci Rep* 7(1)**,** 5680. doi: 10.1038/s41598-017-05972-z.

Bredehoeft, J., and King, M. (2010). Potential contaminant transport in the regional Carbonate Aquifer beneath Yucca Mountain, Nevada, USA. *Hydrogeology Journal* 18**,** 775. doi: 10.1007/s10040-009-0550-z.

Bredehoeft, J., King, M., Jansen, J., Fridrich, C.J., and Reese, S. (2008). Death Valley Lower Carbonate Aquifer monitoring program - wells down gradient of the proposed Yucca Mountain Nuclear Waste Repository. *Inyo County Yucca Mountain Repository Assessment Office***,** 111.

Breuker, A., Köweker, G., Blazejak, A., and Schippers, A. (2011). The deep biosphere in terrestrial sediments in the Chesapeake Bay area, Virginia, USA. *Front Microbiol* 2. doi: 10.3389/fmicb.2011.00156.

Caccavo, F., and Das, A. (2002). Adhesion of dissimilatory Fe(III)-reducing bacteria to Fe(III) minerals. *Geobiology J* 19**,** 161-177.

Canfield, D.E. (1994). Factors influencing organic carbon preservatioin in marine sediments. *Chemical Geology* 114**,** 315-329.

Canfield, D.E., Glazer, A.N., and Falkowski, P.G. (2010). The Evolution and Future of Earth's Nitrogen Cycle. *Science* 330(6001)**,** 192-196. doi: 10.1126/science.1186120.

Caporaso, J.G., Kucynski, J., Stombaugh., Bittinger, K., Bushman, F.D., Costello, E.K., et al. (2010). QIIME allows analysis of high-throughput community sequencing data. *Nature Methods* 7(5)**,** 335-336. doi: 10.1038/nmeth0510-335.

Caporaso, J.G., Lauber, C.L., Walters, W.A., Berg-Lyons, D., Huntley, J., Fierer, N., et al. (2012). Ultra-high-throughput microbial community analysis on the Illumina HiSeq and MiSeq platforms. *ISME J* 6(8)**,** 1621-1624. doi: 10.1038/ismej.2012.8.

Case, D.H., Pasulka, A.L., Marlow, J.J., Grupe, B.M., Levin, L.A., and Orphan, V.J. (2015). Methane Seep Carbonates Host Distinct, Diverse, and Dynamic Microbial Assemblages. *MBio* 6(6)**,** e01348-01315. doi: 10.1128/mBio.01348-15.

Chadwick, G.L., Skennerton, C.T., Laso-Pérez, R., Leu, A.O., Speth, D.R., Yu, H., et al. (2020). Comparative genomics reveals electron transfer and syntrophic mechanisms differentiating methanotrophic and methanogenic archaea. *submitted.*

Chivian, D., Brodie, E.L., Alm, E.J., Culley, D.E., Dehal, P.S., DeSantis, T.S., et al. (2008). Environmental genomics reveals a single-species ecosystem deep with Earth. *Science* 322**,** 275-278. doi: 10.1126/science.1155495.

Clarke, K.R. (1993). Non-parametric multivariate analyses of changes in community structure. *Austral Ecology* 18**,** 117-143. doi: 10.1111/j.1442-9993.1993.tb00438.x.

Cline, J.D. (1969). Spectrophotometric Determination of Hydrogen Sulfide in Natural Waters. *Limnology and Oceanography* 14(3)**,** 454-458. doi: 10.4319/lo.1969.14.3.0454.

Coolen, M.J., and Overmann, J. (2000). Functional exoenzymes as indicators of metabolically active bacteria in 124,000-year-old sapropel layers of the eastern Mediterranean Sea. *Appl Environ Microbiol* 66**,** 2589-2598.

Coolen, M.J.L., Cypionka, H., Sass, A.M., Sass, H., and Overmann, J. (2002). Ongoing modification of Mediterranean Pleistocene sapropels mediated by prokaryotes. *Science* 296**,** 2407-2410.

Cordes, E.E., Cunha, M.R., Galéron, J., Mora, C., Olu-Le Roy, K., Sibuet, M., et al. (2010). The influence of geological, geochemical, and biogenic habitat heterogeneity on seep biodiversity. *Marine Ecology* 31(1)**,** 51-65. doi: 10.1111/j.1439-0485.2009.00334.x.

Cortés, J. (2016). "The Pacific coastal and marine ecosystems," in *Costa Rican Ecosystems,* ed. M. Kappelle. University of Chicago Press), 97-138.

Crémière, A., Lepland, A., Chand, S., Sahy, D., Kirsimäe, K., Bau, M., et al. (2016). Fluid source and methane-related diagenetic processes recorded in cold seep carbonates from the Alvheim channel, central North Sea. *Chemical Geology* 432**,** 16-33. doi: 10.1016/j.chemgeo.2016.03.019.

Davidson, M.M., Silver, B.J., Onstott, T.C., Moser, D.P., Gihring, T.M., Pratt, L.M., et al. (2011). Capture of Planktonic Microbial Diversity in Fractures by Long-Term Monitoring of Flowing Boreholes, Evander Basin, South Africa. *Geomicrobiology Journal* 28(4)**,** 275-300. doi: 10.1080/01490451.2010.499928.

Doronina, N.V., Kaparullina, E.N., and Trotsenko, Y.A. (2014). Methyloversatilis thermotolerans sp. nov., a novel thermotolerant facultative methylotroph isolated from a hot spring. *Int J Syst Evol Microbiol* 64(Pt 1)**,** 158-164. doi: 10.1099/ijs.0.055046-0.

Eder, W., Ludwig, W., and Huber, R. (1999). Novel 16S rRNA gene sequences retrieved from highly saline brine sediments of Kebrit Deep, Red Sea. *Arch Microbiol* 172**,** 213-218.

Edgar, R.C. (2018). Updating the 97% identity threshold for 16S ribosomal RNA OTUs. *Bioinformatics* 34(14)**,** 2371-2375. doi: 10.1093/bioinformatics/bty113.

Edwards, K.J., Bach, W., and McCollom, T.M. (2005). Geomicrobiology in oceanography: microbe-mineral interactions at and below the seafloor. *Trends Microbiol* 13(9)**,** 449-456. doi: 10.1016/j.tim.2005.07.005.

Edwards, K.J., and Rutenberg, A.J. (2001). Microbial response to surface microtopography: the role of metabolism in localized mineral dissolution. *Chemical Geology* 180**,** 19-32. doi: 0009-2541r01.

Etminan, M., Myhre, G., Highwood, E.J., and Shine, K.P. (2016). Radiative forcing of carbon dioxide, methane, and nitrous oxide: A significant revision of the methane radiative forcing. *Geophysical Research Letters* 43(24)**,** 12614-12623. doi: 10.1002/2016GL071930.

Fike, D.A., Houghton, J.L., Moore, S.E., Gilhooly, W.P., Dawson, K.S., Druschel, G.K., et al. (2017). Spatially resolved capture of hydrogen sulfide from the water column and sedimentary pore waters for abundance and stable isotopic analysis. *Marine Chemistry* 197**,** 26-37. doi: 10.1016/j.marchem.2017.10.004.

Flynn, T.M., Sanford, R.A., Ryu, H., Bethke, C.M., Levine, A.D., Ashbolt, N.J., et al. (2013). Functional microbial diversity explains groundwater chemistry in a pristine aquifer. *BMC Microbiology* 13(146). doi: 10.1186/1471-2180-13-146.

Fridrich, C.J., Thompson, R.A., Slate, J.L., Berry, M.E., and Machette, M.N. (2012). Geologic map of the southern Funeral Mountains including nearby groundwater discharge sites in Death Valley National Park, California and Nevada. *U.S.*

Geological Survey Scientific Investigations(Map 3151), 20 p. pamphlet, 21 sheet, scale 21:50,000.

Georgieva, M.N., Paull, C.K., Little, C.T.S., McGann, M., Sahy, D., Condon, D., et al. (2019). Discovery of an Extensive Deep-Sea Fossil Serpulid Reef Associated With a Cold Seep, Santa Monica Basin, California. *Frontiers in Marine Science* 6. doi: 10.3389/fmars.2019.00115.

Giovannoni, S.J., and Cary, S.C. (1993). Transovarial inheritance of endosymbiotic bacteria in clams inhabiting deep-sea hydrothermal vents and cold seeps. *Proc Natl Acad Sci U S A* 90, 5695-5699.

Girguis, P.R., Cozen, A.E., and DeLong, E.F. (2005). Growth and population dynamics of anaerobic methane-oxidizing archaea and sulfate-reducing bacteria in a continuous-flow bioreactor. *Appl Environ Microbiol* 71(7), 3725-3733. doi: 10.1128/AEM.71.7.3725-3733.2005.

Giuffrè, A., Borisov, V.B., Arese, M., Sarti, P., and Forte, E. (2014). Cytochrome bd oxidase and bacterial tolerance to oxidative and nitrosative stress. *Bioenergetics* 1837, 1178-1187. doi: 10.1016/j.bbabio.2014.01.016.

Goffredi, S.K., and Barry, J.P. (2002). Species-specific variation in sulfide physiology between closely related Vesicomyid clams. *Marine Ecology Progress Series* 225, 227-238. doi: 10.3354/meps225227.

Goffredi, S.K., Gregory, A., Jones, W.J., Morella, N.M., and Sakamoto, R.I. (2014). Ontogenetic variation in epibiont community structure in the deep-sea yeti crab, Kiwa puravida: convergence among crustaceans. *Mol Ecol* 23(6), 1457-1472. doi: 10.1111/mec.12439.

Goffredi, S.K., and Orphan, V.J. (2010). Bacterial community shifts in taxa and diversity in response to localized organic loading in the deep sea. *Environ Microbiol* 12(2), 344-363. doi: 10.1111/j.1462-2920.2009.02072.x.

Goffredi, S.K., Tilic, E., Mullin, S.W., Dawson, K.S., Keller, A., Lee, R.W., et al. (2020). Methanotrophic bacterial symbionts fuel dense populations of deep-sea feather duster worms (Sabellida, Annelida) and extend the spatial influence of methane seepage. *Science Advances* 6, eaay8562. doi: 10.1126/sciadv.aay8562.

Graham, U.M., and Ohmoto, H. (1994). Experimental study of formation mechanisms of hydrothermal pyrite. *Geochim. Cosmochim. Acta* 58(10), 2187-2202.

Green-Saxena, A., Dekas, A.E., Dalleska, N.F., and Orphan, V.J. (2014). Nitrate-based niche differentiation by distinct sulfate-reducing bacteria involved in the anaerobic oxidation of methane. *ISME J* 8(1), 150-163. doi: 10.1038/ismej.2013.147.

Gründger, F., Carrier, V., Svenning, M.M., Panieri, G., Vonnahme, T.R., Klasek, S., et al. (2019). Methane-fuelled biofilms predominantly composed of methanotrophic ANME-1 in Arctic gas hydrate-related sediments. *Sci Rep* 9(1), 9725. doi: 10.1038/s41598-019-46209-5.

Grupe, B.M., Krach, M.L., Pasulka, A.L., Maloney, J.M., Levin, L.A., and Frieder, C.A. (2015). Methane seep ecosystem functions and services from a recently discovered southern California seep. *Marine Ecology* 36, 91-108. doi: 10.1111/maec.12243.

Guillot, G., Rousset, F., and Harmon, L. (2013). Dismantling the Mantel tests. *Methods in Ecology and Evolution* 4(4), 336-344. doi: 10.1111/2041-210x.12018.

Han, X., Suess, E., Sahling, H., and Wallmann, K. (2004). Fluid venting activity on the Costa Rica margin: new results from authigenic carbonates. *International Journal of Earth Sciences*. doi: 10.1007/s00531-004-0402-y.

Hao, L., McIlroy, S.J., Kirkegaard, R.H., Karst, S.M., Fernando, W.E.Y., Aslan, H., et al. (2018). Novel prosthecate bacteria from the candidate phylum Acetothermia. *ISME J* 12**,** 2225-2237. doi: 10.1038/s41396-018-0187-9.

Harrison, B.K., Zhang, H., Berelson, W., and Orphan, V.J. (2009). Variations in Archaeal and Bacterial Diversity Associated with the Sulfate-Methane Transition Zone in Continental Margin Sediments (Santa Barbara Basin, California). *Applied and Environmental Microbiology* 75**,** 1487-1499. doi: 10.1128/AEM.01812-08.

Hedges, J.I., and Keil, R.G. (1995). Sedimentary organic matter preservation: an assessment and speculative hypothesis. *Marine Chemistry* 49**,** 81-115.

Hensen, C., Wallmann, K., Schmidt, M., Ranero, C.R., and Suess, E. (2004). Fluid expulsion related to mud extrusion off Costa Rica—A window to the subducting slab. *Geology* 32(3). doi: 10.1130/g20119.1.

Hermansson, M. (1999). The DLVO theory in microbial adhesion. *Colloids Surfaces* B: Biointerfaces(14)**,** 105-119.

Hilario, A., Young, C.M., and Tyler, P.A. (2005). Sperm storage, internal fertilization, and embryonic dispersal in vent and seep tubeworms (Polychaeta: Siboglinidae: Vestimentifera). *Biol Bull* 208(1)**,** 20-28. doi: 10.2307/3593097.

Hirose, T., Kawagucci, S., and Suzuki, K. (2011). Mechanoradical H2 generation during simulated faulting: implications for an earthquake-driven subsurface biosphere. *Geophysical Research Letters* 38(17).

House, C.H., Orphan, V.J., Turk, K.A., Thomas, B., Pernthaler, A., Vrentas, J.M., et al. (2009). Extensive carbon isotopic heterogeneity among methane seep microbiota. *Environ Microbiol* 11(9)**,** 2207-2215. doi: 10.1111/j.1462-2920.2009.01934.x.

Hovland, M. (2002). On the self-sealing nature of marine seeps. *Continental Shelf Research* 22**,** 2387-2394.

Hugenholtz, P., Pitulle, C., Hershberger, K.L., and Pace, N.R. (1998). Novel Division Level Bacterial Diversity in a Yellowstone Hot Spring. *Journal of Bacteriology* 180(2)**,** 366-376. doi: 0021-9193/98/.

Imachi, H., Aoi, K., Tasumi, E., Saito, Y., Yamanaka, Y., Saito, Y., et al. (2011). Cultivation of methanogenic community from subseafloor sediments using a continuous-flow bioreactor. *ISME J* 5(12)**,** 1913-1925. doi: 10.1038/ismej.2011.64.

Imachi, H., Sekiguchi, Y., Kamagata, Y., Loy, A., Qiu, Y.L., Hugenholtz, P., et al. (2006). Non-sulfate-reducing, syntrophic bacteria affiliated with desulfotomaculum cluster I are widely distributed in methanogenic environments. *Appl Environ Microbiol* 72(3)**,** 2080-2091. doi: 10.1128/AEM.72.3.2080-2091.2006.

Imachi, H., Sekiguchi, Y., Kamagata, Y., Ohashi, A., and Harada, H. (2000). Cultivation and In Situ Detection of a Thermophilic Bacterium Capable of Oxidizing Propionate in Syntrophic Association with Hydrogenotrophic Methanogens in a Thermophilic Methanogenic Granular Sludge. *Appl Environ Microbiol* 66**,** 3608-3615.

Inagaki, F., Hinrichs, K.-U., Kubo, Y., Bowles, M.W., Heuer, V.B., Hong, W.-L., et al. (2015). Exploring deep microbial life in coal-bearing sediment down to ~2.5 km below the ocean floor. *Science* 349(6246)**,** 420-424.

Inagaki, F., Kuypers, M.M.M., Tsunogai, U., Ishibashi, J., Nakamura, K., Treude, T., et al. (2006). Microbial community in a sediment-hosted CO2 lake of the southern Okinawa Trough hydrothermal system. *Proc Natl Acad Sci U S A* 103(38)**,** 14164-14169. doi: 10.1073/pnas.0606083103.

Inagaki, F., Suzuki, M., Takai, K., Oida, H., Sakamoto, T., Aoki, K., et al. (2003). Microbial communities assocaited with geological horizons in coastal subseafloor sediments from the Sea of Okhotsk. *Appl Environ Microbiol* 69**,** 7224-7235.

Ino, K., Konno, U., Kouduka, M., Hirota, A., Togo, Y.S., Fukuda, A., et al. (2016). Deep microbial life in high-quality granitic groundwater from geochemically and geographically distinct underground boreholes. *Environ Microbiol Reports* 8(2)**,** 285-294. doi: 10.1111/1758-2229.12379.

Jones, A.A., and Bennett, P.C. (2014). Mineral Microniches Control the Diversity of Subsurface Microbial Populations. *Geomicrobiology Journal* 31**,** 246-261. doi: 10.1080/01490451.2013.809174.

Jørgensen, B.B., and Boetius, A. (2007). Feast and famine — microbial life in the deep-sea bed. *Nature Reviews Microbiology* 5(10)**,** 770-781. doi: 10.1038/nrmicro1745.

Joseph, A. (2017). "Seafloor Hot Chimneys and Cold Seeps: Mysterious Life Around Them," in *Investigating Seafloors and Oceans From Mud Volcanoes to Giant Squid.* Elsevier), 307-375.

Jungbluth, S.P., Glavina Del Rio, T., Tringe, S.G., Stepanauskas, R., and Rappe, M.S. (2017). Genomic comparisons of a bacterial lineage that inhabits both marine and terrestrial deep subsurface systems. *PeerJ* 5**,** e3134. doi: 10.7717/peerj.3134.

Kadnikov, V.V., Mardanov, A.V., Beletsky, A.V., Karnachuk, O.V., and Ravin, N.V. (2019). Genome of the candidate phylum Aminicenantes bacterium from a deep subsurface thermal aquifer revealed its fermentative saccharolytic lifestyle. *Extremophiles* 23(2)**,** 189-200. doi: 10.1007/s00792-018-01073-5.

Khoury, H.N., Eberl, D.D., and Jones, B.F. (1982). Origin of Magnesium clays from the Amargos Desert, Nevada. *Clays & Clay Minerals* 30(5)**,** 327-336.

Kieft, T.L., and Phelps, T.J. (1997). "Life in the slow lane: Activites of microorganisms in the subsurface," in *The Microbiology of the Terrestrial Subsurface,* ed. P.S.H. Amy, D.L. (Boca Raton: CRC Press), 137-163.

Klaucke, I., Masson, D.G., Petersen, C.J., Weinrebe, W., and Ranero, C.R. (2008). Multifrequency geoacoustic imaging of fluid escape structures offshore Costa Rica: Implications for the quantification of seep processes. *Geochemistry, Geophysics, Geosystems* 9(4)**,** n/a-n/a. doi: 10.1029/2007gc001708.

Knittel, K., and Boetius, A. (2009). Anaerobic oxidation of methane: progress with an unknown process. *Annu Rev Microbiol* 63**,** 311-334. doi: 10.1146/annurev.micro.61.080706.093130.

Knittel, K., Losekann, T., Boetius, A., Kort, R., and Amann, R. (2005). Diversity and distribution of methanotrophic archaea at cold seeps. *Appl Environ Microbiol* 71(1)**,** 467-479. doi: 10.1128/AEM.71.1.467-479.2005.

Krukenberg, V., Riedel, D., Gruber-Vodicka, H.R., Buttigieg, P.L., Tegetmeyer, H.E., Boetius, A., et al. (2018). Gene expression and ultrastructure of meso- and thermophilic methanotrophic consortia. *Environ Microbiol* 20(5)**,** 1651-1666. doi: 10.1111/1462-2920.14077.

LaRowe, D.E., and Amend, J.P. (2015). Power limits for microbial life. *Front Microbiol* 6. doi: 10.3389/fmicb.2015.00718.

Lee, Y.M., Hwang, K., Lee, J.I., Kim, M., Hwang, C.Y., Noh, H.J., et al. (2018). Genomic Insight Into the Predominance of Candidate Phylum Atribacteria JS1 Lineage in Marine Sediments. *Front Microbiol* 9**,** 2909. doi: 10.3389/fmicb.2018.02909.

Legendre, P., Fortin, M.J., Borcard, D., and Peres-Neto, P. (2015). Should the Mantel test be used in spatial analysis? *Methods in Ecology and Evolution* 6(11)**,** 1239-1247. doi: 10.1111/2041-210x.12425.

Lenchi, N., Inceoglu, O., Kebbouche-Gana, S., Gana, M.L., Lliros, M., Servais, P., et al. (2013). Diversity of Microbial Communities in Production and Injection Waters of Algerian Oilfields Revealed by 16S rRNA Gene Amplicon 454 Pyrosequencing. *PLoS One* 8(6)**,** e66588. doi: 10.1371/journal.pone.0066588.

Levin, L.A. (2005). Ecology of Cold Seep Sediments: Interactions of Fauna with Flow, Chemistry and Microbes. *Oceanography and Marine Biology* 43**,** 1-46.

Levin, L.A., Baco, A.R., Bowden, D.A., Colaco, A., Cordes, E.E., Cunha, M.R., et al. (2016). Hydrothermal Vents and Methane Seeps: Rethinking the Sphere of Influence. *Frontiers in Marine Science* 3. doi: 10.3389/fmars.2016.00072.

Levin, L.A., Mendoza, G.F., Grupe, B.M., Gonzalez, J.P., Jellison, B., Rouse, G., et al. (2015). Biodiversity on the Rocks: Macrofauna Inhabiting Authigenic Carbonate at Costa Rica Methane Seeps. *PLoS One* 10(7)**,** e0131080. doi: 10.1371/journal.pone.0131080.

Levin, L.A., Ziebis, W., Mendoza, G.F., Growney-Cannon, V., and Walther, S. (2006). Recruitment response of methane-seep macrofauna to sulfide-rich sediments: An in situ experiment. *Journal of Experimental Marine Biology and Ecology* 330(1)**,** 132-150. doi: 10.1016/j.jembe.2005.12.022.

Lilley, M.D., and Von Damm, K.L. (2008). *Diffuse Flow Hydrothermal Fluids from 9° 50′ N, East Pacific Rise: Origin, Evolution and Biogeochemical Controls*. Subseafloor Biosphere at Mid-Ocean Ridges: American Geophysical Union.

Linke, P., Wallmann, K., Suess, E., Hensen, C., and Rehder, G. (2005). In situ benthic fluxes from an intermittently active mud volcano at the Costa Rica convergent margin. *Earth and Planetary Science Letters* 235(1-2)**,** 79-95. doi: 10.1016/j.epsl.2005.03.009.

Linnenbom, V.J. (1958). The Reaction between Iron and Water in the Absence of Oxygen. *J. Electrochem. Soc.* 105(6)**,** 322-324. doi: 10.1149/1.2428838.

Lloyd, K.G., Albert, D.B., Biddle, J.F., Chanton, J.P., Pizarro, O., and Teske, A. (2010). Spatial structure and activity of sedimentary microbial communities underlying a Beggiatoa spp. mat in a Gulf of Mexico hydrocarbon seep. *PLoS One* 5(1)**,** e8738. doi: 10.1371/journal.pone.0008738.

Lloyd, K.G., Alperin, M.J., and Teske, A. (2011). Environmental evidence for net methane production and oxidation in putative ANaerobic MEthanotrophic

(ANME) archaea. *Environ Microbiol* 13(9), 2548-2564. doi: 10.1111/j.1462-2920.2011.02526.x.

Lloyd, K.G., Lapham, L., and Teske, A. (2006). An anaerobic methane-oxidizing community of ANME-1b archaea in hypersaline Gulf of Mexico sediments. *Appl Environ Microbiol* 72(11), 7218-7230. doi: 10.1128/AEM.00886-06.

Lovley, D.R., Baedecker, M., Lonergan, D.J., Cozzarelli, I.M., Phillips, E.J.P., and Siegel, D.I. (1989). Oxidation of aromatic contaminants coupled to microbial iron reduction. *Nature* 339(297-300).

Lu, H., Kalyuzhnaya, M., and Chandran, K. (2012). Comparative proteomic analysis reveals insights into anoxic growth of Methyloversatilis universalis FAM 5 on methanol and ethanol. *Environ Microbiol* 14, 2935-2945. doi: 10.1111/j.1462-2920.2012.02857.x.

Ma, M., Zhang, Y., Guo, Z., and Gu, N. (2013). Facile synthesis of ultrathin magnetic iron oxide nanoplates by Schikorr reaction. *Nanoscale Res. Lett* 8(16).

MacLean, L.C.W., Pray, T.J., Onstott, T.C., Brodie, E.L., Hazen, T.C., and Southam, G. (2007). Mineralogical, Chemical and Biological Characterization of an Anaerobic Biofilm Collected from a Borehole in a Deep Gold Mine in South Africa. *Geomicrobiology Journal* 24(6), 491-504. doi: 10.1080/01490450701572416.

Maclean, L.C.W., Tyliszczak, T., Gilbert, P.U.P.A., Zhou, D., Pray, T.J., Onstott, T.C., et al. (2008). A high-resolution chemical and structural study of framboidal pyrite formed within a low-temperature bacterial biofilm. *Geobiology* 6, 471-480. doi: 10.1111/j.1472-4669.2008.00174.x.

Magnabosco, C., Lin, L.H., Dong, H., Bomberg, M., Ghiorse, W., Stan-Lotter, H., et al. (2018). The biomass and biodiversity of the continental subsurface. *Nature Geoscience* 11(10), 707-717. doi: 10.1038/s41561-018-0221-6.

Marlow, J.J., Steele, J.A., Case, D.H., Connon, S.A., Levin, L.A., and Orphan, V.J. (2014a). Microbial abundance and diversity patterns associated with sediments and carbonates from the methane seep environments of Hydrate Ridge, OR. *Frontiers in Marine Science* 1. doi: 10.3389/fmars.2014.00044.

Marlow, J.J., Steele, J.A., Ziebis, W., Thurber, A.R., Levin, L.A., and Orphan, V.J. (2014b). Carbonate-hosted methanotrophy represents an unrecognized methane sink in the deep sea. *Nat Commun* 5, 5094. doi: 10.1038/ncomms6094.

Mason, O.U., Case, D.H., Naehr, T.H., Lee, R.W., Thomas, R.B., Bailey, J.V., et al. (2015). Comparison of Archaeal and Bacterial Diversity in Methane Seep Carbonate Nodules and Host Sediments, Eel River Basin and Hydrate Ridge, USA. *Microb Ecol* 70(3), 766-784. doi: 10.1007/s00248-015-0615-6.

Mau, S., Sahling, H., Rehder, G., Suess, E., Linke, P., and Soeding, E. (2006). Estimates of methane output from mud extrusions at the erosive convergent margin off Costa Rica. *Marine Geology* 225(1-4), 129-144. doi: 10.1016/j.margeo.2005.09.007.

McGinnis, D.F., Greinert, J., Artemov, Y., Beaubien, S.E., and Wüest, A. (2006). Fate of rising methane bubbles in stratified waters: How much methane reaches the atmosphere? *Journal of Geophysical Research* 111(C9). doi: 10.1029/2005jc003183.

McMahon, S., and Parnell, J. (2014). Weighing the deep continental biosphere. *FEMS Microbiol Ecol* 87, 113-120. doi: 10.1111/1574-6941.12196.

McMurdie, P.J., and Holmes, S. (2014). Waste Not, Want Not: Why Rarefying Microbiome Data is Inadmissible. *PLoS Comput Biol* 10(4). doi: 10.1371/journal.pcbi.1003531.

Mehrer, H. (2007). *Diffusion in Solids*. Springer-Verlag.

Metcalfe, K.S., Murali, R., Mullin, S.W., Connon, S.A., and Orphan, V.J. (2020). Experimentally-validated correlation analysis reveals new anaerobic methane oxidation partnerships with consortium-level heterogeneity in diazotrophy. *bioRxiv*, 2020.2004.2012.038331. doi: 10.1101/2020.04.12.038331.

Meyer-Dombard, D.R., Swingley, W., Raymond, J., Havig, J., Shock, E.L., and Summons, R.E. (2011). Hydrothermal ecotones and streamer biofilm communities in the Lower Geyser Basin, Yellowstone National Park. *Environ Microbiol* 13(8), 2216-2231. doi: 10.1111/j.1462-2920.2011.02476.x.

Miller, K.A., Thompson, K.F., Johnston, P., and Santillo, D. (2018). An Overview of Seabed Mining Including the Current State of Development, Environmental Impacts, and Knowledge Gaps. *Frontiers in Marine Science* 4. doi: 10.3389/fmars.2017.00418.

Miyajima, Y., Ijiri, A., Miyake, A., and Hasegawa, T. (2018). Origin of methane and heavier hydrocarbons entrapped within Miocene methane-seep carbonates from central Japan. *Chemical Geology* 498, 83-95. doi: 10.1016/j.chemgeo.2018.09.014.

Momper, L., Aronson, H.S., and Amend, J.P. (2018). Genomic Description of 'Candidatus Abyssubacteria,' a Novel Subsurface Lineage Within the Candidate Phylum Hydrogenedentes. *Front Microbiol* 9, 1993. doi: 10.3389/fmicb.2018.01993.

Momper, L., Reese, B.K., Zinke, L., Wanger, G., Osburn, M.R., Moser, D., et al. (2017). Major phylum-level differences between porefluid and host rock bacterial communitites in the terrestrial deep subsurface. *Environ Microbiol Reports* 9(5), 501-511. doi: 10.1111/1758-2229.12563.

Moreno-Ulloa, A., Diaz, V.S., Tejeada-Mora, J.A., Macias Contreras, M.I., Diaz Costillo, F., Guerrero, A., et al. (2019). Metabolic and metagenomic profiling of hydrocarbon-degrading microorganisms obtained from the deep biosphere of the Gulf of Mexico. *bioRxiv*. doi: 10.1101/606806.

Morono, Y., Terada, T., Nishizawa, M., Ito, M., Hillion, F., Takahata, N., et al. (2011). Carbon and nitrogen assimilation in deep subseafloor microbial cells. *Proc Natl Acad Sci U S A* 108(45), 18295-18300. doi: 10.1073/pnas.1107763108.

Morono, Y., Wishart, J.R., Ito, M., Ijiri, A., Hoshino, T., Torres, M., et al. (2019). Microbial metabolism and community dynamics in hydraulic fracturing fluids recovered from deep hydrocarbon-rich shale. *Frontiers in Microbiology* 10, 376.

Moser, D.P., Gihring, T.M., Brockman, F.J., Fredrickson, J.K., Balkwill, D.L., Dollhopf, M.E., et al. (2005). Desulfotomaculum and Methanobacterium spp. dominate a 4- to 5-kilometer-deep fault. *Appl Environ Microbiol* 71(12), 8773-8783. doi: 10.1128/AEM.71.12.8773-8783.2005.

Moser, D.P., Onstott, T.C., Fredrickson, J.K., Brockman, F.J., Balkwill, D.L., Drake, G.R., et al. (2003). Temporal Shifts in the Geochemistry and Microbial Community Structure of an Ultradeep Mine Borehole Following Isolation. *Geomicrobiology Journal* 20, 517-548. doi: 10.1080/01490450390249280.

Mouser, P.J., Borton, M., Darrah, T.H., Hartsock, A., and Wrighton, K.C. (2016). Hydraulic fracturing offers view of microbial life in the deep terrestrial subsurface. *FEMS Microbiol Ecol* 92(11). doi: 10.1093/femsec/fiw166.

Mullin, S.W., Wanger, G., Kruger, B.R., Sackett, J.D., Hamilton-Brehm, S.D., Bhartia, R., et al. (2020). Microbial Niche-Specialization in a ~60C Continental Subsurface Aquifer Revealed by In Situ Mineral Colonization. *Front Microbiol* (accepted).

Naehr, T.H., Eichhubl, P., Orphan, V.J., Hovland, M., Paull, C.K., Ussler, W., et al. (2007). Authigenic carbonate formation at hydrocarbon seeps in continental margin sediments: A comparative study. *Deep Sea Research Part II: Topical Studies in Oceanography* 54(11-13)**,** 1268-1291. doi: 10.1016/j.dsr2.2007.04.010.

National Library of Medicine (US), N.C.f.B.I. (1988). "Nucleotide".).

Navarro-Gonzalez, R., Rainey, F.A., Molina, P., Bagaley, D.R., Hollen, B.J., De la Rosa, J., et al. (2003). Mars-Like Soils in the Aracama Desert, Chile, and the Dry Limit of Microbial Life. *Science* 302(5647)**,** 1018-1021. doi: 10.1126/science.1089143.

Nigro, L.M., Hyde, A.S., MacGregor, B.J., and Teske, A. (2016). Phylogeography, Salinity Adaptations and Metabolic Potential of the Candidate Division KB1 Bacteria Based on a Partial Single Cell Genome. *Front Microbiol* 7**,** 1266. doi: 10.3389/fmicb.2016.01266.

Oksanen, J., Blanchet, F.G., Friendly, M., Kindt, R., Legendre, P., McGlinn, D., et al. (2018). "vegan: Community ecology package". 2.5-6 ed. (https://cran.r-project.org, https://github.com/vegandevs/vegan).

Oliveros, J.C. (2007-2015). *Venny. An interactive tool for comparing lists with Venn's diagrams* [Online]. Available: https://bioinfogp.cnb.csic.es/tools/venny/index.html [Accessed].

Onstott, T.C., Magnabosco, C., Aubrey, A.D., Burton, A.S., Dworkin, J.P., Elsila, J.E., et al. (2014). Does aspartic acid racemization constrain the depth limit of the subsurface biosphere? *Geobiology* 12(1)**,** 1-19. doi: 10.1111/gbi.12069.

Oppo, D., De Siena, L., and Kemp, D.B. (2020). A record of seafloor methane seepage across the last 150 million years. *Sci Rep* 10(1)**,** 2562. doi: 10.1038/s41598-020-59431-3.

Orcutt, B., Wheat, C.G., and Edwards, K.J. (2010). Subseafloor Ocean Crust Microbial Observatories Development of FLOCS (FLow through Osmo Colonization System) and Evaluation of Borehole Construction. *Geomicrobiology Journal* 27**,** 143-157. doi: 10.1080/01490450903456772.

Orcutt, B.N., Bach, W., Becker, K., Fisher, A.T., Hentscher, M., Toner, B.M., et al. (2011). Colonization of subsurface microbial observatories deployed in young ocean crust. *ISME J* 5(692-703). doi: 10.1038/ismej.2010.157.

Orphan, V.J., Hinrichs, K.U., Ussler, W., 3rd, Paull, C.K., Taylor, L.T., Sylva, S.P., et al. (2001a). Comparative analysis of methane-oxidizing archaea and sulfate-reducing bacteria in anoxic marine sediments. *Appl Environ Microbiol* 67(4)**,** 1922-1934. doi: 10.1128/AEM.67.4.1922-1934.2001.

Orphan, V.J., House, C.H., Hinrichs, K.U., McKeegan, K.D., and DeLong, E.F. (2001b). Methane-consuming archaea revealed by directly coupled isotopic and phylogenetic analysis. *Science* 293(5529)**,** 484-487. doi: 10.1126/science.1061338.

Orphan, V.J., House, C.H., Hinrichs, K.U., McKeegan, K.D., and DeLong, E.F. (2002). Multiple archaeal groups mediate methane oxidation in anoxic cold seep sediments. *Proc Natl Acad Sci U S A* 99(11)**,** 7663-7668. doi: 10.1073/pnas.072210299.

Orphan, V.J., Turk, K.A., Green, A.M., and House, C.H. (2009). Patterns of15N assimilation and growth of methanotrophic ANME-2 archaea and sulfate-reducing bacteria within structured syntrophic consortia revealed by FISH-SIMS. *Environmental Microbiology* 11(7)**,** 1777-1791. doi: 10.1111/j.1462-2920.2009.01903.x.

Orphan, V.J., Ussler III, W., Naehr, T.H., House, C.H., Hinrichs, K.-U., and Paull, C.K. (2004). Geological , geochemical, and mineralogical heterogeneity of the seafloor around methane vents in the Eel River Basin, off shore California. *Chemical Geology* 205**,** 265-289. doi: 10.1016/j.chemgeo.2003.12.035.

Orsi, W.D., Edgcomb, V.P., Christman, G.D., and Biddle, J.F. (2013). Gene expression in the deep biosphere. *Nature* 499**,** 205-208.

Osburn, M.R., LaRowe, D.E., Momper, L.M., and Amend, J.P. (2014). Chemolithotrophy in the continental deep subsurface: Sanford Underground Research Facility (SURF), USA. *Front Microbiol* 5**,** 610. doi: 10.3389/fmicb.2014.00610.

Pedersen, K., Hallbeck, L., Arlinger, J., Erlandson, A.-C., and Jahromi, N. (1997). Investigation of the potential for microbial contaminatioin of deep granitic aquifers during drilling using 16S rRNA gene sequencing and culturing methods. *J. of Microbiol. Methods* 30**,** 179-192.

Picard, A., Gartman, A., and Girguis, P.R. (2016). What do we really know about the role of microorganisms in iron sulfide mineral formation? *Front Earth Sci* 4. doi: 10.3389/feart.2016.00068.

Plugge, C.M., Balk, M., and Stam, A.J.M. (2002). Desulfotomaculum thermobenzoicum subsp. thermosyntrophicum subsp. nov., a thermophilic, syntrophic, propioonat-oxidizing, spore-forming bacterium. *Intnl. J. of Systematic and Evol. Microbiol.* 52**,** 391-399. doi: 10.1099/ijs.0.01948-0.

Pohlman, J.W., Bauer, J.E., Waite, W.F., Osburn, C.L., and Chapman, N.R. (2010). Methane hydrate-bearing seeps as a source of aged dissolved organic carbon to the oceans. *Nature Geoscience* 4(1)**,** 37-41. doi: 10.1038/ngeo1016.

Ponnamperuma, F.N. (1972). The Chemistry of Submerged Soils. *Advances in Agronomy* 24**,** 29-96. doi: 10.1016/S0065-2113(08)60633-1.

Popa, R., Kinkle, B.K., and Badescu, A. (2004). Pyrite Framboids as Biomarkers for Iron-Sulfur Systems. *Geomicrobiology Journal* 21(3)**,** 193-206. doi: 10.1080/01490450490275497.

Qin, W., Heal, K.R., Ramdasi, R., Kobelt, J.N., Martens-Habbena, W., Bertagnolli, A.D., et al. (2017). Nitrosopumilus maritimus gen. nov., sp. nov., Nitrosopumilus cobalaminigenes sp. nov., Nitrosopumilus oxyclinae sp. nov., and Nitrosopumilus ureiphilus sp. nov., four marine ammonia-oxidizing archaea of the phylum Thaumarchaeota. *Int J Syst Evol Microbiol* 67(12)**,** 5067-5079. doi: 10.1099/ijsem.0.002416.

Quast, C., Pruesse, E., Yilmaz, P., Gerken, J., Schweer, T., Yarza, P., et al. (2013). The SILVA ribosomal RNA gene database project: improved data processing and web-based tools. *Nucleic Acids Res* 41**,** D590-596. doi: 10.1093/nar/gks1219.

R Core Team (2014). "R: A Language and Environment for Statistical Computing". (Vienna, Austria: R Foundation for Statistical Computing).

Ramirez-Llodra, E., Tyler, P.A., Baker, M.C., Bergstad, O.A., Clark, M.R., Escobar, E., et al. (2011). Man and the last great wilderness: human impact on the deep sea. *PLoS One* 6(8)**,** e22588. doi: 10.1371/journal.pone.0022588.

Reeburgh, W. (1967). An Improved Interstitial Water Sampler. *Limnology and Oceanography* 12(1)**,** 163-165. doi: 10.4319/lo.1967.12.1.0163.

Reeburgh, W. (2007a). Oceanic Methane Biogeochemistry. *Chem. Rev.* 107**,** 486-513. doi: 10.1021/cr050362v.

Reeburgh, W. (2007b). Oceanic Methane Biogeochemistry. *Chem. Rev.* 107(2)**,** 486-513. doi: 10.1021/cr050362v.

Rempfert, K.R., Miller, H.M., Bompard, N., Nothaft, D., Matter, J.M., Kelemen, P., et al. (2017). Geological and Geochemical Controls on Subsurface Microbial Life in the Samail Ophiolite, Oman. *Frontiers in Microbiology* 8(56). doi: 10.3389/fmicb.2017.00056.

Ribeiro, A.C.F., Ortona, O., Simões, S.M.N., Santos, C.I.A.V., Prazeres, P.M.R.A., Valente, A.J.M., et al. (2006). Binary mutual diffusion coefficients of aqueous solutions of sucrose, lactose, glucose and fructose in the temperature range from (298.15-328.15) K. *J. Chem. Eng. Data* 51**,** 1836-1840.

Rickard, D. (2019). How long does it take a pyrite framboid to form? *Earth and Planetary Science Letters* 513**,** 64-68. doi: 10.1016/j.epsl.2019.02.019.

Riedinger, N., Strasser, M., Harris, R.N., Klockgether, G., Lyons, T.W., and Screaton, E.J. (2015). Deep subsurface carbon cycling in the Nankai Trough (Japan)-Evidence of tectonically induced stimulation of a deep microbial biosphere. *Geochemistry, Geophysics, Geosystems* 16(9)**,** 3257-3270. doi: 10.1002/2015gc006050.

Roalkvam, I., Dahle, H., Chen, Y., Jorgensen, S.L., Haflidason, H., and Steen, I.H. (2012). Fine-Scale Community Structure Analysis of ANME in Nyegga Sediments with High and Low Methane Flux. *Front Microbiol* 3**,** 216. doi: 10.3389/fmicb.2012.00216.

Roalkvam, I., Jorgensen, S.L., Chen, Y., Stokke, R., Dahle, H., Hocking, W.P., et al. (2011). New insight into stratification of anaerobic methanotrophs in cold seep sediments. *FEMS Microbiol Ecol* 78(2)**,** 233-243. doi: 10.1111/j.1574-6941.2011.01153.x.

Roberts, J.A. (2004). Inhibition and enhancement of microbial surface colonization: the role of silicate composition. *Chemical Geology* 212(3-4)**,** 313-327. doi: 10.1016/j.chemgeo.2004.08.021.

Roberts, J.A., Kenward, P.A., Fowle, D.A., Goldstein, R.H., Gonzalez, L.A., and Moore, D.S. (2013). Surface chemistry allows for abiotic precipitation of dolomite at low temperature. *Proc Natl Acad Sci U S A* 110(36)**,** 14540-14545. doi: 10.1073/pnas.1305403110.

Rogers, J.R., Bennett, P.C., and Choi, W.J. (1998). Feldspars as a source of nutrients for microorganisms. *Amer. Mineralog.* 83**,** 1532-1540.

Rowe, A.R., Yoshimura, M., LaRowe, D.E., Bird, L.J., Amend, J.P., Hashimoto, K., et al. (2017). In situ electrochemical enrichment and isolation of a magnetite-reducing bacterium from a high pH serpentinizing spring. *Environ Microbiol* 19(6), 2272-2285. doi: 10.1111/1462-2920.13723.

Ruff, S.E., Arnds, J., Knittel, K., Amann, R., Wegener, G., Ramette, A., et al. (2013). Microbial communities of deep-sea methane seeps at Hikurangi continental margin (New Zealand). *PLoS One* 8(9), e72627. doi: 10.1371/journal.pone.0072627.

Ruff, S.E., Biddle, J.F., Teske, A.P., Knittel, K., Boetius, A., and Ramette, A. (2015). Global dispersion and local diversification of the methane seep microbiome. *Proc Natl Acad Sci U S A* 112(13), 4015-4020. doi: 10.1073/pnas.1421865112.

Sackett, J.D. (2018). *Prokaryotic Diversity and Aqueous Geochemistry of the Subsurface Environments of the Death Valley Regional Flow System*. Ph.D. Ph.D., University of Nevada, Las Vegas.

Sackett, J.D., Kruger, B.R., Becraft, E.D., Jarett, J.K., Stepanauskas, R., Woyke, T., et al. (2019). Four Draft Single-Cell Genome Sequences of Novel, Nearly Identical *Kiritimatiellaeota* Strains Isolated from the Continental Deep Subsurface. *Microbiology Resource Announcements* 8(11). doi: 10.1128/MRA.01249-18.

Sahl, J.W., Schmidt, R., Swanner, E.D., Mandernack, K.W., Templeton, A.S., Kieft, T.L., et al. (2008). Subsurface Microbial Diversity in Deep -Granitic-Fracture Water in Colorado. *Appl Environ Microbiol* 74(1), 143-152. doi: 10.1128/AEM.01133-07.

Sahling, H., Masson, D.G., Ranero, C.R., Hühnerbach, V., Weinrebe, W., Klaucke, I., et al. (2008). Fluid seepage at the continental margin offshore Costa Rica and southern Nicaragua. *Geochemistry, Geophysics, Geosystems* 9(5). doi: 10.1029/2008gc001978.

Sawlowicz, Z. (2000). Framboids: From their origin to application. *Mineralogical Transactions* 88.

Schikorr, G. (1929). Uber das System Eisen-Wasser. *Zeitschrift für Elektrochemie* 35(2). doi: https://doi.org/10.1002/bbpc.19290350203.

Schreiber, L., Holler, T., Knittel, K., Meyerdierks, A., and Amann, R. (2010). Identification of the Dominant Sulfate-Reducing Bacterial Partner of Anaerobic Methanotrophs of the ANME-2 Clade. *Environ Microbiol* 12, 2327-2340. doi: 10.1111/j.1462-2920.2010.02275.x.

Schulze-Makuch, D., Wagner, D., Kounaves, S.P., Mangelsdorf, K., Devine, K.G., de Vera, J.P., et al. (2018). Transitory microbial habitat in the hyperarid Atacama Desert. *Proc Natl Acad Sci U S A* 115(11), 2670-2675. doi: 10.1073/pnas.1714341115.

Sekiguchi, Y., Yamada, T., Hanada, S., Ohashi, A., Harada, H., and Kamagata, Y. (2003). Anaerolinea thermophila gen. nov., sp. nov. and Caldilinea aerophila gen. nov., sp. nov., novel filamentous thermophiles that represent a previously uncultured lineage of the domain Bacteria at the subphylum level. *Int J Syst Evol Microbiol* 53(6), 1843-1851. doi: 10.1099/ijs.0.02699-0.

Sewell, H.L., Kaster, A.-K., and Spormann, A.M. (2017). Homoacetogenesis in Deep-Sea Chloroflexi, as Inferred by Single-Cell Genomics, Provides a Link to

Reductive Dehalogenation in Terrestrial Dehalococcoidetes. *mBio* 8**,** e02022-02017. doi: 10.1128/mBio.02022-17.

Shima, S., Krueger, M., Weinert, T., Demmer, U., Kahnt, J., Thauer, R.K., et al. (2011). Structure of a methyl-coenzyme M reductase from Black Sea mats that oxidize methane anaerobically. *Nature* 481(7379)**,** 98-101. doi: 10.1038/nature10663.

Shindell, D.T., Faluvegi, G., Koch, D.M., Schmidt, G.A., Unger, N., and Bauer, S.E. (2009). Improved Attribution of Climate Forcing to Emissions. *Science* 326**,** 716-718. doi: 10.1126/science.1174760.

Simon-Lledo, E., Bett, B.J., Huvenne, V.A.I., Koser, K., Schoening, T., Greinert, J., et al. (2019). Biological effects 26 years after simulated deep-sea mining. *Sci Rep* 9(1)**,** 8040. doi: 10.1038/s41598-019-44492-w.

Sivan, O., Adler, M., Pearson, A., Gelman, F., Bar-Or, I., John, S.G., et al. (2011). Geochemical evidence for iron-mediated anaerobic oxidation of methane. *Limnology and Oceanography* 56(1546-1544). doi: 10.4319/lo.2011.56.4.1536.

Sleep, N.H., and Zoback, M.D. (2007). Did earthquakes keep the early crust habitable? *Astrobiology* 7**,** 1023-1032.

Soares Pereira, O. (2020). *The influence of methane seepage on composition and trophic structure of hard substrate macrofauna within the seep and surrounding systems*. Master of Science, University of California, San Diego.

Sousa, D.Z., Visser, M., van Gelder, A.H., Boeren, S., Pieterse, M.M., Pinkse, M.W.H., et al. (2018). The deep-subsurface sulfate reducer Desulfotomaculum kuznetsovii employs two methanol-degrading pathways. *Nat Commun* 9(1)**,** 239. doi: 10.1038/s41467-017-02518-9.

Stadnitskaia, A., Bouloubassi, I., Elvert, M., Hinrichs, K.U., and Sinninghe Damsté, J.S. (2008a). Extended hydroxyarchaeol, a novel lipid biomarker for anaerobic methanotrophy in cold seepage habitats. *Organic Geochemistry* 39(8)**,** 1007-1014. doi: 10.1016/j.orggeochem.2008.04.019.

Stadnitskaia, A., Nadezhkin, D., Abbas, B., Blinova, V., Ivanov, M.K., and Sinninghe Damsté, J.S. (2008b). Carbonate formation by anaerobic oxidation of methane: Evidence from lipid biomarker and fossil 16S rDNA. *Geochimica et Cosmochimica Acta* 72(7)**,** 1824-1836. doi: 10.1016/j.gca.2008.01.020.

Starnawski, P., Bataillon, T., Ettema, T.J.G., Jochum, L.M., Schreiber, L., Chen, X., et al. (2017). Seabed microbial community assembly and evolution. *Proc Natl Acad Sci U S A* 114**,** 2940-2945. doi: 10.1073/pnas.1614190114.

Stokke, R., Roalkvam, I., Lanzen, A., Haflidason, H., and Steen, I.H. (2012). Integrated metagenomic and metaproteomic analyses of an ANME-1-dominated community in marine cold seep sediments. *Environ Microbiol* 14(5)**,** 1333-1346. doi: 10.1111/j.1462-2920.2012.02716.x.

Stookey, L.L. (1970). Ferrozine—A New Spectrophotometric Reagent for Iron. *Analytical Chemistry* 42(7)**,** 779-781.

Sweeney, R.E., and Kaplan, I.R. (1973). Pyrite Framboid Formation: Laboratory Synthesis and Marine Sediments. *Econ Geol* 68**,** 618-634.

Sylvan, J.B., Sia, T.Y., Haddad, A.G., Briscoe, L.J., Toner, B.M., Girguis, P.R., et al. (2013). Low temperature geomicrobiology follows host rock composition along a geochemical gradient in lau basin. *Front Microbiol* 4**,** 61. doi: 10.3389/fmicb.2013.00061.

Takai, K., Moser, D.P., DeFlaun, M., Onstott, T.C., and Fredrickson, J.K. (2001). Archaeal Diversity in Waters from Deep South African Gold Mines. *Applied and Environmental Microbiology* 67(12), 5750-5760. doi: 10.1128/aem.67.21.5750-5760.2001.

Takami, H., Noguchi, H., Takaki, Y., Uchiyama, I., Toyoda, A., Nishi, S., et al. (2012). A Deeply Branching Thermophilic Bacterium with an Ancient Acetyl-CoA Pathway Dominates a Subsurface Ecosystem. *PloS ONE* 7, e30559. doi: 10.1371/journal.pone.0030559.

Tavormina, P.L., Ussler III, W., and Orphan, V.J. (2008). Planktonic and Sediment-Associated Aerobic Methanotrophs in Two Seep Systems along the North American Margin. *Applied and Environmental Microbiology* 74, 3985-3995. doi: 10.1128/AEM.00069-08.

Telling, J., Boyd, E.S., Bone, N., Jones, E.L., Tranter, M., Macfarlane, J.W., et al. (2015). Rock comminution as a source for hydrogen for subglacial ecosystems. *Nature Geoscience* 8, 851-854. doi: 10.1038/NGEO2533.

Teske, A., Hinrichs, K.U., Edgcomb, V., de Vera Gomez, A., Kysela, D., Sylva, S.P., et al. (2002). Microbial diversity of hydrothermal sediments in the Guaymas Basin: evidence for anaerobic methanotrophic communities. *Appl Environ Microbiol* 68(4), 1994-2007. doi: 10.1128/aem.68.4.1994-2007.2002.

Teske, A., and Sørensen, K.B. (2008). Uncultured archaea in deep marine subsurface sediments: have we caught them all. *ISME J* 2, 3-18. doi: 10.1038/ismej.2007.90.

Thatje, S., Smith, K.E., Marsh, L., and Tyler, P.A. (2015). Evidence for protracted and lecithotrophic larval development in the yeti crab Kiwa tyleri from hydrothermal vents of the East Scotia Ridge, Southern Ocean. *Sexuality and Early Development in Aquatic Organisms* 1(2), 109-116. doi: 10.3354/sedao00011.

Thomas, J.M., Moser, D.P., Fisher, J.C., Reihle, J., Wheatley, A., Hershey, R.L., et al. (2013). Using Water Chemistry, Isotopes and Microbiology to Evaluate Groundwater Sources, Flow Paths and Geochemical Reactions in the Death Valley Flow System, USA. *Procedia Earth and Planetary Science* 7, 842-845. doi: 10.1016/j.proeps.2013.03.033.

Thurber, A.R., Jones, W.J., and Schnabel, K. (2011). Dancing for food in the deep sea: bacterial farming by a new species of Yeti crab. *PLoS One* 6(11), e26243. doi: 10.1371/journal.pone.0026243.

Tiago, I., and Verissimo, A. (2013). Microbial and functional diversity of a subterrestrial high pH groundwater associated to serpentinization. *Environ Microbiol* 15(6), 1687-1706. doi: 10.1111/1462-2920.12034.

Tivey, M.K. (2007). Generation of Seaflooor Hydrothermal Vent Fluids and Associated Mineral Deposits. *Oceanography* 20(1), 50-65.

Toner, B.M., Lesniewski, R.A., Marlow, J.J., Briscoe, L.J., Santelli, C.M., Bach, W., et al. (2013). Mineralogy Drives Bacterial Biogeography of Hydrothermally Inactive Seafloor Sulfide Deposits. *Geomicrobiology Journal* 30(4), 313-326. doi: 10.1080/01490451.2012.688925.

Torres, M.E., McManus, J., Hammond, D.E., de Angelis, M.A., Heeschen, K.U., Colbert, S.L., et al. (2002). Fluid and chemical fluxes in and out of sediments hosting methane hydrate deposits on Hydrate Ridge, OR, I: Hydrological

provinces. *Earth and Planetary Science Letters* 201**,** 525-540. doi: 10.1016/S0012-821X(02)00733-1.

Trembath-Reichert, E., Morono, Y., Ijiri, A., Hoshino, T., Dawson, K.S., Inagaki, F., et al. (2017). Methyl-compound use and slow growth characterize microbial life in 2-km-deep subseafloor coal and shale beds. *Proc Natl Acad Sci U S A* 114(44)**,** E9206-E9215. doi: 10.1073/pnas.1707525114.

Treude, T., Boetius, A., Knittel, K., Wallmann, K., and Jørgensen, B.B. (2003). Anaerobic oxidation of methane above gas hydrates at Hydrate Ridge, NE Pacific Ocean. *Marine Ecology Progress Series* 264**,** 1-14.

Tryon, M.D., Brown, K.M., Torres, M.E., Tréhu, A.M., McManus, J., and Collier, R.W. (1999). Measurements of transience and downward fluid flow near episodic methane gas vents, Hydrate Ridge, Cascadia. *Geology* 27**,** 1075-1078. doi: 10.1130/0091-7613(1999)027<1075:MOTADF>2.3.CO;2.

Tryon, M.D., Wheat, C.G., and Hilton, D.R. (2010). Fluid sources and pathways of the Costa Rica erosional convergent margin. *Geochemistry, Geophysics, Geosystems* 11(4)**,** n/a-n/a. doi: 10.1029/2009gc002818.

Tuson, H.H., and Weibel, D.B. (2013). Bacteria-surface interactions. *Soft Matter* 9(18)**,** 4368-4380. doi: 10.1039/C3SM27705D.

USGS (2018). *National Water Information System - Groundwater Levels for Inyo-BLM1* [Online]. USGS Nevada Water Science Center. Available: https://nwis.waterdata.usgs.gov/nwis/gwlevels/?site_no=362402116280901 [Accessed 2018].

Van Dover, C.L. (1994). In Situ Spawning of Hydrothermal Vent Tubeworms (Riftia pachyptila). *The Biological Bulletin* 186(1)**,** 134-135.

Walker, C.B., de la Torre, J.R., Klotz, M.G., Urakawa, H., Pinel, N., Arp, D.J., et al. (2010). Nitrosopumilus maritimus genome reveals unique mechanisms for nitrification and autotrophy in globally distributed marine crenarchaea. *Proc Natl Acad Sci U S A* 107(19)**,** 8818-8823. doi: 10.1073/pnas.0913533107.

Walker, J.J., and Pace, N.R. (2007). Endolithic microbial ecosystems. *Annu Rev Microbiol* 61**,** 331-347. doi: 10.1146/annurev.micro.61.080706.093302.

Wanger, G., Southam, G., and Onstott, T.C. (2007). Structural and Chemical Characterization of a Natural Fracture Surface from 2.8 Kilometers Below Land Surface: Biofilms in the Deep Subsurface. *Geomicrobiology Journal* 23(6)**,** 443-452. doi: 10.1080/01490450600875746.

Watsuji, T.-o., Tsubaki, R., Chen, C., Nagai, Y., Nakagawa, S., Yamamoto, M., et al. (2017). Cultivation mutualism between a deep-sea vent galatheid crab and its chemosynthetic epibionts. *Deep Sea Research Part I: Oceanographic Research Papers* 127**,** 13-20. doi: 10.1016/j.dsr.2017.04.012.

Weiss, S., Xu, Z.Z., Peddada, S., Amir, A., Bittinger, K., Gonzalez, A., et al. (2017). Normalization and microbial differential abundance strategies depend upon data characteristics. *Microbiome* 5(1)**,** 27. doi: 10.1186/s40168-017-0237-y.

Wilkins, M.J., Daly, R.A., Mouser, P.J., Trexler, R., Sharma, S., Cole, D.R., et al. (2014). Trends and future challenges in sampling the deep terrestrial biosphere. *Front Microbiol* 5**,** 481. doi: 10.3389/fmicb.2014.00481.

Wrighton, K.C., Castelle, C.J., Wilkins, M.J., Hug, L.A., Sharon, I., Thomas, B.C., et al. (2014). Metabolic interdependencies between phylogenetically novel fermenters

and respiratory organisms in an unconfined aquifer. *The ISME Journal* 8(7)**,** 1452-1463. doi: 10.1038/ismej.2013.249.

Xie, S., Lipp, J.L., Wegener, G., Ferdelman, T.G., and Hinrichs, K.-U. (2013). Turnover of microbial lipids in the deep biosphere and growth of benthic archaeal populations. *Proc Natl Acad Sci U S A* 110(15)**,** 6010-6014. doi: 10.1073/pnas.1218569110.

Yee, N., Fein, J.B., and Daughney, C.J. (2000). Experimental study of the pH, ionic strength, and reversibility behavior of bacteria-mineral adsorption. *Geochim. Cosmochim. Acta* 64(4)**,** 609-617.

Zaitseva, S., V., Lavrentieva, E.V., Radnagurueva, A.A., Baturina, O.A., Kabilov, M.R., and Barkhutova, D.D. (2017). Distribution of Acetothermia-dominated microbial communities in alkaline hot springs of Baikal Rift Zone. *PeerJ Preprints* 5(e3492v1). doi: 10.7287/peerj.preprints.3492v1.